

MODELING, ANALYSIS, CONTROL AND DESIGN APPLICATION  
GUIDELINES OF DOUBLY FED INDUCTION GENERATOR (DFIG)  
FOR WIND POWER APPLICATIONS

by

Tarek Masaud

A thesis submitted to the Faculty and the Board of Trustees of the Colorado School of Mines in partial fulfillment of the requirements for the degree of Doctor of Philosophy (Electrical Engineering).

Golden, Colorado

Date \_\_\_\_\_

Signed: \_\_\_\_\_  
Tarek Masaud

Signed: \_\_\_\_\_  
Dr. Pankaj K. Sen  
Thesis Advisor

Golden, Colorado

Date \_\_\_\_\_

Signed: \_\_\_\_\_  
Dr. Randy L. Haupt  
Professor and Head  
Department of Electrical Engineering & Computer Science

## ABSTRACT

Double Fed Induction Generators (DFIG) has been widely used for the past two decades in large wind farms. However, there are many open-ended problems yet to be solved before they can be implemented in some specific applications. This dissertation deals with the general analysis, modeling, control and applications of the DFIG for large wind farm applications. A detailed “d-q” model of DFIG along with other applications is simulated using the MATLAB/Simulink platform. The simulation results have been discussed in detail in both sub-synchronous and super-synchronous mode of operation. An improved vector control strategy based on the rotor flux oriented vector control has been proposed to control the active power output of the DFIG. The new vector control strategy is compared with the stator flux oriented vector control which is commonly used. It is observed that the new improved vector control method provides a better active power tracking accuracy compare with the stator flux oriented vector control.

The behavior of the DFIG –based wind farm under the various grid disturbances is also studied in this dissertation. The implementation of the Flexible AC Transmission System devices (FACTS) to overcome the voltage stability issue for such applications is investigated. The study includes the implementation of both a static synchronous compensator (STATCOM), and the static VAR compensator (SVC) as dynamic reactive power compensators at the point of common coupling to support DFIG-based wind farm during disturbances. Integrating FACTS protect the grid connected DFIG-based wind farm from going offline during and after the disturbances. It is found that the both devices improve the transient performance and therefore helps the wind turbine generator system to remain in service during grid faults. A comparison between the performance of the two devices in terms of the amount of reactive power injected, time response and the application cost has been discussed in this dissertation.

Finally, the integration of the battery energy storage system (BESS) into a grid connected DFIG- based wind turbine as a proposed solution to smooth out the output power during wind speed variations is also addressed.

## TABLE OF CONTENTS

ABSTRACT.....	iii
LIST OF FIGURES.....	viii
LIST OF TABLES.....	xii
LIST OF SYMBOLS.....	xiii
LIST OF ABBREVIATIONS.....	xvi
ACKNOWLEDGMENT.....	xvii
CHAPTER 1 INTRODUCTION.....	i
1.1 An Overview of Wind Energy Growth.....	1
1.2 Introduction to Wind Energy Conversion System.....	1
1.2.1 Aerodynamic Components.....	4
1.2.2 Types of Wind Turbines.....	5
1.2.3 Operation Regions and Control of Wind Turbines.....	6
1.2.4 Wind Turbine Generators.....	8
1.3 Motivation of the Research.....	10
1.4 Literature Review.....	14
1.5 Objectives and Dissertation Outlines.....	16
CHAPTER 2 MODELING AND CONTROL OF DOUBLY FED INDUCTION GENERATOR BASED WIND TURBINE.....	19
2.1 Introduction.....	21
2.2 Components of DFIG.....	21
2.3 Principle of Operation of DFIG.....	22
2.3.1 Sub-synchronous Mode of Operation.....	23
2.3.2 Super-synchronous Mode of Operation.....	23
2.4 Generalized Induction Machine Dynamic Modeling (d-q Model).....	24
2.4.1 d-q Equivalent Circuit of Induction Machine.....	25
2.5 Doubly Fed Induction Generator Model (d-q Model).....	26
2.5.1 Dynamic Modeling of DFIG.....	26
2.6 Fundamentals of Vector Control of Induction Machines.....	26
2.7 Design of GSC Controller of DFIG.....	29

2.8	Design of RSC Controller of DFIG.....	30
2.8.1	RSC Controller Based on Stator Flux Oriented Vector Control.....	31
2.8.2	RSC Controller Based on Rotor Flux Oriented Vector Control.....	35
2.9	Simulation Results and Discussion.....	37
2.10	Summary.....	45
<b>CHAPTER 3 INTEGRATION OF FLEXIBLE AC TRANSMISSION SYSTEM (FACTS) DEVICES INTO DFIG-BASED WIND FARM.....</b>		<b>46</b>
3.1	DFIG-Based Wind Farm and Grid.....	46
3.2	FACTS Devices Overview.....	47
3.2.1	Shunt Capacitors.....	47
3.2.2	Static Var Compensator (SVC).....	48
3.2.3	Static Synchronous Compensator (STATCOM).....	50
3.3	Test System.....	52
3.4	Disturbances Mitigation in the DFIG-based Wind Farm System Using the STATCOM.....	53
3.4.1	The System Output at Steady State Conditions Without any compensation.....	54
3.4.2	Single Line to Ground Fault (SLGF) With STATCOM and RSC Blocking.....	55
3.4.3	Line to Line Fault (L-L) With STATCOM and RSC Blocking.....	58
3.4.4	Voltage Sag of 30% at Bus 120Kv With STATCOM and RSC Blocking.....	60
3.5	Disturbances Mitigation in the DFIG-based Wind Farm System Using the SVC.....	61
3.5.1	Single Line to Ground Fault (SLGF) With SVC and RSC Blocking.....	62
3.5.2	Line to Line Fault (L-L) With SVC and RSC Blocking.....	62
3.5.3	Voltage Sag of 30% at Bus 120Kv With SVC and RSC Blocking.....	64
3.6	Economic Comparison of STATOM and SVC .....	64
3.7	STATCOM and SVC Performance Comparison.....	65

3.8 Summary.....	66
CHAPTER 4 SMOOTHING OUTPUT POWER OF A GIRD CONNECTED DFIG-BASED WIND TURBINE USING BATTERY ENRGY STORAGE SYSTEM (BESS).....	68
4.1 Introduction.....	68
4.2 An overview of Energy Storage Devices.....	69
4.2.1 Flywheel.....	70
4.2.2 Supercapacitors.....	71
4.2.3 Superconducting Magnetic Energy Storage System (SMES).....	72
4.2.4 Batteries.....	72
4.2.5 Fuel Cells.....	73
4.2.6 Compressed Air Energy Storage (CAES).....	73
4.2.7 Pumping Hydro Energy Storage.....	74
4.3 Why Battery Energy Storage System (BESS) for DFIG.....	76
4.4 System Configuration and Principle of Operation.....	77
4.4.1 Design and Sizing of BESS.....	77
4.5 Proposed Control Strategy.....	78
4.5.1 Grid Side Converter (GSC) Controller.....	79
4.5.2 Rotor Side Converter (RSC) Controller.....	80
4.6 A Grid Connected DFIG Model with BESS.....	80
4.6.1 Grid Connected DFIG Model.....	82
4.6.2 BESS Sizing.....	82
4.6.3 BESS Model.....	84
4.7 Simulation Results and Discussion.....	85
4.7.1 The System Output at Steady State Conditions without BESS.....	85
4.7.2 The System Performance with the BESS and The Proposed Control Strategy.....	85
4.8 Summary.....	89
CHAPTER 5 CONCLUSIONS AND FUTURE WORK.....	91
5.1 Summary.....	91
5.2 Contributions.....	93

5.3 Future Work.....	94
5.4 List of Publications.....	95
REFERENCES.....	97
APPENDIX A: SYSTEM PARAMETES.....	107
APPENDIX B: MATLAB/Simulink.....	109
APPENDIX C: PRINCIPLE OF d-q TRANSFORMATION.....	120
APPENDIX D: SUPPLEMENTAL FILES.....	125

<b>LIST OF FIGURES</b>	<b>Page</b>
Figure 1.1 U.S wind power capacity growth 2001-2012.....	1
Figure 1.2 The total installed wind power capacity in U.S by state (2012).....	2
Figure 1.3 Global Cumulative installed wind capacity 1996-2012.....	2
Figure 1.4 U.S. vs Worldwide – Installed wind power capacity 2001-2012.....	3
Figure 1.5 The total installed power capacity in U.S. at the end of 2011.....	4
Figure 1.6 Block diagram of the components of the wind energy conversion system connected to the grid.....	5
Figure 1.7 Tip speed Ratio (TSR) versus Power Coefficient ( $C_p$ ).....	7
Figure 1.8 Horizontal axis wind turbine (HAWT) and vertical axis wind turbine (VAWT).....	8
Figure 1.9 Steady state power curve of wind turbine.....	9
Figure 1.10 Typical configuration of type 1 WTG.....	11
Figure 1.11 Typical configuration of type 2 WTG.....	12
Figure 1.12 Typical configuration of a grid connected DFIG-based wind farm.....	13
Figure 1.13 Typical configuration of type 4 WTG.....	14
Figure 2.1 Configuration of DFIG wind Energy conversion system using back-to-back converter.....	22
Figure 2.2 Power flow of DFIG system.....	25
Figure 2.3 Dynamic $d^e$ - $q^e$ equivalent circuit of induction machine.....	27
Figure 2.4 Separately excited DC machine and vector controlled induction machine.....	30
Figure 2.5 Phasor diagram of stator flux- oriented vector control.....	31
Figure 2.6 Vector control scheme of RSC.....	34
Figure 2.7 Phasor diagram of rotor flux- oriented vector control.....	35
Figure 2.8 Simulink implementation of inner control loop of rotor flux oriented vector control.....	36
Figure 2.9a Stator currents of DFIG in super-synchronous mode.....	38
Figure 2.9b Rotor Currents of DFIG in super-synchronous mod.....	39
Figure 2.9c Electrical Torque of DFIG in super-synchronous mode .....	39
Figure 2.9d The rotor and the synchronous speed of DFIG in super-synchronous mode .....	39
Figure 2.9e The stator active power of DFIG in super-synchronous mode.....	40
Figure 2.9f The stator reactive power of DFIG in super-synchronous mode.....	40
Figure 2.10a The stator currents of DFIG in sub-synchronous mode .....	40

Figure 2.10b The rotor currents of DFIG in sub-synchronous mode.....	41
Figure 2.10c The rotor and synchronous speed of DFIG in sub-synchronous mode.....	41
Figure 2.10d The electromagnetic torque of DFIG in sub-synchronous mode.....	41
Figure 2.10e The stator active power of DFIG in sub-synchronous mode.....	42
Figure 2.10f The stator reactive power of DFIG in sub-synchronous mode.....	42
Figure 2.11a The stator active power tracking the reference power using stator flux oriented vector control.....	43
Figure 2.11b The control of $i_{qr}$ component in the stator flux oriented vector control.....	43
Figure 2.11c The stator active power tracking the reference power using rotor flux oriented vector control.....	43
Figure 2.11d The control of $i_{qr}$ component in the rotor flux oriented vector control.....	44
Figure 2.11e The control of the rotor current in the rotor flux oriented vector control.....	44
Figure 3.1 Typical SVC Configuration.....	49
Figure 3.2 Equivalent circuit and control system of SVC.....	49
Figure 3.3 Equivalent Circuit of STATCOM.....	51
Figure 3.4 Control System Block Diagram of STATCOM.....	51
Figure 3.5 Single Line Diagram of the Test System.....	52
Figure 3.6a Wind speed profile.....	54
Figure 3.6b DFIG generated active and reactive power.....	54
Figure 3.6c The voltage and current at point of common coupling (Bus B575).....	55
Figure 3.6d DC link Capacitor voltage and turbine speed.....	55
Figure 3.7a PCC (Bus B575) voltage during SLGF.....	56
Figure 3.7b Interrupted operation of the wind turbine during a SLGF.....	56
Figure 3.7c PCC (Bus B575) voltage during SLGF with a STATCOM.....	57
Figure 3.7d Reactive power injected by the STATCOM during SLGF.....	57
Figure 3.7e Uninterrupted operation of the wind turbine with a STATCOM during SLGF.....	57
Figure 3.8a PCC (Bus B575) voltage during line to line fault.....	58
Figure 3.8b PCC (Bus B575) voltage during line to line fault with a STATCOM.....	59
Figure 3.8c Reactive power injected by the STATCOM during line to line fault.....	59
Figure 3.8d The overshoot of the DC link voltage during Line to Line fault without STATCOM.....	59
Figure 3.8e The overshoot of the DC link voltage during Line to Line fault with STATCOM.....	60

Figure 3.9a PCC (Bus B575) voltage during a voltage sag Of 30% at Bus 120kV.....	60
Figure 3.9b PCC (Bus B575) voltage during Sag of 30% at Bus 120kV with a STATCOM.....	61
Figure 3.9c Reactive power injected by the STATCOM during sag of 30% at 120k.....	61
Figure 3.10a PCC (Bus B575) Voltage during SLGF with a SVC.....	62
Figure 3.10b Reactive power injected by the SVC during SLGF.....	62
Figure 3.10c PCC (Bus B575) Voltage during Line to Line Fault with SVC.....	63
Figure 3.10d Reactive Power Injected by the SVC during Line to Line Fault.....	63
Figure 3.10e The Overshooting of the DC link Voltage during Line to Line Fault with SVC.....	63
Figure 3.10f PCC (Bus B575) Voltage during Sag of 30% at Bus 120kV with SVC.....	64
Figure 3.10g Reactive Power Injected by the SVC during the sag of 30% at the 120kV bus.....	64
Figure 4.1 Battery Energy Storage System (BESS) connected to the DC Link of the rotor converter of DFIG.....	69
Figure 4.2 Classification of energy storage technologies.....	70
Figure 4.3 Working Scheme of Supercapacitor.....	71
Figure 4.4 Layout of a compressed air energy storage facility.....	74
Figure 4.5 Layout of a pumped hydroelectric energy storage facility.....	75
Figure 4.6 General power curve of a wind-turbine showing the characteristics of the generated power ( $P_{gen}$ ) and the average power ( $P_{avg}$ ).....	78
Figure 4.7 Schematic Diagram of Proposed Control Strategy for RSC and GSC of a DFIG with BESS.....	81
Figure 4.8 Depth of discharge % vs. Number of cycles for typical deep-cycle Lead-Acid battery.....	83
Figure 4.9 Thevenin Equivalent circuits of the BESS.....	85
Figure 4.10 Performance of DFIG-based wind turbine without the BESS and the proposed control at rated wind speed of 14m/s.....	86
Figure 4.11 (a) Applied stepwise wind speed profile.....	87
Figure 4.11 (b) Battery output power.....	87
Figure 4.11 (c&d) Generated active and reactive power.....	87
Figure 4.11 (e &f) DC Link voltage and rotor speed .....	88
Figure 4.12 (a) Random wind speed profile.....	88
Figure 4.12 (b) Battery output power.....	88

Figure 4.12 (c &d) Generated active and reactive power..... 89  
Figure 4.12 (e &f) DC Link voltage and rotor speed..... 89

## LIST OF TABLES

Page

Table 1.1	Table 1.1 Average rate of wind power capacity growth.....	3
Table 2.1	Comparison of a simple hand calculation with simulation results for stator power and current.....	38
Table 3.1	Installation cost comparison of shunt controllers.....	65
Table 3.2	The installation cost calculation of the SVC application .....	65
Table 3.3	The installation cost calculation of the STATCOM application .....	65
Table 3.4	STATCOM compared to SVC performance.....	66
Table 4.1	Energy storage devices characteristics.....	76
Table.4.2	Sizing of BESS bank.....	84

## LIST OF SYMBOLS

TSR	Tip speed ratio
$C_P$	Power coefficient
$n_s$	Synchronous speed
$n_{Rotor}$	Rotor speed
$n_{\phi,Stator}$	Speed of the rotating magnetic field induced in the stator
$n_{\phi,Rotor}$	Speed of the rotating magnetic field induced in the rotor
$f_{Stator}$	Frequency of the stator voltages
$f_{Rotor}$	Frequency of the rotor voltages and currents
$f_{Grid}$	Grid frequency
$P_g$	Air gap power
$P_r$	Slip power
$P_m$	Mechanical power
$S$	Slip
$d^s - q^s$	Stator (stationary) direct and quadrature axes
$d^r - q^r$	Rotor direct and quadratic axes
$d^e - q^e$	Synchronously rotating direct and quadratic axes
$\theta$	Orientation angle
$v_{qs}^s, \text{ and } v_{ds}^s$	Stator voltages on the stationary reference frame
$F_{ij}$	The flux linkage
$v_{qs}, v_{ds}, v_{qr}, \text{ and } v_{dr}$	Stator and rotor voltages on d–q axis
$i_{qs}, i_{ds}, i_{qr}, \text{ and } i_{dr}$	Stator and rotor currents on d–q axis
$F_{mq}, F_{md}$	q and d axis magnetizing flux linkage
$L_{ls}$	Leakage inductance of stator windings
$L_{lr}$	Leakage inductance of rotor windings

$L_s$	Stator inductance
$L_r$	Rotor inductance
$L_m$	Magnetizing inductance
$R_s$ and $R_r$	Stator and rotor resistances
$X_{ls}$ and $X_{lr}$	Stator and rotor leakage reactance's
$p$	Number of poles
$J$	Moment of inertia
$T_e$	Electromagnetic torque
$T_L$	Load torque (mechanical torque)
$P_s$ and $Q_s$	Stator active and reactive power
$P_{gen}$	Generated output active power
$P_{avg}$	Average active power
$\omega_e$ and $\omega_r$	Stator angular electrical frequency and the rotor angular speed
$\omega_b$	Angular electrical base frequency
$\psi_s$	Stator flux
$\psi_{ds}$	Stator flux component on d axes
$\psi_{qs}$	Stator flux component on q axes
$\psi_{ds}^s$	Stator flux component on the d axes of the stationary reference Frame
$\psi_{qs}^s$	Stator flux component on the q axes of the stationary reference frame
$k_i$	Integral constant of the PI controller
$k_p$	Proportional constant of the PI controller
$I_a$	Armature current
$I_f$	Field current
$\psi_a$	Armature flux
$\psi_f$	Field flux

$V_{ref}$	Reference Voltage
$C$	Capacitance
$g$	Acceleration due to gravity
$S_C$	Energy Storage capacity of the pumped hydro storage plant
$\eta_P$	Pump efficiency
$\eta_T$	Turbine efficiency
$R_s$	Equivalent internal & external resistance of battery
$C_b$	Battery capacitance
$V_b$	Battery nominal voltage
$P_b$	Battery capacity
$E_b$	Total rating of the battery bank
$R_b$	Parallel circuit resistance of the battery equivalent circuit
$V_{OCMin}$ and $V_{OCMax}$	Minimum and maximum open circuit voltage of the battery

## LIST OF ABBREVIATIONS

BESS	Battery energy storage system
CAES	Compressed air energy storage
DFIG	Doubly-fed induction generator
ESS	Energy storage system
FSWT	Fixed speed wind turbine generators
FACTS	Flexible AC transmission systems devices
FC	Fixed capacitor
G	Generator
GSC	Grid-side converter
HAWT	Horizontal axis wind turbines
IG	Induction generator
IGBT	Insulated gate bipolar transistor
MDOD	Maximum depth of discharge of the battery
PCC	Point of common coupling
PLL	Phase-locked loop
P.u	per unit
PWM	Pulse width modulation
PCS	Power conversion system
PHES	Pumped hydro energy storage
RSC	Rotor-side converter
SVC	Static Var compensator
STATCOM	Static synchronous compensator
SLGF	Single-line-to-ground fault
SMES	Superconducting magnetic energy storage system
TCR	Thyristor controlled reactor
TSC	Thyristor switched capacitor
VAWT	Vertical axis wind turbines
VSWT	Variable Speed Wind Turbine Generators

VSC	Voltage source converter
WECS	Wind energy conversion system
WT	Wind turbine

## ACKNOWLEDGMENT

First and foremost, I would like to express my sincere gratitude to my advisor Prof. **P.K. Sen** for his continuous support of my Ph.D study and research, his patience, motivation, enthusiasm, and immense knowledge. His guidance significantly helped me throughout the research and writing of this dissertation. I could not have imagined having a better advisor and mentor for my PhD study.

In addition, I would like to thank the rest of my academic committee: Prof. **David Munoz**, Dr. **Eduard Muljadi**, Dr. **Kathryn Johnson**, and Dr. **Ravel F. Ammerman** for their encouragement, insightful comments, help and support.

I would also like to thank my parents, for their continual support, generous love, never-ending patience, and inspiration. I am also thankful to my friends for their valuable support and time, especially my colleague **Keun Lee** for his support and assistance.

I would like also to thank the **Ministry of Higher Education and Scientific Research of Libya** for the scholarship I have received during my PhD Study.

Finally, I dedicate my PhD to my brother, **Abdulhamed**, whom we lost in an automobile accident in 2004. He was 21. He was full of life, dreams and goals. This dedication will serve to keep his spirit alive.

# CHAPTER 1

## INTRODUCTION

### 1.1 Wind Energy Growth: An Overview

The worldwide installed capacity for large wind power applications has grown significantly over the time period of 2005-2009 [3]. In the United States, the installed wind power capacity was 35,000MW at the end of 2009, while the worldwide installed capacity reached 160,000MW [3]. According to the American Wind Energy Association (AWEA), the total U.S. wind power capacity was 60,007MW at the end of 2012, as shown in Figure 1.1 [13]. This means that the total U.S. wind power capacity has grown by 71.4% over the time period of 2009-2012 (45,100 wind turbines installed across the U.S. at the end of 2012 [13]). Figure 1.2 shows an updated map of the installed wind power capacity in the US at the end of 2012 [12]. The top 2 states for new wind power capacity installations in 2012 were Texas (12,212 MW), and California (5,549 MW). According to the global wind energy council (GWEC), the worldwide wind power capacity installed was 282,430MW at the end of 2012, with a growth average rate of 77.7% over the time period of 2009-2012 Figure 1.3 [14].

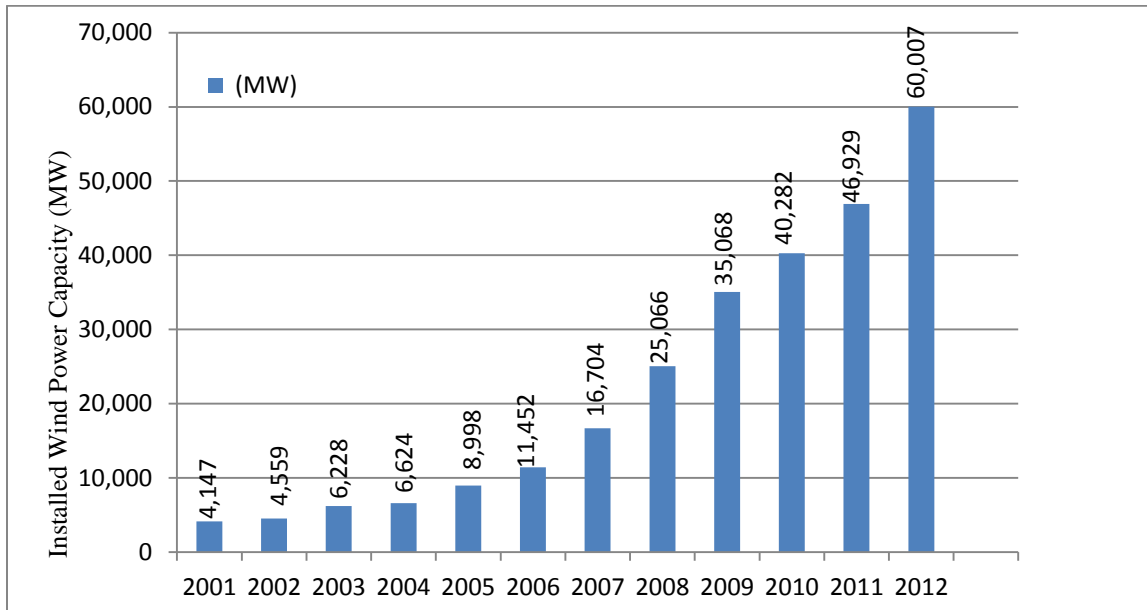


Figure 1.1 U.S wind power capacity growth during 2001-2012

### 2012 Year End Wind Power Capacity (MW)

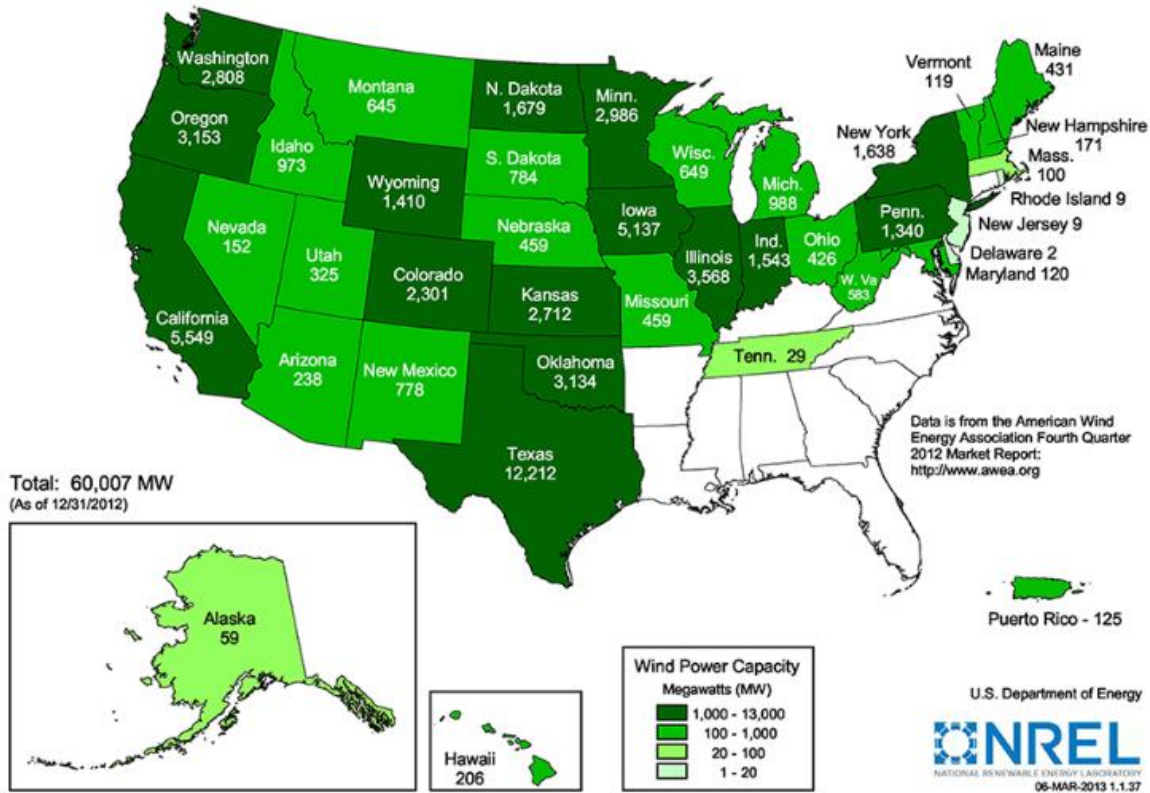


Figure 1.2 Total installed wind power capacity in U.S by state (2012) [12]

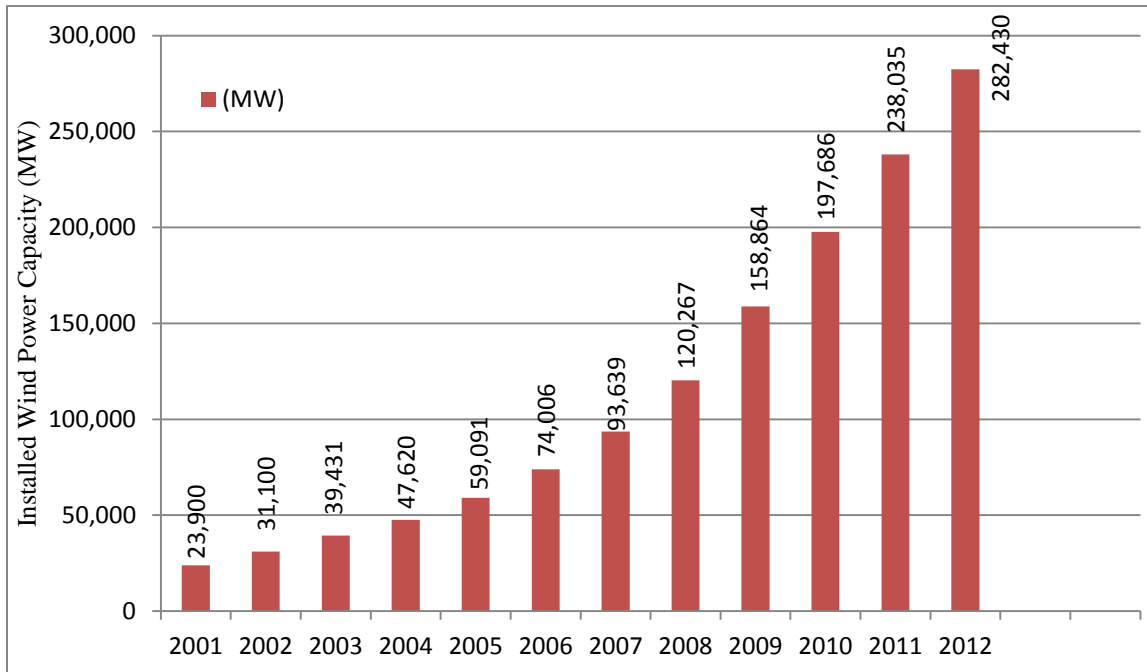


Figure 1.3 Global Cumulative installed wind capacity 2001-2012

Figure 1.4 shows the cumulative installed wind capacity in the U.S. and the corresponding worldwide values. In 2001, the U.S. installed wind power capacity was 17.35% of the global installed wind power capacity, while in 2012 the value increased to 21.24%. Table 1.1 compares the annual growth of wind power capacity in the U.S. and worldwide in the last 4 years.

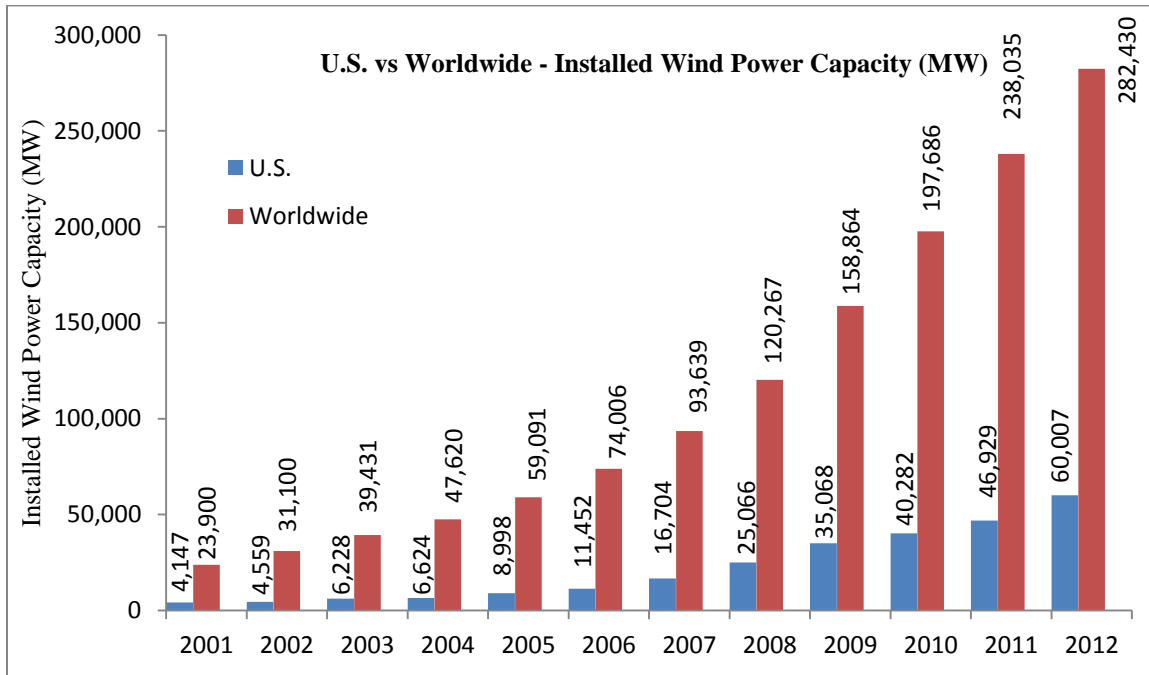


Figure 1.4 U.S. vs Worldwide – installed wind power Capacity during 2001-2012

Table 1.1 Average rate of wind power capacity growth

Time Period	Annual Growth (U.S.)	Annual Growth (Worldwide)
2008-2009	39.90%	32.09%
2009-2010	14.86%	24.43%
2010-2011	16.50%	20.41%
2011-2012	27.86%	18.65%

The U.S. Department of Energy lays the framework for America to produce 20% of its electrical energy generation from wind by 2030 [10], which included a contribution of 4% to the nation’s total electricity from offshore wind power. The report also states that, based on the

installed wind power capacity at the end of 2006 (11.6 GW), an additional 300 GW need to be installed to achieve the 20% wind power goal.

According to the U.S. Energy Information Administration (EIA) [108], the total installed power capacity at the end of 2011 is 1054.8 GW. Figure 1.5 shows the share of total installed power capacity in U.S. at the end of 2011. The graph depicts that wind power capacity is 4.28% (45.2GW) of the total installed power capacity.

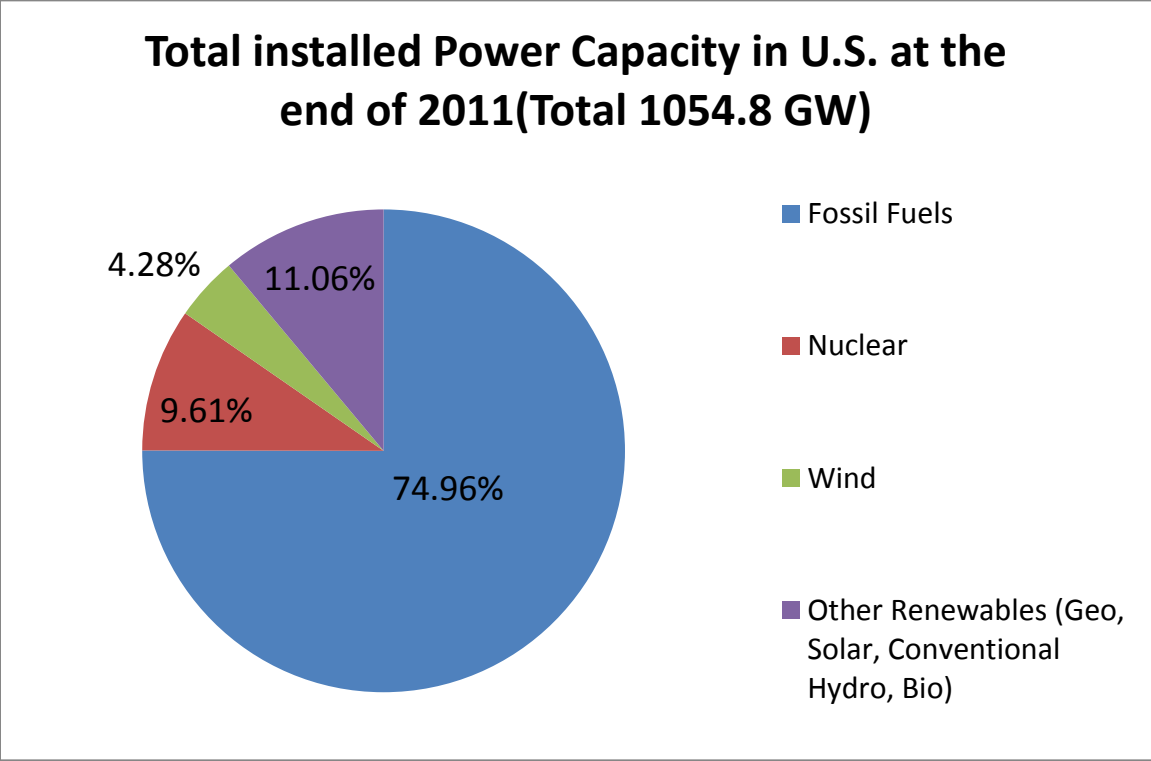


Figure 1.5 The total installed power capacity in U.S. at the end of 2011

### 1.2 Introduction to Wind Energy Conversion System

Wind Energy Conversion System (WECS) converts wind energy into useful mechanical energy in a wind-turbine that is used as the prime-mover to power an electrical (Doubly Fed Induction Generator or DFIG) generator. The WECS basically consists of two major components: (i) turbine and associated control including the gear box, and (ii) electrical (DFIG including the rotor converter system and associated control), as shown in Figure 1.6, one such design.

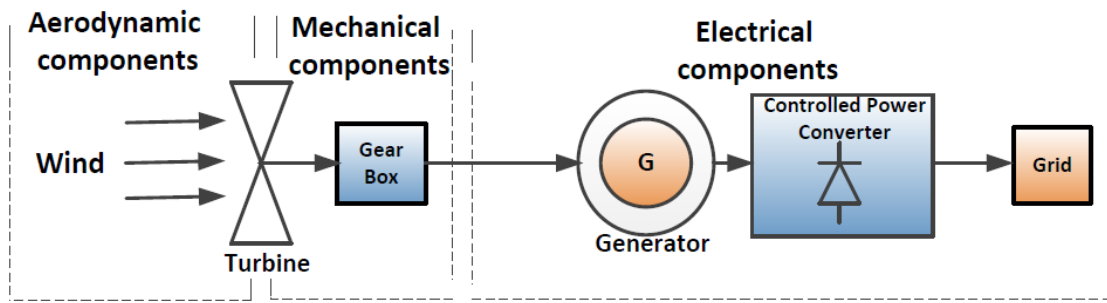


Figure 1.6 Block diagram of the components of the wind energy conversion system connected to the grid

### 1.2.1 Aerodynamic Components

A wind turbine is a device that extracts kinetic energy from the wind and converts it into electrical energy. Wind turbine power production depends on the interaction between the blade (rotor) and the wind speed and mass. The wind turbine performance quantities like the power output, speed, torque, etc. are determined by the aerodynamic forces generated by the wind. The two main dimensionless parameters to characterize the aerodynamic operation and mechanical performance of wind turbines are the tip speed ratio (TSR) and the power coefficient ( $C_p$ ).

“Tip Speed Ratio” of wind turbine is the ratio between the linear speed of the tip of the blade and the actual velocity of the wind.

$$\text{TSR} (\lambda) = \frac{\omega R}{v} \quad (1.1)$$

$\lambda$  is the tip speed ratio,  $\omega$  is the rotor angular velocity,  $R$  is the rotor radius, and  $v$  is wind speed. If the rotor of the wind turbine turns too slowly, most of the wind will pass undisturbed through the opening between the blades, extracting little power. On the other hand, if the rotor turns too fast, the rotating blades will obstruct the wind flow, which reduce the power extraction. Therefore, it is necessary in the design of wind turbines to obtain maximum rotor efficiency, match the angular velocity of the rotor to the wind speed or the optimal TSR.

If TSR is too low the wind turbine will tend to slow and/or stall. If the tip speed ratio is too high the turbine will spin very fast through turbulent air, power will not be optimally extracted and the wind turbine will be highly stressed and at risk of structural failure.

The “power coefficient” of a wind turbine describes how efficiently a wind turbine converts the energy in the wind into electricity. This is defined as,

$$\text{Power Coefficient } (C_p) = \frac{\text{Electricity produced by wind turbine}}{\text{Total energy available in the wind}} \quad (1.2)$$

The theoretical maximum power coefficient of a wind turbine is approximately 59% (called “Betz Limit”) [3]. Good modern-day wind turbines generally have a power coefficient in the range of 35% - 40% [2]. This value below the theoretical limit (“Betz Limit”) is due to the inefficiencies and losses attributed to different configurations, rotor blades profiles, finite wings, friction, and turbine designs.

Figure 1.7 shows that the maximum power extraction occurs at the optimal TSR [7] in which the lowest difference can be seen between the actual TSR curve (blue curve) and the constant TSR line (dashed line). This difference represents the uncaptured power by the wind turbine. Frictional losses, finite wing size, and turbine design losses account for part of the uncaptured wind power, and are supplemented by the fact that a wind turbine is not operating at the optimal TSR across its operating range of wind speeds [3, 7]. However, The rotor speed can be controlled (main strategy) to maintain an optimal TSR at different wind speeds to extract maximum possible energy from the wind (maximum  $C_p$ ).

### 1.2.2 Types of Wind Turbines

Wind turbines are classified into two general types: horizontal axis wind turbines (HAWT) and vertical axis wind turbines (VAWT), as shown in Figure 1.8 [8]. Initially, vertical axis designs were considered superior, (no need for a yaw system) and the location of their gears and generating equipment at the tower base. However, the following disadvantages caused the VAWT to have a diminished presence in the commercial market.

- Reduced aerodynamic efficiency: much of the blade surface is close to the axis.
- The housing is usually at ground level, so it is not feasible to also have the gearbox of a large VAWT at ground level due to the weight and cost of the transmission shaft. This limit the size.

In HAWT, the wind turbine blades rotate around an axis that is parallel to the ground and wind flow. Almost all the larger turbines employed in modern wind farms are HAWT, because

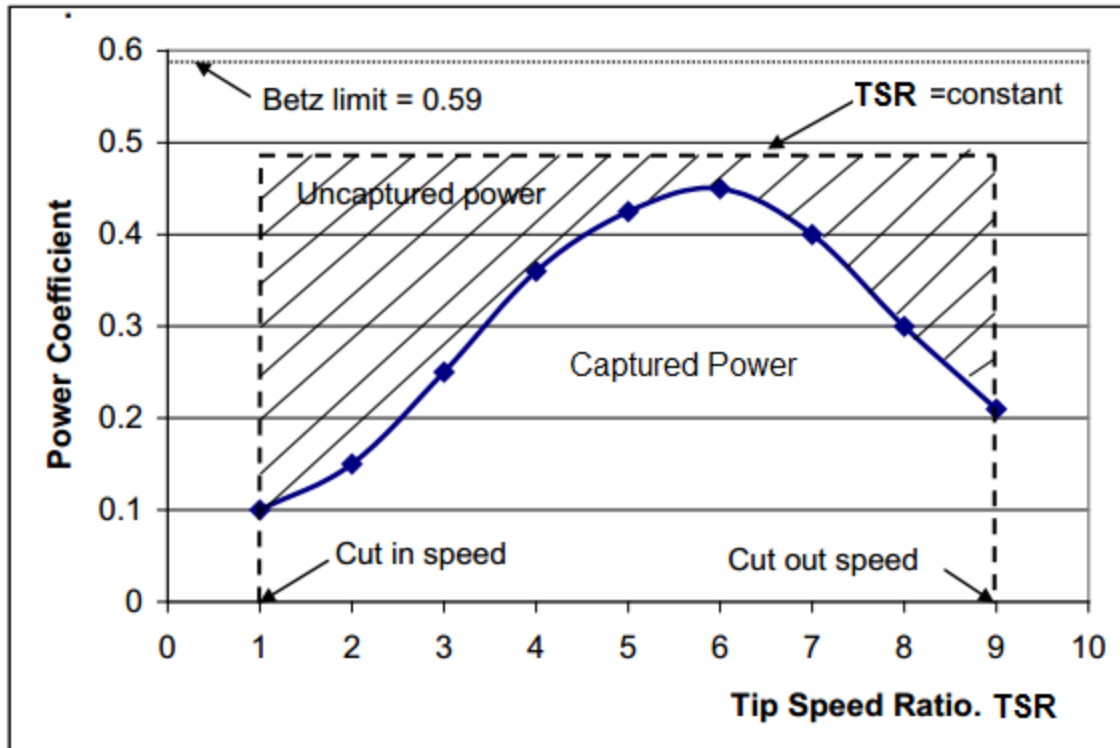


Figure 1.7 Tip speed Ratio (TSR) versus Power Coefficient ( $C_p$ ) [7]

they are more suitable for harnessing a higher amount of wind energy. However, HAWT are subjected to reversing gravitational loads (the structural load is reversed when the blade goes from upwards to downwards position), which impose a limit on the size of such turbines [3, 5].

Typical modern wind turbine has two basic operating modes: fixed or variable wind speed turbines. A wind turbine can also be variable pitch or constant pitch, which means that the blades may or may not be able to rotate about their longitudinal axes.

The rotor of the fixed speed wind turbine rotates at a fixed angular speed and connected to a conventional squirrel cage induction generator that has the same frequency of the grid to which it is connected, regardless of wind speed variation. The fixed speed wind turbine has the advantage of being simple and robust construction and lower capital cost.

The disadvantages include:

- Cannot extract maximum energy from wind (not optimal).
- Generates more mechanical stress on gearbox during variable wind speed.
- Do not have the capability of independent control of active and reactive power delivered to the grid because of the generator type (conventional induction generator).

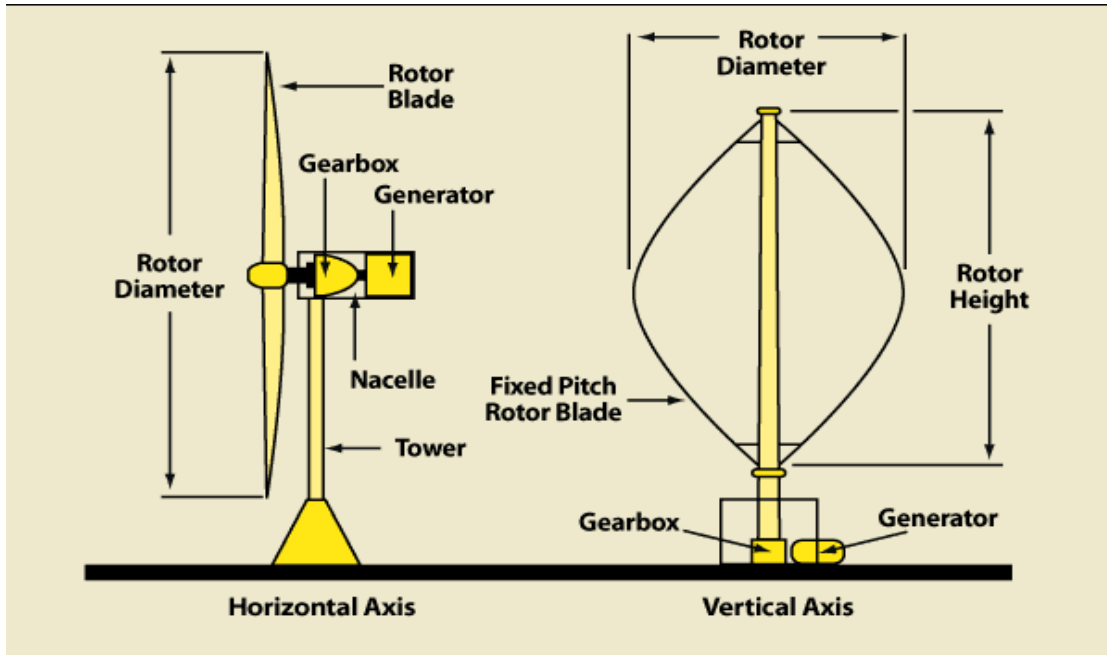


Figure 1.8 Horizontal axis wind turbine (HAWT) and vertical axis wind turbine (VAWT) [8]

The main advantages and disadvantages of the variable speed wind turbine can be summarized as below.

Advantages:

- Variable speed turbine can operate at ideal tip-speed ratios over a larger range of wind speeds, so capturing maximum energy from wind and have efficient operation.
- Due to the type of generator and type of power converter used, it has the ability to supply power at a constant voltage and frequency while rotor speed varies.
- Control of active and reactive power supplied to the grid.

The disadvantage that the machine generates variable frequency current/voltage requiring a power (electronics) converter.

The modern wind turbine industry has shifted toward variable speed wind turbines because of their better overall performance. They take full advantage of variations in the wind speed, encounter lower mechanical stress and less power fluctuations, and provide 10-15% higher energy output compared with constant speed operation [16, 18].

### 1.2.3 Operating Regions and Control of Wind Turbine

As discussed earlier, the present day application is focused on the variable speed wind turbine. The control approaches for such applications vary depending on the operation region.

The variable speed wind turbine has three control regions, as shown in Figure 1.9 [15]. The power coefficient  $C_p$ , is defined mathematically as the ratio of the rotor power to the power available in the wind  $P_{wind}$  [3]:

$$C_p = \frac{P}{P_{Wind}} \quad (1-3)$$

and

$$P_{Wind} = \frac{1}{2} \rho A v^3 \quad (1-4)$$

where,  $\rho$  is the air density ( $\text{kg/m}^3$ ),  $A$  is the rotor swept area ( $\text{m}^2$ ),  $v$  is the wind speed ( $\text{m/s}$ ),  $P$  is the aerodynamic rotor power (turbine power) in kW.

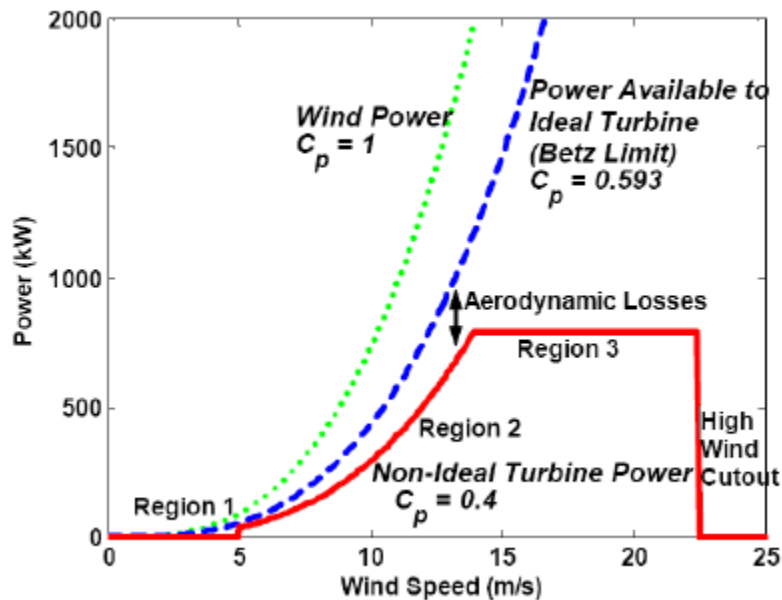


Figure 1.9 Steady state power curve of an example wind turbine [15]

**Region 1**, the section of the solid red curve which is located prior to the wind speed of 5m/s (“cut-in” wind speed). The wind turbine in this region is considered to be starting up. In general, the purpose of the control strategy in region 1 is for monitoring the wind speed to decide whether it fall within the turbine operation specifications and, if so, performing the necessary routines needed in starting up the turbine. The implementation of the modern control techniques is not crucial in this region [15].

**Region 2**, Illustrated by the cubic area of the solid red curve (from cut in speed 5 m/s to the rated wind speed 14m/s, in this example), is an operational region in which it is favorably to extract as much power as possible from the wind [15].The generator torque and yaw control techniques are widely deployed for most of the time in region 2 with maintaining the blade pitch constant at optimal value for maximum energy extraction [15].

**Region 3** is the region above the rated wind speed (from rated wind speed 14m/s to the “cut-out” speed 23m/s, in this example), the wind turbine must maintain a constant speed and a constant rated power output. Pitch control on blades is done in order to shed additional power. In order to control blade pitch, proportional integral derivative (PID) is the most efficient and yet simple control standard technique in industry that limits speed and power [15].

#### **1.2.4 Wind Turbine Generators**

Wind Turbine Generators (WTG) in the current market can be classified broadly into two types according to their operation speed and the size of the associated converters: Fixed Speed Wind Turbine Generators (FSWT) and Variable Speed Wind Turbine Generators (VSWT). As discussed earlier, the variable-speed, variable-pitch wind turbines utilizing DFIG are the most popular in the wind power industry, especially for multi-megawatt wind turbine generators. The DFIG consists of a wound rotor induction generator with the stator side connected directly to the constant frequency three-phase grid and the rotor windings connected to the grid through a bidirectional back-to-back ac/dc/ac voltage source converter. Its output power can be controlled via pitch control as well as back-to-back converter control. Below is a snapshot summary of the different design characteristics of wind turbine generators applied in various wind power plants.

**Type 1: Wind Turbine Generator (Fixed Speed Wind Turbine Generator)** Type 1 is a conventional Squirrel-Cage Induction Generator (SCIG) and is connected to the step-up transformer directly, as shown in Figure 1.10. The turbine speed is nearly fixed to the electrical grid synchronous speed, and generates real power ( $P$ ) when the turbine shaft rotates slightly faster than the synchronous speed creating a negative slip (positive value for the slip and power for motoring convention). The highest rotor operational speed is very small about 1% above the synchronous speed [95, 96]. Design simplicity, and the low cost are the main advantages of this type. However, this design requires a large amount of reactive power to excite the machine and draws a very high starting current (like a conventional induction motor starting at full-voltage).

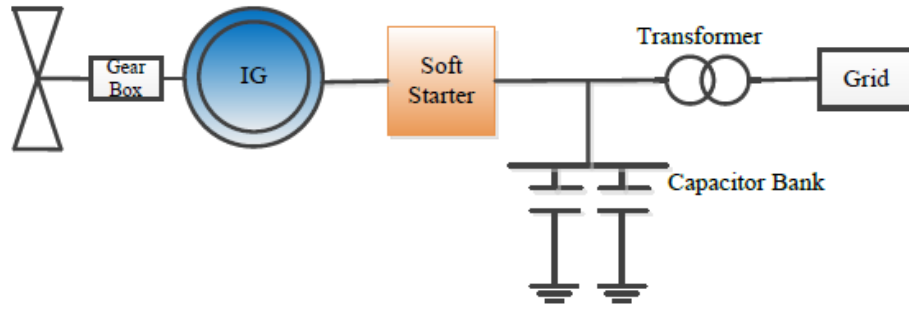


Figure 1.10 Typical configuration of Type 1 WTG

These machines also do not have any control on the electrical side and the turbine speed has to be within a very narrow bandwidth. The generator typically employs a soft starter device and discrete steps of capacitor banks [95, 96]. This design is utilized in low-head hydro units, where the speed could be effectively controlled with the governor. There are some limited applications (small scale residential type use) of this design in wind power systems.

**Type 2: Wind Turbine Generator (Limited Variable Speed Wind Turbine Generator)** is a wound-rotor induction generator and is connected directly to the step-up transformer in a similar way to Type 1 with regards to the machines stator circuit. However, variable external resistors are inserted into the rotor circuit, as shown in Figure 1.11 and the rotor power is controlled by power electronics. The variable resistors can control the rotor currents quite rapidly so as to keep constant power even during gusting conditions, and can influence the machine’s dynamic response during grid disturbances.

Adding the rotor resistance enables a higher operational speed of 10% above the synchronous speed [96]. This feature enables some ability to control the speed, with the blades’ pitching mechanisms and move the turbines operation to a tip speed ratio to achieve a better energy capture. Similar to a Type 1 WTG, a Type 2 WTG always requires reactive power, which is typically supplied by switched capacitor units or dynamic reactive power compensators to meet the grid interconnection standards [99].

**Type 3: Wind Turbine Generator (Variable Speed Wind Turbine Generator)** is also known as Doubly Fed Induction Generator (DFIG). It is a variable wind speed turbine generator with a partial power electronic conversion associated in the rotor circuit. The term “doubly fed”

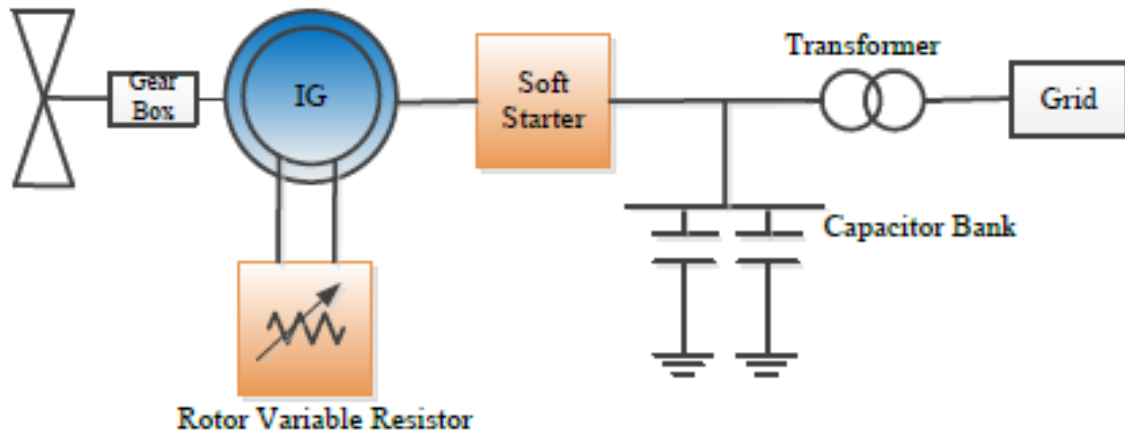


Figure 1.11 Typical configuration of Type 2 WTG

refers to the fact that the power and reactive power are fed to the grid directly from the stator and via the bidirectional converter from the rotor circuit. This system allows a variable-speed operation over a range of  $\pm 25\%$  (compared to about 1%-2% for the Type 1 and 2) around the synchronous speed [32]. The converter compensates for the difference between the mechanical rotor speed and electrical frequencies by injecting a rotor current with a variable frequency. Hence, the operation and behavior of the DFIG is governed by the power converter and its controllers. Figure 1.12 shows a general configuration of a grid-connected DFIG-based wind turbine.

The rotor power converter circuit consists of two components, the Rotor Side Converter (RSC) and the Grid Side Converter (GSC), which are controlled independently. The RSC controls the active and reactive power by controlling the rotor current, while the GSC controls the DC link voltage and DFIG terminal voltage (or power factor) of the overall DFIG system by controlling amount of reactive power exchanged with the power grid. Stator side always feeds active power to the grid whereas active power is fed into or out of the rotor depending on the operating conditions of the drive. In super-synchronous speed, power flows from the rotor via the converter to the grid, whereas it flows in the opposite direction in sub-synchronous speed of the drive.

Advantages of DFIG wind turbine system include:

- It has the ability to control reactive power and decouple control of active and reactive

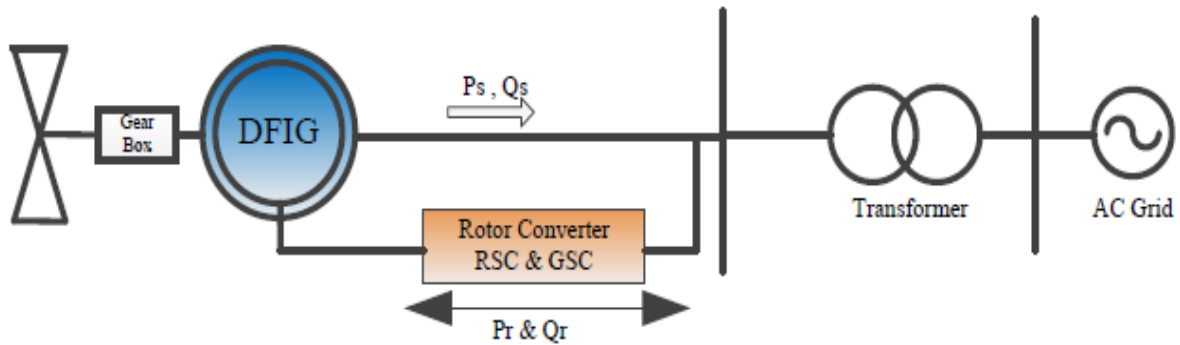


Figure 1.12 Typical configuration of a grid connected DFIG-based wind turbine.

- power by independently controlling the rotor excitation current. So power factor control can be implemented in this system.
- DFIG is a wound-rotor induction machine which is simple in construction and cheaper than the synchronous machine. In DFIG, converter rating is typically between 25-30% of total system power, which results: reduced converter costs compared to full-scale power converters used in Type 4 machines, less harmonics injection to the connected grid, and improved overall efficiency (approximately 2-3% more than a full-scale frequency converter) of the wind turbine system [36].
- In the case of a weak grid, where the voltage may fluctuate, the DFIG can produce or absorb reactive power to or from the grid within its capacity, to regulate the terminal voltage.
- Higher energy conversion efficiency compared with the conventional induction generator.
- A smaller power rated DFIG can be used with a higher power rated wind turbine.

Disadvantages of DFIG wind turbine system include:

- A need for slip rings and a gear box that requires frequent maintenance.
- Limited reactive power capability and fault ride through capability.

**Type 4: Wind Turbine Generator (Variable Speed Wind Turbine Generator)** is a variable wind speed turbine generator (either induction or synchronous: conventional or permanent magnet) with a full power electronic conversion. This type provides a great deal of flexibility in design and operation as the output of the rotating machine is supplied to the grid through a full-scale back-to-back power converter [97]. The turbine is able to rotate at its optimal

aerodynamic speed, resulting in a widely variable AC output from the machine. In addition, the gearbox may be eliminated, such that the machine spins at the slow turbine speed and generates an electrical frequency well below that of the grid. This is not a problem for a Type 4 design, as the inverters convert the supplied power and provides the ability to supply reactive power to the grid much as a STATCOM [97]. The typical configuration of Type 4 machine is shown in Figure 1.13.

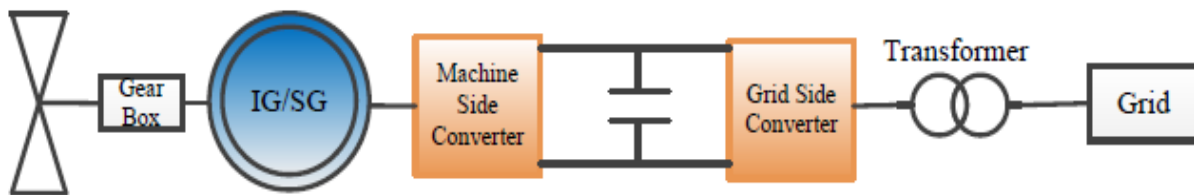


Figure 1.13 Typical configuration of type 4 WTG

The main advantages of Type 4 are: less mechanical stress, less noisy, aerodynamically efficient, and no gearbox, operates at lower speeds, this can translate into increased reliability of the wind turbine, and can vary the grid side converter current, allowing control of the effective power factor of the machines over a wide range. However, large converter size, expensive, heavy and large generator, and complex generator are the main disadvantages of this type.

### 1.3 Motivation of the Research

Renewable energy application as an integral part of the “big” energy picture has gained a tremendous amount of interest in recent years due to their environmental friendly characteristics and finite resources of fossil fuel. Nowadays, wind farms are being planned and/or utilized around the world in large numbers, and the power ratings of wind turbines both, individually and on farms, are increasing. DFIG are invariably the choice when it comes to multi-megawatt variable-speed variable-pitch wind turbine.

DFIG- based wind turbine provides power conversion at lower cost and reduced mechanical stress due to its unique feature which is partial size rate rotor power converter needed to achieve the full control of the machine at variable wind speed.

Typically, DFIG - based wind turbines are installed far away (hundreds of miles are very common) from the load centers where the electric power grid is weak and characterized by low short-circuit ratios and voltage regulation problems. Limited reactive power capability is a major drawback of DFIG-based wind turbine when it is connected to a weak power grid.

Hence, in order to integrate DFIG into the modern power system, it is important to assess wind turbines dynamic behavior, steady state performance, and impacts on the interconnected power network with regard to its active and reactive power capability and voltage control. It is expensive and technically demanding to control the bus voltage at weak remote power grid using conventional power stations located elsewhere in the grid. Typically, an external local reactive power source is required and more economical. With fast advancement in power electronics technology, FACTS devices with excellent dynamic responses are technically and economically feasible in power system application. Therefore, reactive power compensation using both Static synchronous compensator (STATCOM) and static Var compensator (SVC) at the point of common coupling (PCC) can be a feasible technique in order to enhance the reactive power capability and voltage controllability of the DFIG-based wind farm system and improving the dynamic and steady state stability of both the wind turbine system as well as the interconnected weak power system.

Another critical factor associated with wind power applications is intermittency which is the fluctuation of the output power of wind turbine due to wind speed variation. The size of the wind farm and the stability of the grid to which is connected play a significant factor on the potential occurrence of frequency deviation which may be caused by the active power variation. Such frequency deviation might mistakenly trigger the protective relays that have a tripping threshold of 1% [40]. Maintaining the DFIG- based wind farm in service during the grid fault is also becoming very critical due to wind turbine's increasing market penetration. Therefore, integration of energy storage systems (ESS) into DFIG-based wind turbine is an attractive approach for reducing the fluctuation of the output power of DFIG-based wind turbine due to wind speed variation.

This dissertation is motivated for a better understanding of the DFIG-based turbine in terms of modeling, vector control and its interaction to the power grids with the FACTS devices as well as with the energy storage system.

## 1.4 Literature Review

There is a plethora of information available in public domain dealing with various issues in wind power systems like system applications, design, control strategy and policy related. For the past 20-25 years hundreds (or thousands) of researchers globally had contributed to this subject. There are still many open questions. With the advancement of the power electronics and digital control techniques, new ideas and control strategies are being addressed routinely. There are a group of researchers looking into the policy, carbon emission, global warming, global politics, energy independence, etc. related topics and renewable energy applications. Wind is the most used and developed non-hydro renewable energy source. Others are looking into the system integration, and system issues like voltage stability, protection and control. Yet researchers are also looking into the design and application related problem including economics. It is impossible to cite them all and/or discuss them in this section. By no means, this literature review is exhaustive. It provides a cursory look at the problem more related to this dissertation topic. Omission of any literature is inadvertent and unintentional.

The U.S Department of Energy's report [10] states a long term plan for accomplishing 20% of the US electrical energy generation from wind by 2030. Variable-speed turbines can increase the energy production by 10-15% in comparison to a fixed-speed wind turbine depending on the site conditions and design parameters [16, 18]. The use of DFIG with large wind turbines that operate at variable speed in order to enhance the efficiency of energy transfer and optimize the performance of wind turbine has been accepted as the best choice at this time [32, 37].

Literature [32, 33, 35] state that DFIG wind turbines can provide decoupled active and reactive power control of the generator which results in more efficient energy production, improved power quality and improved dynamic performance. Enhancing the performance of the vector control (decoupled control) approach has been an attractive contribution for large amount of research [33, 35].

Control of the DFIG is more complicated than the control of a standard induction machine. In order to control the DFIG, the rotor current is controlled by a power electronic converter in the rotor circuit [31, 35]. One common way of controlling the rotor current is by means of field-oriented vector control. Several vector control schemes for the DFIG have been proposed. In existing technology, the stator-flux orientation frame is commonly used in the DFIG control scheme design, and analysis in which the position of the stator-flux space is estimated through

measurement of the stator-flux space vector in  $d^s$ - $q^s$  stationary reference frame [26, 39, 40, 41]. The estimation of the position of the stator-flux oriented vector control is attractive from the parameter variation point of view, because the stator resistance is the only parameter under consideration, which can be compensated somewhat easily [42]. However, integration of low-voltage, low-frequency signals for flux estimation becomes difficult because a single-stage integrator with a large time constant tends to build up DC offset at the integrator output [43]. In addition, in the stator flux orientation frame, the flux is influenced both by load changes and stator power supply variations. The flux response to a disturbance is a damped oscillation [44, 45].

It becomes extremely important to analyze, compare and improve the performance and control mechanism of the DFIG using different oriented frames. Consequently, vector control based on rotor flux oriented orientation frame is an alternative method to overcome the disadvantages associated with the stator flux calculation mentioned above.

Recently, the utility companies have been asked to fulfill certain criteria (grid codes) for the interconnection of wind turbines to the power grid. The grid codes mainly demand that wind turbines to have low voltage ride-through capability and reactive power capability [49]. The first specification seeks to improve transient stability in a power system with a high penetration of wind energy, while the second specification aims to support steady state voltage regulation in such a power system [49]. Another key requirement for wind power interconnection is that the power factor at the PCC must remain between 0.95 leading and 0.95 lagging [53]. The reason for this ruling is that reactive power capability for a wind plant is a significant additional cost compared to conventional units, which possess inherent reactive power capability [53].

The work presented in [49, 50, 51] was based on the fact that the DFIG has a limited reactive power capability. This limitation in the reactive power capability of the DFIG and the need for an external dynamic reactive power compensation can be observed when it is connected to a remotely weak power grid and during fault period [46, 47, 48]. The goal is to maintain the DFIG based wind farm in service during the fault by providing a controlled dynamic reactive power compensation assuming that during the fault periods the utilities would immediately disconnect the wind farm when an external reactive compensation source does not exist. With reactive power compensation, the possibility of tripping many of wind turbines in a large wind

farm during grid faults would be lower and prevent influencing the overall power system voltage stability [46, 52].

Many researches and studies have been done in order to maintain DFIG-based wind farm in service during a grid fault. Dynamic reactive power compensation using FACTS devices has been widely investigated as a significant solution to achieve uninterrupted operation of a wind farm equipped with DFIG during grid faults [46, 48, 57]. Static synchronous compensator (STATCOM) and Static Var Compensator (SVC) are the two options available to provide controlled dynamic reactive power compensation. However, the focus of [46, 47, 48] was to investigate the DFIG behavior with the STATCOM for voltage support during grid faults. A comparative study of the application of both STATCOM and SVC to enhance the capability of a wind farm (equipped with DFIGs) during the fault has not been reported in the literature, especially in relation to the economic aspects of each application. No literature has been found that compares the use of SVC and STATCOM to provide a voltage regulation of the DFIG wind farm terminal for different fault conditions.

Integration of a properly sized energy storage system into the DFIG-based wind turbine to mitigate the power fluctuations due to wind speed variation is one of the most commonly proposed applications. Many investigations have been done for technical and/or economical advantages of a configuration of a wind power unit with energy storage, such as batteries [65], fuel cells [88], a superconducting magnetic energy storage (SMES) [78] and a super-capacitor [67]. However, the type of energy storage devices, their cost, and their corresponding control topology makes a difference in specific applications. A composite evaluation of such applications summary is not available in literature.

In summary, based on literature, the first issue that has been addressed in this dissertation is to develop a new vector control approaches which has been the core of recent and future research studies. Secondly, a comparison study between the integration of the different types of FACTS devices (STATCOM & SVC) into DFIG-based wind farm in terms of performance and installation cost has not been well investigated. Finally, in terms of energy storage system (ESS) applications into DFIG-based wind turbine, the literature emphasized that the type of energy storage devices and the control strategy adopted has opened the opportunities for more contributions to enhance the overall system performance.

## 1.5 Objectives and Dissertation Outlines

The first objective of this dissertation is to develop a code in MATLAB/Simulink platform, a composite dynamic model and analyze the various steady state and dynamic performance of the grid connected DFIG-based wind turbine connected to the power grid. This, however, does not include the aerodynamic and the turbine model. That is left to be added in a future work. Second objective is to study in depth the various control strategy for the DFIG including vector control for the active power. A new vector control approach to control the active power output of the DFIG has been proposed in this work. The implementation of the proposed rotor flux oriented vector control is simpler in terms of the orientation angle calculation compared to the stator-flux oriented vector control method. It is easier to estimate a rotor flux vector position than a stator-flux space vector position.

The third objective in this dissertation is to produce a comparative study that provides a clear understanding of the advantages of FACTS devices into DFIG-based wind farm in order to maintain DFIG-based wind farm in service during grid fault. This work also includes the selection of the optimum FACT device that meets both cost and performance requirements for specific fault conditions.

Finally, an idea about how to smooth out the output power for a grid connected DFIG along with the frequency control is presented. The proposed strategy includes integrating a Battery Energy Storage System (BESS) into the DC link of the rotor converter. Control strategies for grid side and rotor side converters placed in the rotor circuit of the DFIG are used for the charging and discharging process of BESS, depending on the available wind energy. The BESS was designed to handle the required power fluctuation.

The simulation for all the studies is carried out in a MATLAB/Simulink environment using SimPowerSystem toolbox. This is the most common approach taken by a large number of researchers because of the flexibility of the tool boxes and availability of well-tested component models. The details of the codes and models utilized in this research are all added in detail in the Appendix for any future work and reference.

This dissertation is organized into five chapters. Chapter One provides an introduction to the Wind Energy Conversion System (WECS) and the motivation and objectives of the thesis. Chapter Two describes the modeling and control of the grid- connected DFIG system, different operation modes of the DFIG-based wind turbine system and the vector control strategies to

control the active power output of the DFIG. In Chapter Three, the integration of FACTS devices into DFIG has been investigated as a significant solution to achieve uninterrupted operation of a wind farm equipped with DFIGs during different grid fault conditions. Chapter Four, investigates the integration of the BESS into a DFIG-based wind turbine in order to reduce the fluctuation of the output power due to wind speed variation. Finally, in Chapter Five, a summary of the research contributions and extensions for future work are presented. Expanded Appendices are added for the completeness of this research and all future work.

## CHAPTER 2

### THEORY, MODELING AND CONTROL OF DOUBLY FED INDUCTION GENERATOR

#### 2.1 Introduction

Wind energy technology has grown significantly in the last few decades. Capacity (rating) of a single wind turbine has increased from a few kW ranges to machines producing 1-5 MW [50, 90]. Wind energy generation can be classified into three broad categories based on the total power output capacity. (a) Utility scale, which corresponds to large wind turbine (900kW - 3.5MW) each, is mainly used to generate bulk power for energy market. (b) Industrial scale corresponds to medium sized turbines (50kW-600kW) each, which are mainly used by industries for remote grid production to meet local power requirement, and (c) Residential scale which corresponds to small sized turbines (both 1-phase and 3-phase) (400W-50kW) each, is mainly utilized for battery charging or to supply light loads.

The increasing reliability of large scale wind turbines system (wind farm) as an integral part of the grid has led to a corresponding decrease in cost, with availability of modern machines reaching 97-99% [89]. Much of the advancement has been made in the components dealing with the grid integration, the electrical machine, the power converters and the control capability. However, there are still many challenges and unresolved issues. It is now possible to control the real and reactive power of the machine for a variable speed operation. This area of control strategy has become a very challenging research topic, and technology is being developed that offers great deal of future capability. It requires an understanding of overall power systems and system integration, machines and applications of power electronic converters and control schemes put together on a common platform.

Wind turbines based on the doubly fed induction generators (DFIG) technology (Type 3) are widely used worldwide. Compared to wind turbines using fixed speed induction generators (Type 1), DFIG-based wind turbines offer several advantages, including variable speed operation and four-quadrant active and reactive power capabilities. Such a system also results in lower converter costs and lower power losses compared to a system based on a fully fed synchronous generator (Type 4) with full-rated converter. Typically DFIG costs much less compared to other machines of similar rating due to the lower power rating of the rotor converter which is the significant cost compared to the full-rated converter.

## 2.2 Components of DFIG

DFIG, as mentioned earlier, is basically a conventional wound-rotor induction machine in which the stator is directly connected to the grid<sup>1</sup> through a transformer, and the connection of the rotor to the stator (and grid) is via a back-to-back voltage source convertor. The rotor converter system consists of a grid side converter (GSC) and rotor side converter (RSC) connected via a DC link. A simplified schematic diagram of a DFIG based wind energy generation system is shown in Figure 2.1.

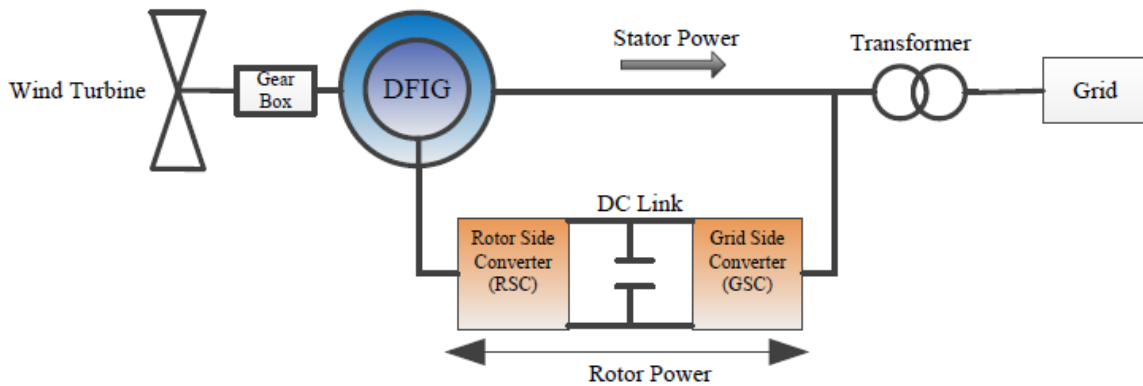


Figure 2.1 Configuration of DFIG wind Energy conversion system (one single generator) using back-to-back converter

The generator is called DFIG because the power is fed from both stator and the rotor circuits to the grid. The rotor circuit handles typically about 25-30% of the generator rated power, this percentage allows the DFIG to have about  $\pm 30\%$  operational speed range around the synchronous speed and reduces the rating and the cost of the rotor converter [28, 36]. The size of the converter is not related to the total generator power but to the selected speed range and, hence, to the “slip” power, thus the cost of the converter increases when the speed range becomes wider. The selection of the speed range, therefore, is based on the economic optimization of investment costs and on increased efficiency. Since the DFIG is connected to the grid, the high transient currents due to the grid disturbances may destroy the power electronic devices of the rotor converter. A protection system called “crowbars” are being used in which the rotor winding can be short circuited during the fault period via a small resistance and released when the fault is cleared.

<sup>1</sup> The term “Grid” is used in a broad sense. The machine is connected to the low side of the transformer. In a wind farm application, the machines are connected to the collector system and step-up to the grid voltage by a large step-up transformer in a substation.

## 2.3 Principle of Operation of DFIG

Large doubly fed electric machines in the industry are three-phase wound-rotor type. Although their principles of operation have been known for decades, the massive application has only recently entered and is almost exclusively due to the advent of wind power technologies. The DFIG operates in both sub-synchronous (rotor speed lower than synchronous speed) and super-synchronous (rotor speed higher than synchronous speed) modes which allows an operational speed range of about  $\pm 30\%$  around the synchronous speed.

The main advantage of doubly fed induction generator when used in wind turbines is that it has the ability to maintain the amplitude and the frequency of the output voltage essentially constant at grid values, no matter the speed of the wind turbine rotor. Because of this, doubly-fed induction generator can be directly connected to the AC power network and remain synchronized at all times. Other advantages include the ability to control reactive power from the rotor circuits to the grid, which enables the DFIG to support the voltage stability and power factor correction at the point of common coupling (PCC).

The feature of controlling the rotor speed to overcome the wind speed variation is done by adjusting the frequency of the AC voltages and currents fed to the rotor windings. This principle can be understood by explaining the sub-synchronous and super synchronous modes of operation discussed below.

### 2.3.1 Sub-synchronous Mode of Operation

When the rotor speed of the generator  $n_{Rotor}$  is below the synchronous speed  $n_s$  the rotor frequency  $f_{Rotor}$  of the voltage induced increases accordingly and (according to the normal convention) is of positive polarity. This positive polarity means that the phase sequence of the AC currents injected into the generator rotor windings will make the rotor magnetic field rotate in the same direction as the generator rotor, and as a result of controlling the phase sequence of injected current the rotor “receives” power from the grid through the rotor converters (GSC and RSC). This approach to control the power flow in the rotor winding of DFIG in the sub-synchronous mode can be explained by understanding the power flow equations of an induction machine, as explained below [24, 71].

$$P_g = P_m + P_r = (1 - s)P_g + sP_g \quad (2.1)$$

$P_g$  is the air gap power,  $P_m$  is the mechanical power transferred between the rotor and the shaft, and  $P_r$  is the “slip” power ( $sP_g$ ) that is transferred between the rotor converters and the electrical grid in the case of DFIG. The slip “s” is defined by:

$$s = \frac{n_s - n_{Rotor}}{n_s}$$

The conventional induction motor with short circuited rotor windings runs at a speed lower than its synchronous speed. The mechanical power  $P_m$  is considered positive when transferred from the rotor to the shaft and then driving the mechanical load (like pump or fan). In this case the slip is positive ( $0 < s < 1$ ), the air gap power that is transferred from the stator to the rotor will be positive. If the direction of flow for both  $P_g$  and  $P_m$  is reversed (i.e.  $P_g$  and  $P_m$  have negative values) the machine will operate in the generator mode (DFIG in sub-synchronous mode). The slip power  $P_r$  will also be negative and will be supplied by the converters (RSC and GSC) to the rotor in which the rotor-side converter (RSC) operates as an inverter and the grid side converter (GSC) as a rectifier. The reversion of the slip power direction in the rotor circuit is done by reversing the phase sequence of the AC voltage or current that is injected into the rotor winding of the DFIG. Figure 2.2 shows the slip power flow directions of the DFIG in both sub-synchronous (grid to rotor) and super-synchronous (rotor to grid) modes.

### 2.3.2 Super-synchronous Mode of Operation

Similarly, when the generator rotor speed  $n_{Rotor}$  increases above the synchronous speed  $n_s$ , the frequency  $f_{Rotor}$  of the ac currents that need to be fed into the generator rotor windings increases accordingly and is of negative polarity now. The negative polarity of the frequency  $f_{Rotor}$  indicates that the phase sequence of the three-phase AC currents fed into the rotor windings must make the rotor magnetic field rotate in the direction opposite to that of the generator rotor. This means that above the synchronous speed the slip (s) is negative ( $s < 0$ ), the DFIG operates in the super-synchronous mode, where the slip power  $P_r$  is controlled by controlling the phase sequence of the injected currents to the rotor windings of the DFIG. In this mode, the slip power will be positive and transferred from the generator rotor to the grid through the rotor converters of the DFIG, where the RSC operates as a rectifier and the GSC as an inverter.

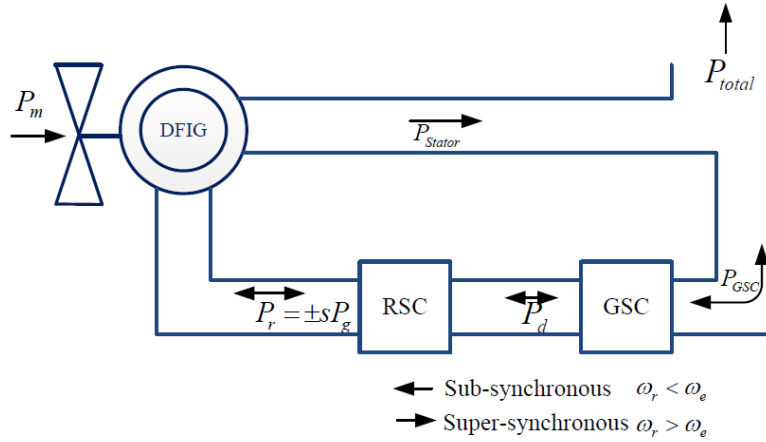


Figure 2.2 Power flow of DFIG system

## 2.4 Generalized Induction Machine Dynamic Modeling (d-q Model)

Having a mathematical model for transient analysis is the first step needed to study the application of the induction machine (motor or generator). The d-q model of induction machine is the most widely used, which provides numerous advantages in terms of induction machine control. The result from transforming the 3-phase induction machine model to 2-phase (d-q) equivalent circuit is that all time varying inductances in the voltage equations due to both self and mutual inductance varying (coupling effect) between the stator and rotor winding can be eliminated. Hence, this will minimize the computational nightmare. All the inductances in the transformed model will be time in-variant and can be solved easily using standard numerical techniques. Equation (2.2) explains this concept with the induced voltage equations in the cases of time varying inductance.

$$v(t) = \frac{d}{dt}(L(t)i_L(t)) = L(t)\frac{d}{dt}i_L(t) + i_L(t)\frac{d}{dt}L(t) \quad (2.2)$$

For time in-variant (or constant) inductance, solving the induced voltage equation is much less complex as shown in equation (2.3).

$$v(t) = \frac{d}{dt}(Li_L(t)) = L\frac{d}{dt}i_L(t) \quad (2.3)$$

The principle of a d-q transformation and the equations used in this transformation are discussed in details in Appendix C.

### 2.4.1 d-q Equivalent Circuit of Induction Machine

In the d-q transformation which is widely used, the induction machine can be represented as “decoupled” d-q equivalent circuit in the rotating reference frame  $d^e - q^e$ . Figure 2.3<sup>2</sup> shows the  $d^e - q^e$  dynamic equivalent circuit of the induction machine, in which there is no time-varying inductances and thus simplifies the mathematical solution [25].

All the induction machine equations for the dynamic d-q model are well known and can be found in [25, 26] and have been used in developing the d-q model of the doubly fed induction generator (DFIG), as shown the next section.

## 2.5 Doubly Fed Induction Generator Model (d-q Model)

The d-q dynamic model of DFIG would be very beneficial in terms of studying the behavior under sub-synchronous and super-synchronous modes of operation and applying the vector control approach to control the output active and reactive power. This model is used to implement vector control approach in order to control the output active power of the DFIG.

### 2.5.1 Dynamic Modeling of DFIG

Based on the  $d^e - q^e$  equivalent circuit model of the induction machine shown in Figure 2.3, the main equations of MATLAB/Simulink modeling of doubly fed induction generator in flux linkage form derived in [25] are shown below.

$$\frac{dF_{qs}}{dt} = \omega_b [v_{qs} - \frac{\omega_e}{\omega_b} F_{ds} + \frac{R_s}{X_{ls}} (F_{mq} + F_{qs})] \quad (2.4)$$

$$\frac{dF_{ds}}{dt} = \omega_b [v_{ds} + \frac{\omega_e}{\omega_b} F_{qs} + \frac{R_s}{x_{ls}} (F_{md} + F_{ds})] \quad (2.5)$$

$$\frac{dF_{qr}}{dt} = \omega_b [v_{qr} - \frac{(\omega_e - \omega_r)}{\omega_b} F_{dr} + \frac{R_r}{x_{lr}} (F_{mq} - F_{qr})] \quad (2.6)$$

$$\frac{dF_{dr}}{dt} = \omega_b [v_{dr} + \frac{(\omega_e - \omega_r)}{\omega_b} F_{qr} + \frac{R_r}{x_{lr}} (F_{md} - F_{dr})] \quad (2.7)$$

---

<sup>2</sup> The notations and the variables are all standard for induction machine dynamic models and are self-explanatory. It is recommended that Reference [25, 26] be consulted for additional information.

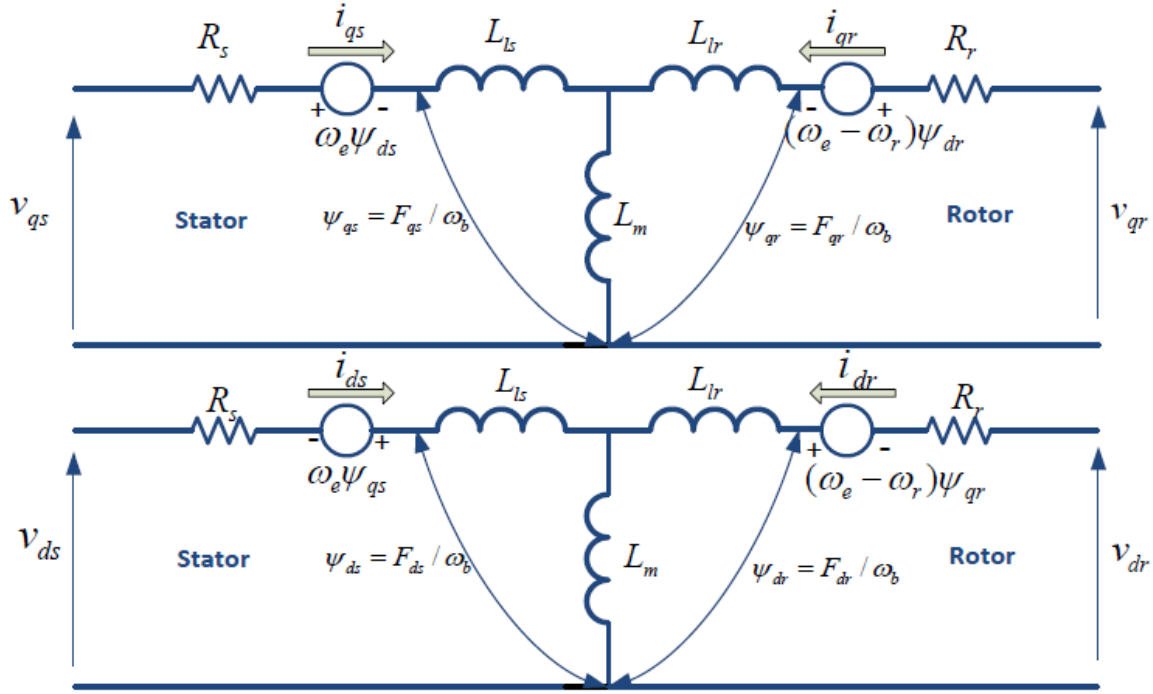


Figure 2.3 Dynamic  $d^e - q^e$  equivalent circuit of induction machine

$$F_{mq} = x_{ml}^* \left( \frac{F_{qs}}{x_{ls}} + \frac{F_{qr}}{x_{lr}} \right) \quad (2.8)$$

$$F_{md} = x_{ml}^* \left( \frac{F_{ds}}{x_{ls}} + \frac{F_{dr}}{x_{lr}} \right) \quad (2.9)$$

$F_{ij}$  is the flux linkage ( $i = d$  or  $q$ , and  $j = s$  or  $r$ );  $v_{qs}, v_{ds}, v_{qr}$ , and  $v_{dr}$  are the stator and rotor voltages on d-q axis;  $\omega_e$  and  $\omega_r$  are the stator angular electrical frequency and the rotor angular electrical frequency respectively;  $\omega_b$  is angular electrical base frequency;  $F_{ij} = \psi_{ij}^* \omega_b$ ,  $\psi_{ij}$  is the flux;  $R_s$  and  $R_r$  are the stator and rotor resistances;  $x_{ls}$  and  $x_{lr}$  are the stator and rotor leakage reactances;  $x_m$  is the magnetizing reactance,  $F_{mq}, F_{md}$  are q and d axis magnetizing flux linkage; and  $x_{ml}^* = \left( \frac{1}{x_m} + \frac{1}{x_{ls}} + \frac{1}{x_{lr}} \right)$ .

The stator and rotor currents can be calculated as following.

$$i_{qs} = \frac{1}{x_{ls}} (F_{qs} - F_{mq}) \quad (2.10)$$

$$i_{ds} = \frac{1}{x_{ls}} (F_{ds} - F_{md}) \quad (2.11)$$

$$i_{qr} = \frac{1}{x_{lr}} (F_{qr} - F_{mq}) \quad (2.12)$$

$$i_{dr} = \frac{1}{x_{lr}} (F_{dr} - F_{md}) \quad (2.13)$$

The electromagnetic torque, the stator active and reactive output power are calculated using the formulas below.

$$T_e = \frac{3}{2} \left( \frac{p}{2} \right) \frac{1}{\omega_b} (F_{ds} i_{qs} - F_{qs} i_{ds}) \quad (2.14)$$

$$T_e - T_L = J \frac{2}{P} \frac{d\omega_r}{dt} \quad (2.15)$$

$$P_s = \frac{3}{2} (v_{ds} i_{ds} + v_{qs} i_{qs}) \quad (2.16)$$

$$Q_s = \frac{3}{2} (v_{qs} i_{ds} - v_{ds} i_{qs}) \quad (2.17)$$

Where,  $i_{qs}, i_{ds}, i_{qr}$  and  $i_{dr}$  are the stator and rotor currents on d-q axis;  $T_e$  is the electromagnetic torque;  $p$  is the number of pole;  $J$  is the moment of inertia;  $T_L$  is the load torque (mechanical torque); and  $P_s$  and  $Q_s$  are the stator active and reactive power.

The set of equations from (2.4) to (2.17) have been implemented in MATLAB/Simulink to model the doubly fed induction generator and utilized for the entire study in this Chapter. The mechanical torque, stator and rotor input voltages and the synchronous speed are the inputs of this DFIG model and the electrical magnetic torque, stator and rotor currents, rotor speed, and the stator output active and reactive power are the outputs. The model can be run either in sub-synchronous mode or super-synchronous mode. Using a positive load torque will operate the model in the sub-synchronous mode  $\omega_e > \omega_r$ , while applying a negative load torque will operate the model in the super-synchronous mode  $\omega_r > \omega_e$ .

The model also included a back-to back AC-DC-AC PWM converter. It included both rotor side converter (RSC) and the grid side converter (GSC). The complete MATLAB/Simulink model is shown in appendix B. The software code is also included for future reference.

## 2.6 Fundamentals of Vector Control of Induction Machines

A vector-controlled induction machine operates very similarly like a separately excited DC machine in which the flux and torque can be controlled independently by the field current ( $I_f$ ) and the armature current ( $I_a$ ) respectively. Figure 2.10 shows the comparison between the principals of a separately excited DC machine and vector controlled induction machine.

In the case of a DC machine the electro-magnetic (developed) torque is given as a function of both armature and field currents as:

$$T_e = K I_a I_f \quad (2.18)$$

Where,  $I_a$  and  $I_f$  are the armature and the field currents, respectively. The armature current produces the armature flux  $\psi_a$  (in phase) which is perpendicular to the field flux  $\psi_f$  produced by the field current  $I_f$ . This means that both armature flux and the field flux are naturally decoupled as shown in Figure 2.4. Because of this decoupling, when the armature torque is controlled by controlling  $I_a$ , the flux  $\psi_f$  is not affected, and the opposite is true which means that when the field flux  $\psi_f$  is controlled by controlling the field current  $I_f$ , the armature torque is not affected. This decoupled performance can be extended to a vector-controlled induction as shown in Figure 2.4. In this case, the stator current component on the d- axis  $i_{ds}$  corresponds to the field current in the case of a DC machine, and the stator component on the q-axis  $i_{qs}$  corresponds to the armature current. This means that in a vector controlled machine, both  $i_{ds}$  and  $i_{qs}$  are mutually orthogonal (hence, decoupled) where the torque component  $i_{qs}$  is aligned with q-axis, and the flux component  $i_{ds}$  is aligned with the d-axis. The electromagnetic torque of a vector-controlled induction machine can be expressed as a function of both  $i_{ds}$  and  $i_{qs}$  as following.

$$T_e = K i_{ds} i_{qs} \quad (2.19)$$

$i_{qs}$  and  $i_{ds}$  are the torque and flux components. Therefore, the electromagnetic torque and the flux can be controlled independently by controlling  $i_{qs}$  and  $i_{ds}$  respectively.

Vector control is one of the most common methods applied to DFIG to control the flow of active and reactive power between the stator and the grid. It can be applied on both rotor side converter (RSC) and grid side converter (GSC). The objective of the RSC is to govern both the stator-side active and reactive powers independently, while the objective of the GSC is to keep the dc-link voltage constant regardless of the magnitude and direction of the rotor power [31]. The GSC control scheme can also be designed to regulate the reactive power. The design of the RSC Controller to control the stator active power of the DFIG is the main focus of this study.

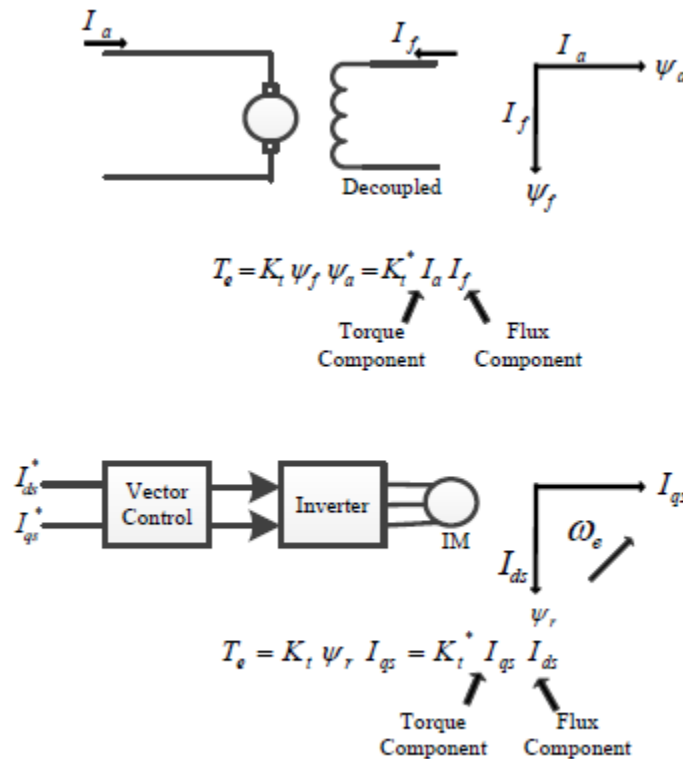


Figure 2.4 Separately Excited DC machine and vector controlled induction machine

## 2.7 Design of GSC Controller of DFIG

The main objective of the GSC controller is to keep the DC-link voltage constant regardless of the magnitude and direction of the rotor power. It can also be designed to regulate the reactive power output of the DFIG. More details about designing the GSC controller can be

found in [33] and [34] and is beyond the scope of this study. Controlling the stator active power of the DFIG is the main objective of the RSC controller and discussed next.

## 2.8 Design of RSC Controller of DFIG

The main objective of the RSC controller is to control the stator active and reactive power of the DFIG independently by controlling the rotor current component ( $i_{qr}$  and  $i_{dr}$ ). The RSC control scheme consists of two cascaded control loops. The inner current control loops regulate independently the  $d$ -axis and  $q$ -axis rotor current components,  $i_{dr}$  and  $i_{qr}$ , according to some synchronously rotating reference frame [31]. The stator flux oriented reference frame is most popular. In this study, a new rotor flux-oriented vector control approach is proposed and compared with the commonly used stator flux-oriented vector control. the following section expands both methods in detail.

### 2.8.1 RSC Controller Based on Stator Flux Oriented Vector Control

In the stator-flux oriented reference frame, the  $d$ -axis is aligned with the stator flux linkage vector  $\psi_s$ , namely,  $\psi_{ds} = \psi_s$  and  $\psi_{qs} = 0$  as shown in Figure 2.5.

The stator flux is estimated using the stator machine equation in stationary reference frame ( $d^s - q^s$ ), as shown below.

$$\psi_{ds}^s = \int v_{ds}^s - R_s i_{ds}^s \quad (2.20)$$

$$\psi_{qs}^s = \int v_{qs}^s - R_s i_{qs}^s \quad (2.21)$$

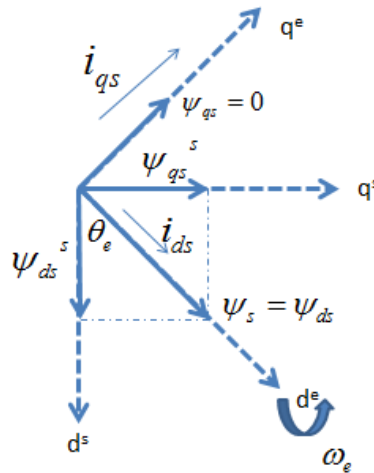


Figure 2.5 Phasor diagram of stator flux- oriented vector control

From the  $d^s - q^s$  components of the stator flux, the stator flux angle  $\theta_e$  used in this orientation is obtained as below.

$$\theta_e = \tan^{-1} \left( \frac{\psi_{qs}^s}{\psi_{ds}^s} \right) \quad (2.22)$$

The dynamic machine equations (2.4) – (2.7) can then be rewritten in terms of flux and rearranging, we obtain.

$$v_{ds} = R_s i_{ds} - \omega_e \psi_{qs} + \frac{d\psi_{ds}}{dt} \quad (2.23)$$

$$v_{qs} = R_s i_{qs} + \omega_e \psi_{ds} + \frac{d\psi_{qs}}{dt} \quad (2.24)$$

$$v_{dr} = R_r i_{dr} - (\omega_e - \omega_r) \psi_{qr} + \frac{d\psi_{dr}}{dt} \quad (2.25)$$

$$v_{qr} = R_r i_{qr} + (\omega_e - \omega_r) \psi_{dr} + \frac{d\psi_{qr}}{dt} \quad (2.26)$$

Where

$$F_{ij} = \psi_{ij} * \omega_b$$

$$\begin{cases} \psi_{ds} = L_s i_{ds} + L_m i_{dr} \\ \psi_{qs} = L_s i_{qs} + L_m i_{qr} \\ \psi_{dr} = L_r i_{dr} + L_m i_{ds} \\ \psi_{qr} = L_r i_{qr} + L_m i_{qs} \end{cases} \quad (2.27)$$

As stated before, the reference frame attached to the stator flux at steady conditions, gives the following conditions:

$$\psi_{ds} = \psi_s \text{ and } \psi_{qs} = 0 \quad (2.28)$$

By substituting (2.28) in (2.23) to (2.27) and rearranging we obtain a set of simplified equations:

$$\begin{cases} v_{ds} = R_s i_{ds} \\ v_{qs} = R_s i_{qs} + \omega_e \psi_{ds} \end{cases} \quad (2.29)$$

$$i_{qs} = \frac{-L_m}{L_s} i_{qr} \quad (2.30)$$

$$i_{ds} = \frac{L_m}{L_s} (i_{ms} - i_{dr}) \quad (2.31)$$

where

$$i_{ms} = \frac{v_{qs} - R_s i_{qs}}{\omega_e L_m} \quad (2.32)$$

Substituting (2.30), (2.31) and (2.32) in the stator active and reactive power equations (2.16) and (2.17), the stator active and reactive power can be obtained as a function of the rotor currents, as shown below:

$$P_s = \frac{-3}{2} \frac{L_m^2}{L_s} \omega_e i_{ms} i_{qr} \quad (2.33)$$

$$Q_s = \frac{3}{2} \frac{L_m^2}{L_s} \omega_e i_{ms} (i_{ms} - i_{dr}) \quad (2.34)$$

By substituting (2.27), (2.31) and (2.32) in (2.25) and (2.26), we obtain:

$$v_{dr} = R_r i_{dr} + \sigma L_r \frac{di_{dr}}{dt} - (\omega_e - \omega_r) \sigma L_r i_{qr} \quad (2.35)$$

$$v_{qr} = R_r i_{qr} + \sigma L_r \frac{di_{qr}}{dt} + (\omega_e - \omega_r) \left( \frac{\sigma L_r i_{dr} + L_m^2 i_{ms}}{L_s} \right) \quad (2.36)$$

Where

$$\sigma = 1 - \frac{L_m^2}{L_s L_r}$$

If  $R_s$  (the stator resistance) is ignored, which is an acceptable practice to simplify the analysis for large electrical machines, the final expression of stator real and reactive power is given as below.

$$P_s = \frac{-3}{2} \frac{L_m}{L_s} i_{qr} \quad (2.37)$$

$$Q_s = \frac{3}{2} \frac{L_m}{L_s} \left( \frac{v_{qs}}{\omega_e L_m} - i_{dr} \right) \quad (2.38)$$

Where,  $v_{qs}$  is constant and equal to the stator voltage. Equations (2.37) and (2.38) suggest that both  $P_s$  and  $Q_s$  can be controlled independently by regulating the rotor current components  $i_{qr}$  and  $i_{dr}$ , respectively. The reference values of  $i_{dr}$  and  $i_{qr}$  can be determined from the outer power control loops by feeding the error of the active and reactive power to PI controllers as shown in Figure 2.6.

From equations (2.35) and (2.36), the inner current control loop can be designed using PI controllers. The final form of the inner current control loop is shown below.

$$v_{dr} = (k_p + \frac{k_i}{s})(i_{dr}^* - i_{dr}) - s\omega_e \sigma L_r i_{qr} \quad (2.39)$$

$$v_{qr} = (k_p + \frac{k_i}{s})(i_{qr}^* - i_{qr}) + s\omega_e (\sigma L_r i_{dr} + \frac{L_m^2}{L_s} i_{ms}) \quad (2.40)$$

Where,  $k_i$  and  $k_p$  are the integral and proportional gains of the PI controller. Figure 2.6 shows the overall vector control scheme of the RSC [26]. The compensated outputs of the two current controllers,  $v_{dr}$  and  $v_{qr}$ , are used by the PWM module to generate the IGBT gate control signals to drive the IGBT converter.

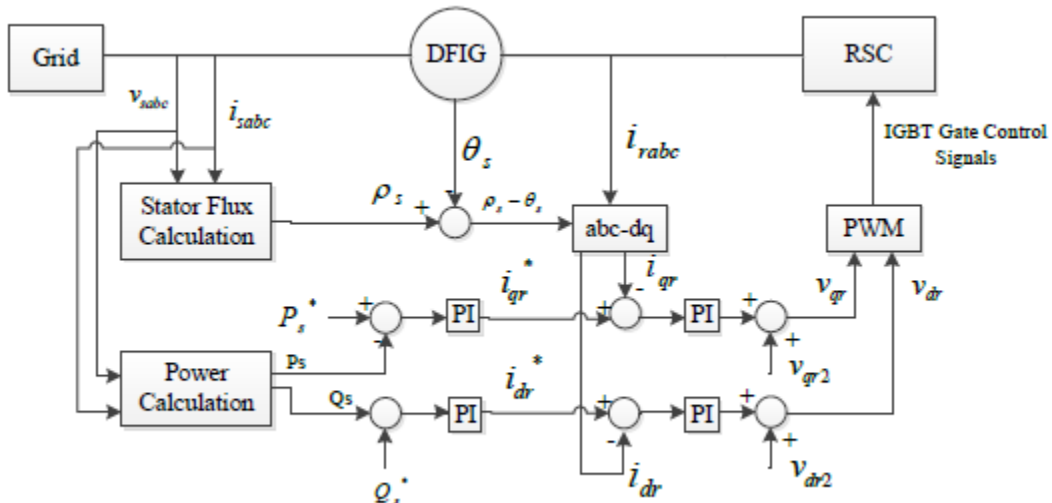


Figure 2.6 Vector control scheme of RSC



Where  $\psi_r = \psi_{dr}$ , and since the stator is connected to a stiff grid with a constant voltage, it's practical to assume the stator flux constant. The stator flux angle  $\theta_e$  (orientation angle) used in this control is obtained as following:

$$\omega_e = \omega_r + \omega_{sl} \quad (2.43)$$

$$\theta_e = \int \omega_e dt \quad (2.44)$$

In the super-synchronous mode,  $\omega_{sl}$  will be negative, to verify that the rotor angular speed is higher than the electrical synchronous speed, and to ensure the validation of equation (2.43).  $v_{qr}$  and  $i_{qr}$  in equation (2.42) must be calculated directly from the inner control loop by using the PI controllers. The Simulink implementation of the inner control loop, which derives from equation (2.42), is shown in Figure 2.8. The output of the inner control loop ( $v_{dr}$  and  $v_{qr}$ ) will be applied as a gate commands to the rotor side converter (PWM inverter) to control the rotor currents, which independently control the stator active and reactive power. The implementation of both rotor flux and stator flux oriented vector control using MATLAB/Simulink is shown in Appendix B.

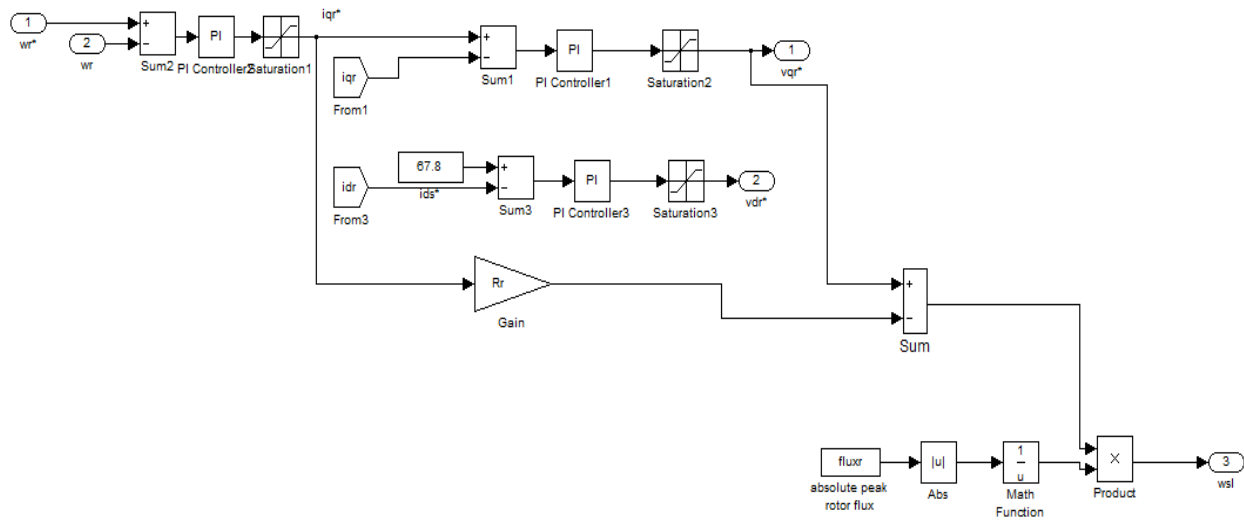


Figure 2.8 Simulink implementation of inner control loop of rotor flux oriented vector control

## 2.9 Simulation Results and Discussion

To test the DFIG model, the model has been run using MATLAB/Simulink under steady state conditions. The machine parameters used in the model testing are shown in the appendix A. Figure 2.9a –Figure 2.9f, and Figure 2.10a –Figure 2.10f show the output of the DFIG model in both super-synchronous and sub-synchronous modes. At the super-synchronous mode, the rotor speed accelerates to higher than the synchronous speed (Figure 2.9d), and in the sub-synchronous speed, the rotor speed accelerates freely to less than the synchronous speed (Figure 2.10d). In the super-synchronous mode, the machine reaches steady state conditions after approximately 0.3s, while in the sub-synchronous mode, it takes approximately 1.0s.

According to the convention of the active power, it is negative when the machine “generates” active power in the super-synchronous mode, while it is positive when the machine “absorbs” active power in the sub-synchronous mode.

In order to validate the obtained steady state results, hand calculation can be quickly performed to calculate the steady state conditions (stator current, stator power) and compare it with the model results. The machine parameters used to run the DFIG model is shown in Table A1 in appendix A. It is 30kW 3-phase induction machine, 220/230V, 50 Hz. Some assumptions have been made such as the generator efficiency (95%), power factor (0.95), and machine slip (0.02 which is the typical value [111]). All the calculation is done assuming the machine is operating in the super-synchronous mode (generating mode).

### 1- Stator current

The mechanical power 30kw, 3-phase, v 230v, pf assumed to be 0.95 (assumed the generator efficiency is 0.95), the output Electrical power is:

$$\text{Generator Efficiency} = \frac{\text{Electrical Power}}{\text{Mechanical Power}}$$

$$0.95 = \frac{P_{Elec}}{30kW} \Rightarrow P_{Elec} = 0.95 \times 30kW = 28.5kW$$

$$I_{Stator} = \frac{28500W}{\sqrt{3} * 230 * 0.95} = 75A(rms)$$

$$I_{Stator,max} = 79 * \sqrt{2} = 106 \approx 100A$$

The simulation results in super-synchronous modes show 100A as a stator current amplitude Figure 2.9a, which is very close to the calculated value (106A).

2- 30Nm is the load torque applied to run the model, assuming the slip is 0.02 which is the typical value for an induction machine. The rotor speed can be calculated as following:

$$\omega_r = (1 - (-s)) = 314 * (1 + 0.02) = 320 \text{ rad/s}$$

The mechanical power =  $30\text{Nm} \times 320 \text{ rad/s} = 9600 \text{ W}$ , The generator electrical power =  $0.95 \times 9600 = 9100 \text{ W}$

For a less efficient machine, this value can be lower. For example, for 80% efficiency; the output electrical power is 7680 W which is close to 6200W given by the model as shown in Figure 2.9e. Table 2.1 compares the estimated hand calculation values of the steady state stator power and current with the simulated values generated by the introduced DFIG model in the super-synchronous mode (generating mode). The small difference between the compared numbers has to do with assumed machine efficiency, power factor, and the normal error associated with simulation results compared with the real applications.

Table 2.1 Comparison of a simple hand calculation with simulation results for stator power and current

	Approximate Steady State hand Calculation	Steady State Results(Model Results in super-synchronous)
Stator Current (Amplitude)	106 Amp	100Amp
Stator active Power (Watt)	7680 W	6200 W

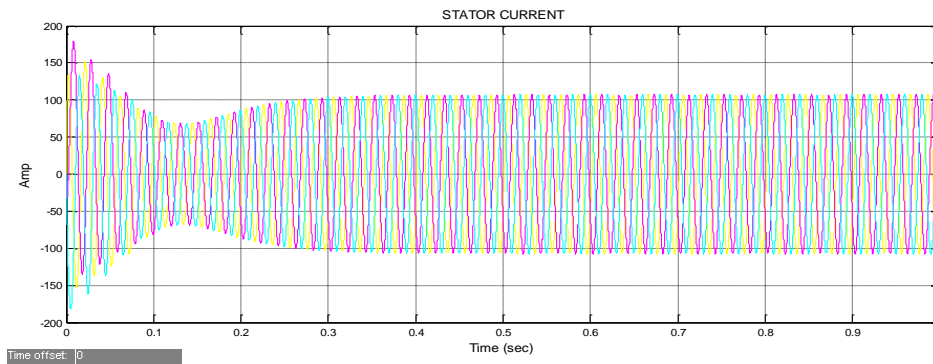


Figure 2.9a Stator currents of DFIG in super-synchronous mode

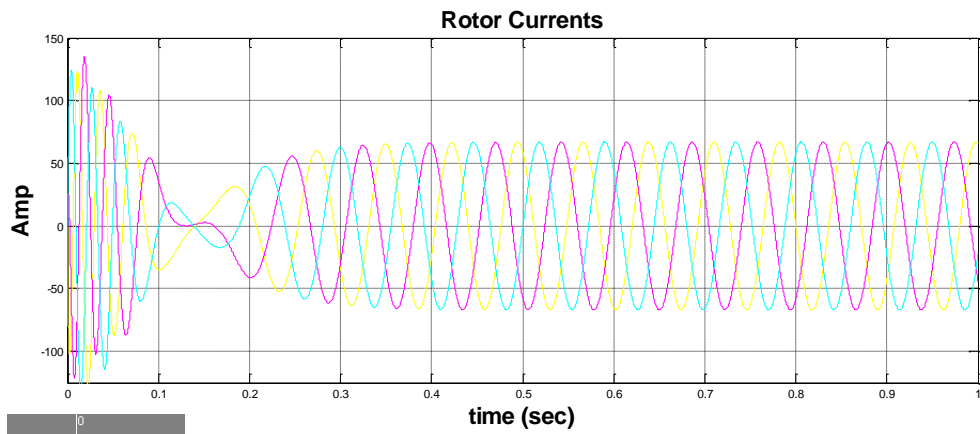


Figure 2.9b Rotor Currents of DFIG in super-synchronous mode

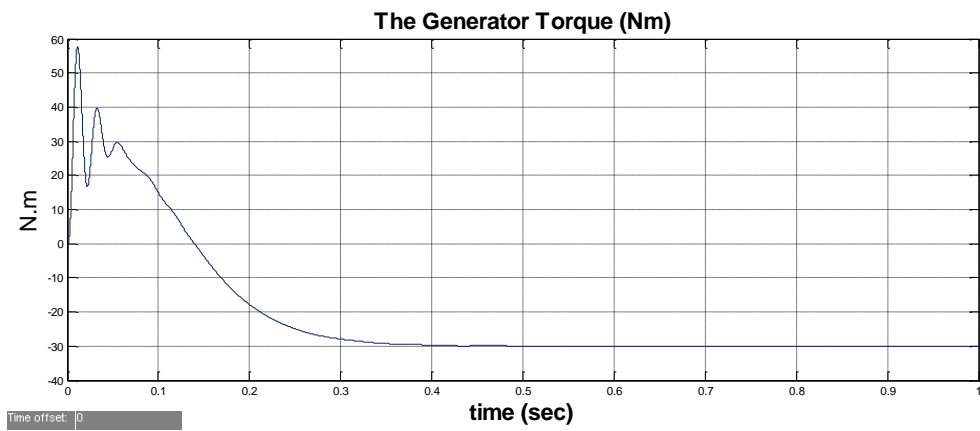


Figure 2.9c Electrical Torque of DFIG in super-synchronous mode

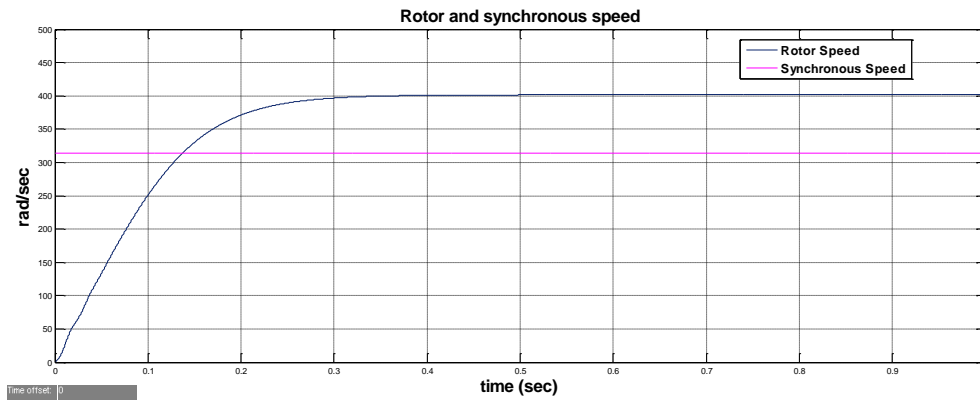


Figure 2.9d Rotor and the synchronous speed of DFIG in super-synchronous mode

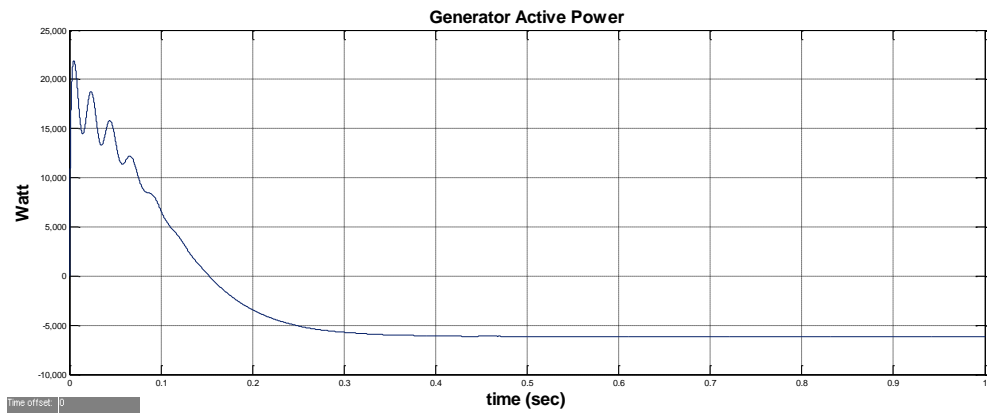


Figure 2.9e Stator active power of DFIG in super-synchronous mode

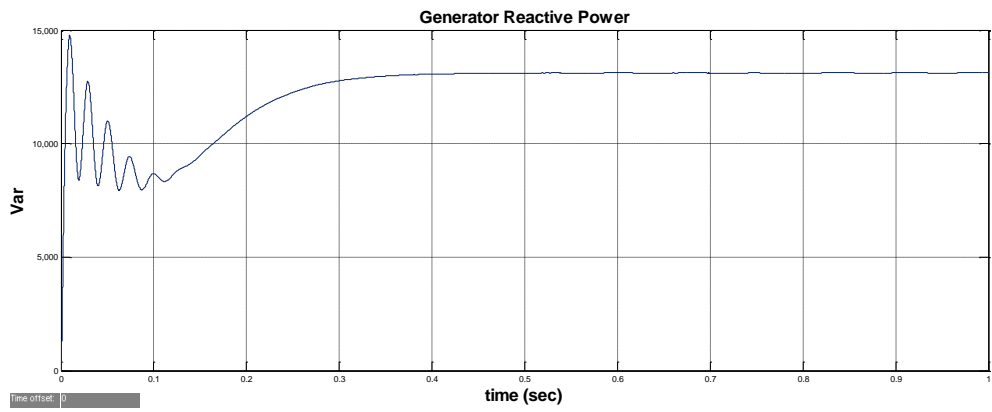


Figure 2.9f Stator reactive power of DFIG in super-synchronous mode

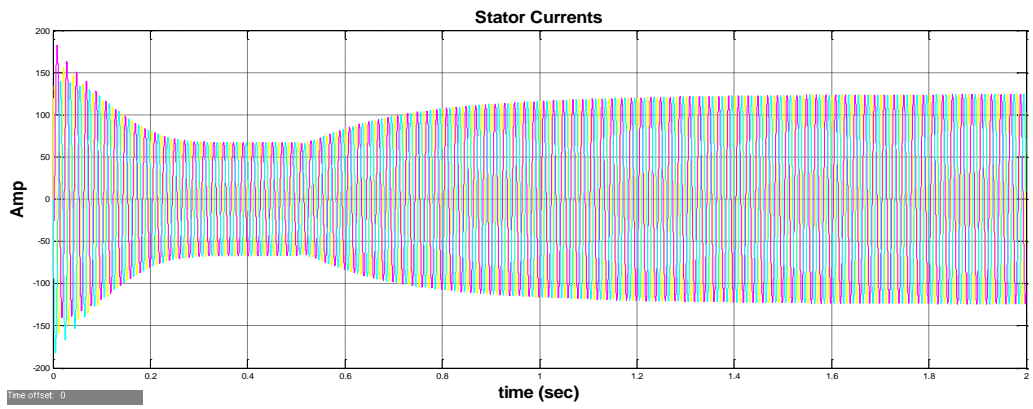


Figure 2.10a Stator currents of DFIG in sub-synchronous mode

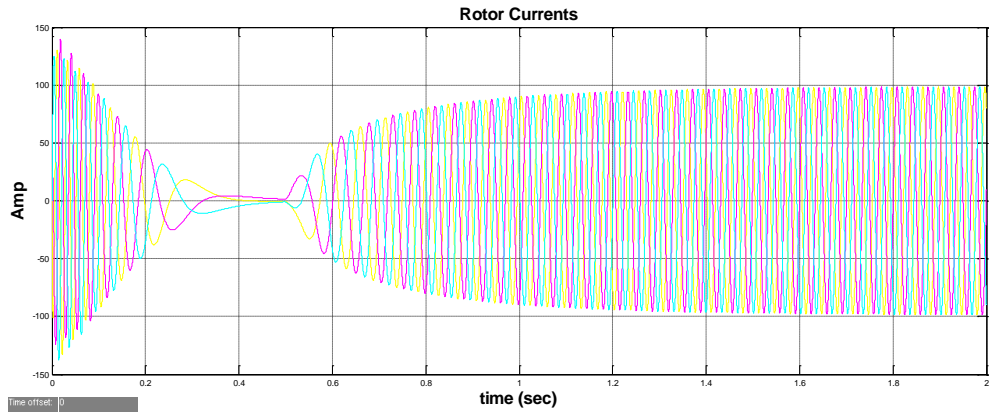


Figure 2.10b Rotor currents of DFIG in sub-synchronous mode

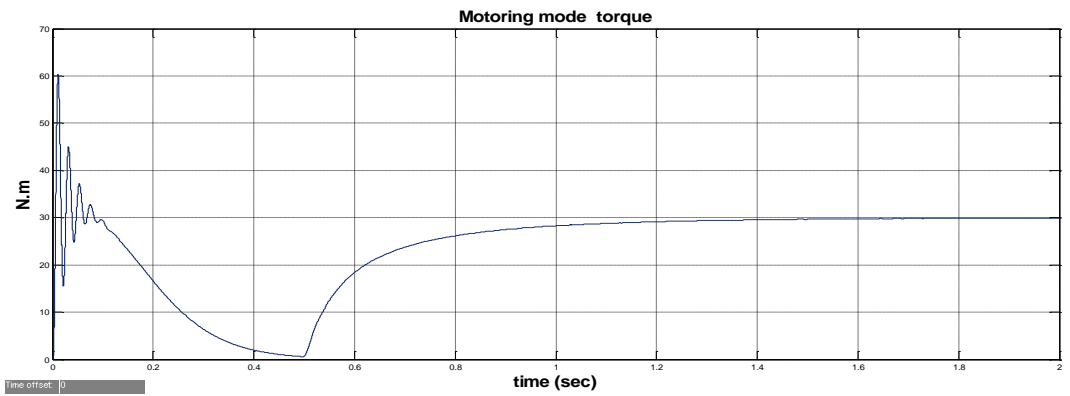


Figure 2.10c Electromagnetic torque of DFIG in sub-synchronous mode

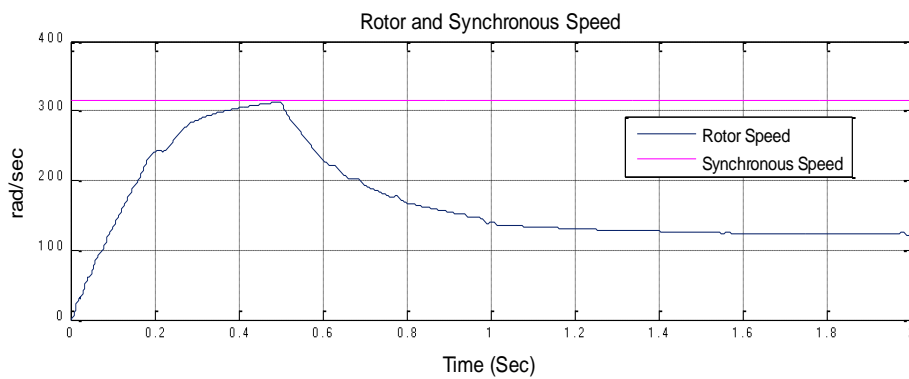


Figure 2.10d Rotor and synchronous speed of DFIG in sub-synchronous mode

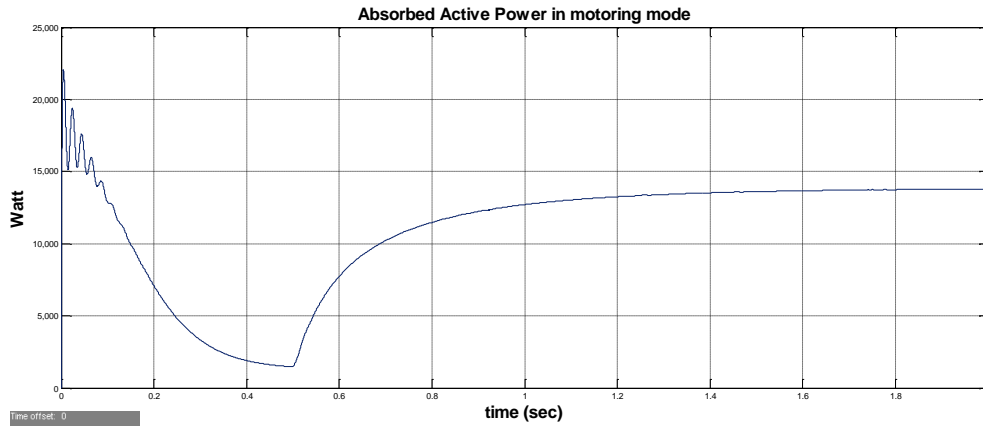


Figure 2.10e Stator active power of DFIG in sub-synchronous mode

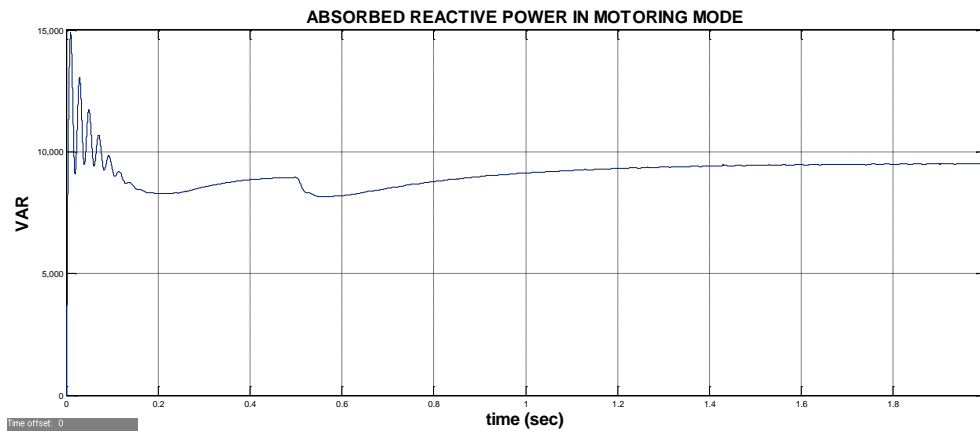


Figure 2.10f Stator reactive power of DFIG in sub-synchronous mode

The vector control algorithm based on the stator flux-oriented reference frame has also been run in MALABT/Simulink platform, and a reference stator active power (or electrical torque) was applied to the outer control loop, while a constant rotor current in d axis ( $i_{dr}$ ) was applied for the reactive power loop instead of a reference value of reactive power. The stator active power tracks the applied reference value as expected and is shown in Figure 2.11a. Due to the integration of low-voltage, low-frequency signals for the orientation angle estimation, DC offset builds up at the integrator output which affects the accuracy of the tracking process. The reactive power control is beyond the scope of this study.

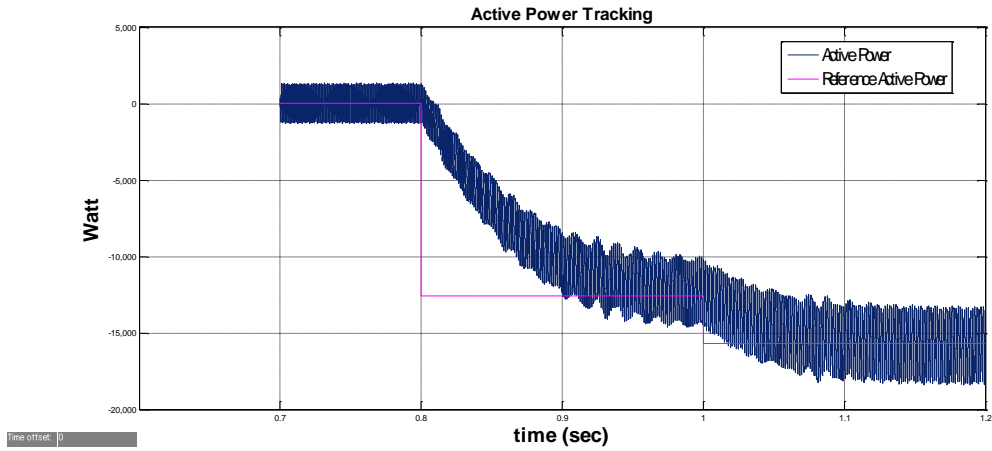


Figure 2.11a Stator active power tracking the reference power using stator flux oriented vector control

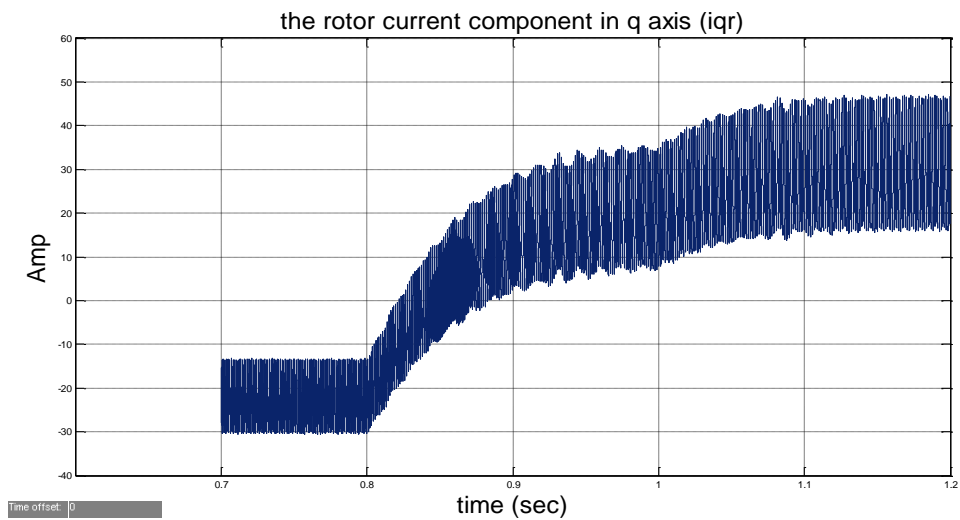


Figure 2.11b the control of  $i_{qr}$  component in the stator flux oriented vector control

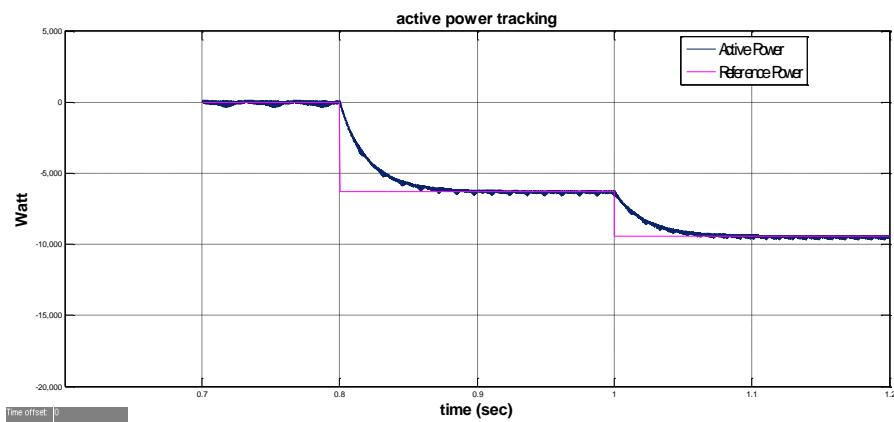


Figure 2.11c Stator active power tracking the reference power using rotor flux oriented vector control

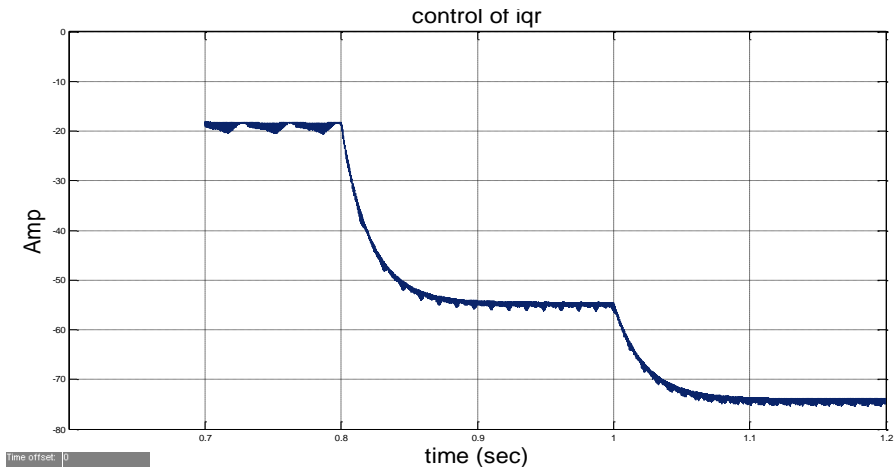


Figure 2.11d Control of  $i_{qr}$  component in the rotor flux oriented vector control

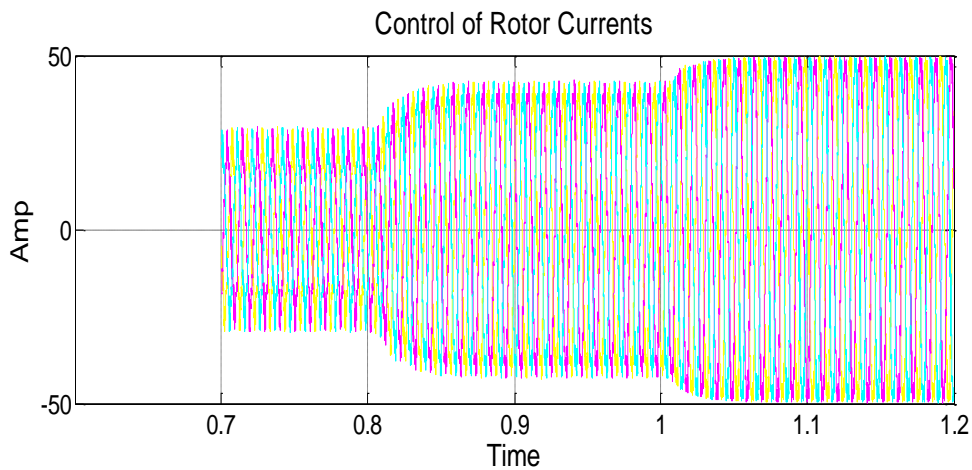


Figure 2.11e Control of the rotor current in the rotor flux oriented vector control

The simulated results have confirmed that the active power was controlled by the rotor current component on q axis  $i_{qr}$ . Figure 2.11b shows the variation in  $i_{qr}$ , which corresponds the variation in the active power. The change in  $i_{qr}$  follows exactly the change in the step reference power at 0.8s and 1.0s, which results in the same step change in the stator active power.

Similar response was obtained when the vector control was run using the rotor flux-oriented vector control. The active power tracking is shown in Figure 2.11c. Figure 2.11d shows the variation in  $i_{qr}$  that corresponds the variation in the active power when the rotor flux oriented vector control is applied. The change in  $i_{qr}$  follows exactly the change in the step reference power at 0.8s and 1.0s, which results the same step change in the stator active power. Figure

2.11e shows the control of the rotor current that follows the variation of the reference active power and  $i_{qr}$ .

## **2.10 Summary**

In this chapter, basic and fundamentals of modeling and control of DFIG is presented. A detailed DFIG model in MATLAB/Simulink is discussed at length and implemented. The simulation results confirm the validity of the model and compare very well with the steady state performance evaluation. Vector control strategy based in stator flux-oriented reference frames is implemented for a decoupled control of active power in the DFIG. The simulation shows satisfactory results. In addition, a new vector control strategy based on the rotor flux-oriented reference frame is presented and compared with the stator flux oriented vector control. The results confirm the validity of the new vector control strategy. The new proposed vector control strategy provides more accurate active power tracking compared with the stator flux-oriented vector control.

## CHAPTER 3

### INTEGRATION OF FLEXIBLE AC TRANSMISSION SYSTEM (FACTS) DEVICES INTO DFIG-BASED WIND FARM

#### 3.1 DFIG-Based Wind Farm and Grid

A wind farm is a large number (several hundreds) of wind turbines (typically combined capacity of 100's of MW) in the same location used to produce electric power and connected to a bulk power transmission system (115kV and above). Integration of large wind farms into bulk power systems presents multiple challenges mentioned earlier to system operation and security. One particular challenge to system security is vulnerability to common-mode tripping due to short circuit faults. Wind generators may have to be disconnected from the grid once the system has a disturbance, such as a short circuit fault, lightning strike on transmission lines, etc. Tripping generators normally has a negative impact on system stability, especially if the penetration of wind power to the grid reaches a very high level.

In case of DFIG-based wind farm and during a grid fault, blocking the RSC of the DFIG is widely used strategy in order to protect the RSC from overcurrent protection. The grid side converter (GSC) cannot provide sufficient reactive power and voltage support due to its small power capability, and there might be a risk of voltage instability. As a result, utilities, usually immediately disconnect the wind turbines, a common practice, from the grid to prevent such a contingency and reconnect them when normal operation has been restored [46, 52]. With the rapid increase in penetration of wind power in power systems, tripping of many wind turbines in a large wind farm during grid faults may begin to influence the overall power system voltage stability. Dynamic reactive power compensation using FACTS devices has been widely investigated as a significant solution for voltage instability problem and to achieve uninterrupted operation of a wind farm equipped with DFIGs during grid faults. Static synchronous compensator (STATCOM) and Static VAR Compensator (SVC) are the two options available to provide controlled dynamic reactive power compensation because of their quick response design. The focus of references [46], [47] and [48] was to investigate the DFIG behavior with the STATCOM for voltage support during grid faults. Use of SVC, however, has not been addressed in published literature. In addition, a comparative study of the application of both STATCOM and SVC to enhance the capability of a wind farm (equipped with DFIGs) during the fault is worth investigating, especially in relation to the economic costs of such application. This chapter

investigates and compares the implementation of two FACTS devices, STATCOM and SVC connected at the point of common coupling, to overcome the voltage stability issue and maintain stable voltage for DFIG-based wind farm. The performance of the two devices in terms of the amount of reactive power injected (kVAR), the application cost, and improving the overshooting in the DC link voltage is presented.

### **3.2 FACTS Devices Overview**

FACTS are defined as “Alternating current transmission systems incorporating power electronic-based and other static controllers to enhance controllability and increase power transfer capability” [93]. One of the major causes of voltage instability is the reactive power limit of the system. The voltage fluctuation limit of a bus in the power system depends on the reactive power support (and control) that the bus can receive from the system. When the system approaches the Maximum Loading Point (MLP) or voltage collapse point, both real and reactive power losses increase rapidly. Therefore, the reactive power supports have to be local and adequate.

In terms of wind energy applications, there are times when wind farms are subjected to short duration disturbances due to short circuits. During these disturbances the system voltage rapidly collapses. Smaller scale wind turbines are normally disconnected from the system until healthy conditions have been restored. For larger wind farms, it is often a requirement that they remain connected to the system during such disturbances and also provide support to the system to aid recovery to a pre-disturbance state.

Fixed or switched shunt capacitor bank are used as a traditional method to provide reactive power compensations for steady-state operation. They do not, however, enhance the transient behavior and cannot control the overvoltage problem.

#### **3.2.1 Shunt Capacitor**

A shunt capacitor or a group of capacitors (capacitor bank) is a reactive power source which typically placed in parallel across the PCC to provide the following benefits:

- Improved power factor.
- Improved voltage quality.
- Compensate the reactive power.
- Reduced losses and investment.

Utilities use shunt capacitors at distribution and utilization voltages to provide reactive power near the inductive loads that require it. This reduces the total current flowing on the distribution feeder, which improves the voltage profile along the feeder, frees additional feeder capacity, and reduces losses ( $I^2R$ ). While in transmission level (69kV and above) shunt capacitor serves to increase power transfer capability of the transmission system without requiring new lines or larger conductors. In addition, shunt capacitors improve the voltage at the receiving end of the transmission system which is necessary especially when the transmission system is pushed beyond its design limits as a result of decreased capital spending on network upgrades. The low cost of the shunt capacitor installation is the most significant advantage of the shunt capacitor application. The maximum capacitive power generated by a shunt capacitor is proportional to the square of the system voltage. This is the main disadvantage of shunt capacitor; the injected amount of reactive power is reduced with the fall of the system voltage, when it is most needed [62]. Shunt capacitor is uncontrolled reactive power compensator source which means it has to be switched on and out of service. This is one of the disadvantages of shunt capacitor compared with the controlled reactive power compensators (SVC & STATCOM).

### **3.2.2 Static VAR Compensator (SVC)**

The SVC is a shunt device of the FACTS family using power electronics. They regulate voltage at its terminals by controlling the amount of reactive power injected into or absorbed from the power system [94]. When system voltage is low, the SVC generates reactive power. When system voltage is high, it absorbs reactive power. The variation of reactive power is performed by switching three-phase capacitor banks and inductor banks connected on the secondary side of a coupling transformer. Both the capacitor and reactor banks are switched on and off using controlled power electronic devices such as thyristor switches [57].

There are two popular configurations of SVC. One is a fixed capacitor (FC) and thyristor controlled reactor (TCR) configuration and the other one is a thyristor switched capacitor (TSC) and TCR configuration. The typical SVC configuration and the one line diagram of the SVC equivalent circuit and its control system are shown in Figure 3.1 and Figure 3.2.

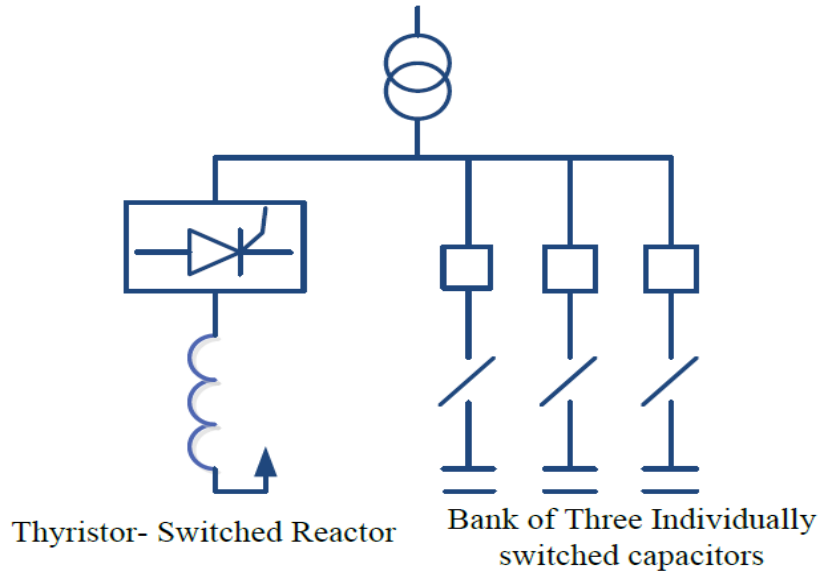


Figure 3.1 Typical SVC configuration

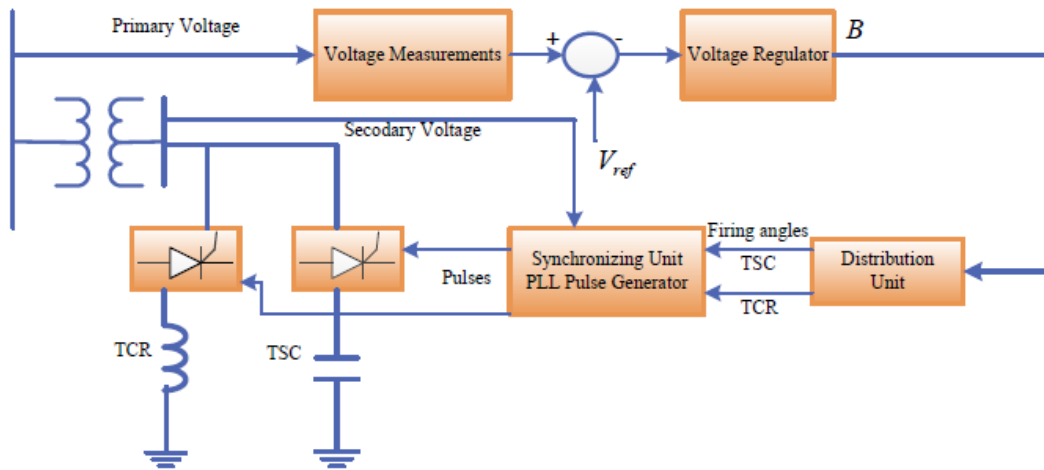


Figure 3.2 Equivalent circuit and control system of SVC [56]

The control system consists of: [56]

- A measurement system measuring the positive-sequence voltage to be controlled.
- A voltage regulator that uses the voltage error (difference between the measured voltage  $V_m$  and the reference voltage  $V_{ref}$ ) to determine the SVC reactive power needed to keep the system voltage constant.

- A distribution unit that determines the TSCs (and eventually TCRs) that must be switched in and out, and computes the firing angle ( $\alpha$ ) of TCRs.
- A synchronizing system using a phase-locked loop (PLL) synchronized on the secondary voltages and a pulse generator that send appropriate pulses to the thyristors.

### 3.2.3 Static Synchronous Compensator (STATCOM)

STATCOM is another very popularly used Flexible AC Transmission System (FACTS) device that is capable of generating and/or absorbing reactive power and is applied to voltage support at a given bus [58].

It consists of a Voltage Source converter (VSC) and a DC energy storage device connected in shunt to the distribution network through a coupling transformer [46, 47]. The VSC converts the DC voltage across the storage device into a set of three-phase AC output voltages. It can continuously generate or absorb reactive power by varying the amplitude of the converter voltage with respect to the line bus voltage so that a controlled current flows through the tie reactance between the STATCOM and the distribution network. When system voltage is low, the STATCOM generates reactive power. When system voltage is high, it absorbs reactive power [62]. The VSC uses forced-commutated power electronic devices (GTOs, IGBTs or IGCTs) to synthesize its terminal voltage from a DC voltage source. . The major features of STATCOM are quick response time, less space requirement, optimum voltage platform, higher operational flexibility and excellent dynamic characteristics under various operating conditions [102].

The real and reactive power injected by the STATCOM is given by equations (3.1) and (3.2) [102].

$$P = \frac{V_1 V_2 \sin \delta}{X} \quad (3.1)$$

$$Q = \frac{V_1(V_1 - V_2 \cos \delta)}{X} \quad (3.2)$$

$\delta$  is the angle difference between  $V_1$  and  $V_2$ . In steady state operation, the voltage  $V_2$  generated by the VSC is in phase with  $V_1$  ( $\delta = 0$ ), so that only reactive power is flowing ( $P = 0$ ). Therefore, Equations (3.2) can be rewritten as following:

$$Q = \frac{V_1(V_1 - V_2)}{X} \quad (3.3)$$

Equation (3.3) gives the amount of reactive power produced or absorbed by a STATCOM. If  $V_2$  is lower than  $V_1$ , reactive  $Q$  (lagging VAR) is flowing from  $V_1$  to  $V_2$  (STATCOM is absorbing reactive power). On the reverse, if  $V_2$  is higher than  $V_1$ ,  $Q$  is flowing from  $V_2$  to  $V_1$  (STATCOM is generating reactive power).

The overall scheme of the STATCOM circuit is shown in Fig 3.3, and the control system block diagram is shown in Fig 3.4.

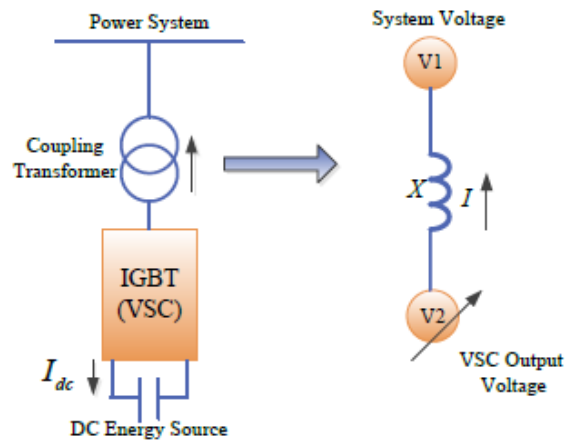


Figure 3.3 Equivalent circuit of STATCOM

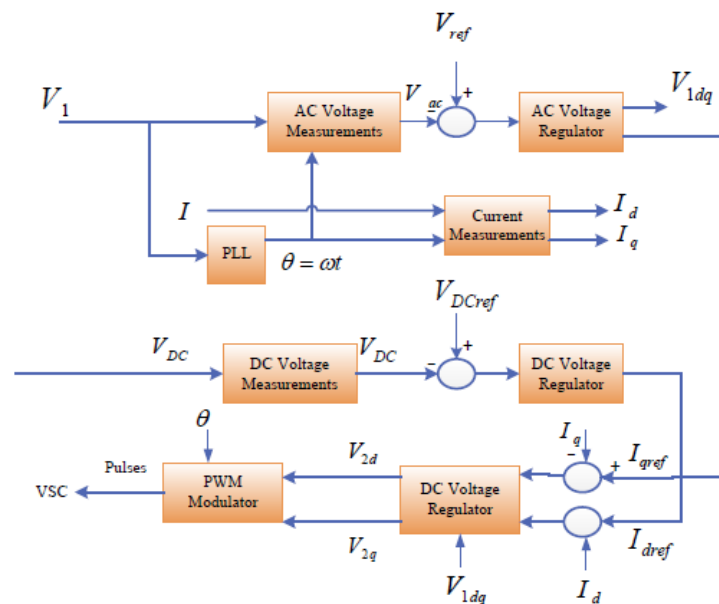


Figure 3.4 Control system block diagram of STATCOM [56]

### 3.3 Test System

Figure 3.5 shows the single line diagram of the test system used for this study [56]. This test system is available in MATLAB/Simulink Library and is widely used for grid connected applications because it strikes a balance between detail and simplicity. The grid model consists of a 120kV, 60Hz grid supply point, feeding a 25kV distribution system through 120-25kV, 47MVA step-down transformer, which is feeding a 575V system through a 25kV-575V, 12MVA step-down transformer.

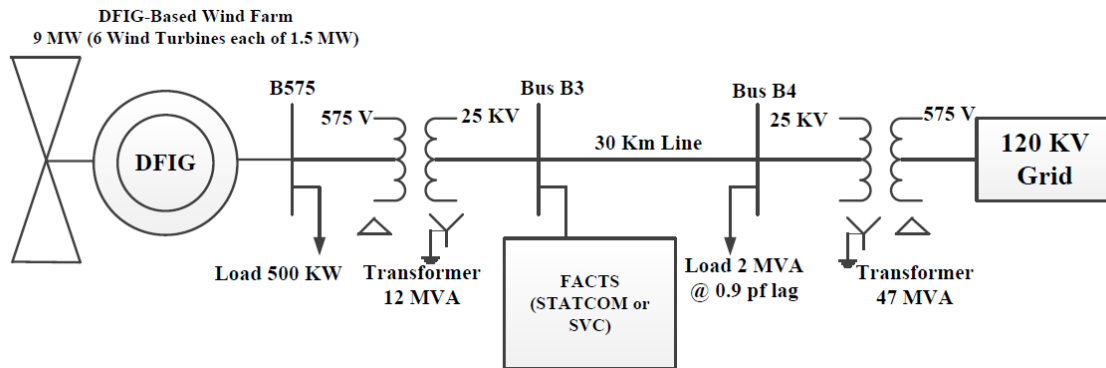


Figure 3.5 Single line diagram of the test system

There are two loads in the system; one load of 2MVA, 0.9 pf (lag) at 30 km from transmission line, and a static load of 500-kW at 575V bus. The 25kV, 30-km long line is represented as nominal- $\pi$  line. A DFIG-based wind farm consists of six DFIG-based wind turbines connected at 575V bus, each with 1.5MW (for a total of 9MW) which have a protection system monitoring voltage, current, speed and the DC link voltage. In this model, the wind speed increases slowly from 8m/sec and reaches the final constant value of 14m/sec in 16 sec. All the tests here are studied after the system reaches steady state (i.e. after 16 seconds). The GSC in DFIG maintains the DC link voltage to almost constant value at 1,200V during normal operating conditions. The STATCOM (or SVC) is shunt connected at the sending end bus B3) (25kV bus) to provide dynamic reactive power compensation. The parameters of the system components are given in Appendix A (Table A2).

In this study, the wind farm of 9 MW is represented using a SimPowerSystem toolbox [56] in MATLAB/Simulink. Six DFIG-based wind turbines are represented as one equivalent DFIG driven by a single equivalent wind turbine. Each individual DFIG wind turbine represents a

1.5MW wind turbine generator (WTG) system which results a total of 9 MW DFIG-based Wind farm. The parameters of the equivalent wind turbine and DFIG are given in Appendix A (Table A2). The simulation analysis was carried out using MATLAB/ Simulink software for various cases discussed in the next section. The cases include the effect of the short circuit fault and the corresponding voltage sag on the DFIG-based wind farm connected to a power system. Section 3.4 deals with the STATCOM applications and the results in Section 3.5 correspond to the SVC.

### **3.4 Disturbance Mitigation in the DFIG-based Wind Farm System Using the STATCOM**

The presence of DFIG-based wind farms into a weak power system raises serious concerns about system stability, and voltage regulation. Utilities require that, during normal operation, wind farms should be capable of regulating voltage or reactive power to maintain a smooth voltage profile at the point of interconnection, protecting against voltage instability caused by faults. The rotor converter of the DFIG consists of a rotor-side converter (RSC) and a grid-side converter (GSC) connected back-to-back by a dc-link capacitor. During the fault periods, the RSC is blocked in order to avoid damaging it due to the high fault currents. When the RSC is blocked the capacity of the GSC is not sufficient to supply the required reactive power at the PCC to regulate the voltage and avoid tripping the wind farm. This section presents a complete study of the integration of STATCOM into a grid connected DFIG-based wind farm to improve the voltage stability and mitigate tripping the wind farm during different fault conditions.

In this study, the wind farm is represented using a SimPowerSystem toolbox in MATLAB/Simulink. 6 wind turbines and DFIGs are represented as one equivalent DFIG driven by a single equivalent wind turbine. Each individual DFIG wind turbine represents a 1.5MW wind turbine generator (WTG) system.

The simulation analysis was carried out using MATLAB/ Simulink software, as shown in Appendix B. Different cases studied on the test system, shown in Figure.3.5. The cases include the effect of the short circuit fault and the voltage sag on the DFIG-based wind farm connected to a power system. In addition, the evaluation of using of the STATCOM to provide dynamic reactive power compensation for mitigating transient disturbances in a DFIG-based wind farm has been meaningfully addressed and analyzed.

### 3.4.1 The System Output at Steady State Conditions without any Compensation

The system was initially run at the steady state condition to confirm the steady state output conditions of the DFIG-based wind farm. A step wind speed profile has been applied with initial wind speed of 8m/s and then at  $t=5$ s wind speed increases to 14m/s. The control mode of the DFIG-based wind farm block was set to voltage regulation mode of reference voltage of 1 Pu on the base of generator rating ( $6 \times 1.5$ MVA and  $V=575$  V) at bus B575. At  $t = 5$  s, the generated active power starts increasing smoothly (together with the turbine speed) to reach its rated value of 9 MW in approximately 18 s. Over that time frame, the turbine speed will have increased from 0.8 pu to 1.21 pu of generator synchronous speed. The reactive power is controlled to maintain a 1 pu voltage at PCC (Bus B575) and the equivalent DC link voltage of the DFIG-based wind farm at 1200V. The overall performance of the system is shown in Figure 3.6a through Figure 3.6d.

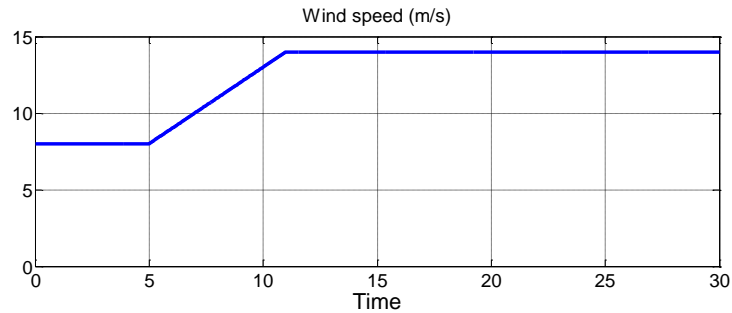


Figure 3.6a Wind speed profile

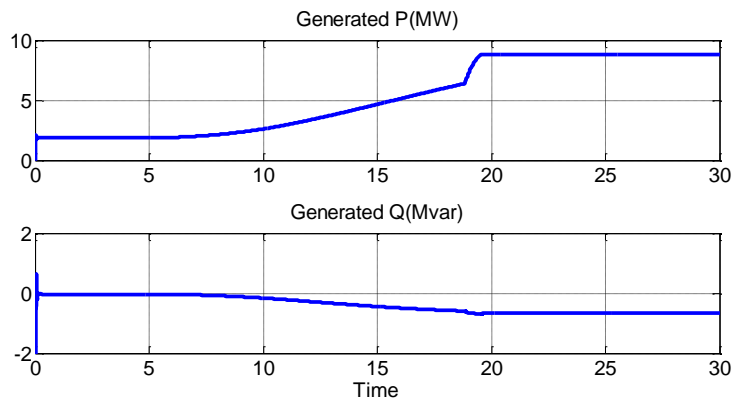


Figure 3.6b DFIG generated active and reactive power

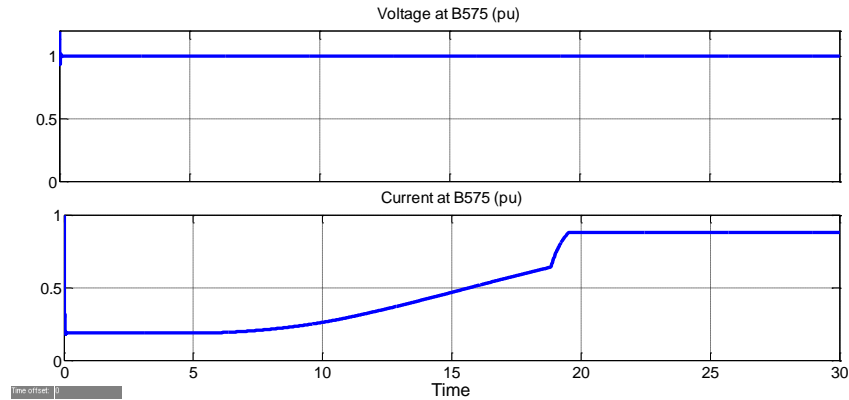


Figure 3.6c The voltage and current at point of common coupling (Bus B575)

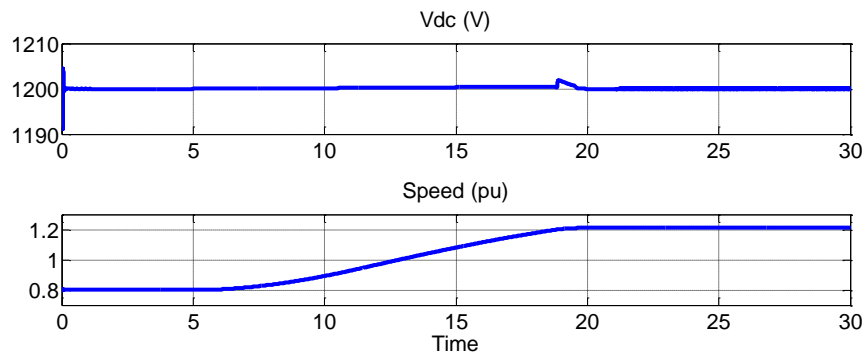


Figure 3.6d DC link capacitor voltage and turbine speed

### 3.4.2 Single Line to Ground Fault (SLGF) With STATCOM and RSC Blocking

Grid fault has a significant effect on the wind farm even when the fault is located far away from the PCC of the wind farm. Voltage sag at the PCC leads to overcurrent in the rotor circuit, DC link voltage fluctuations and a change in speed. Therefore, the RSC must be blocked to avoid being destroyed by the overcurrent in the rotor circuit. A temporary single line to ground fault is applied for 9 cycles to the bus B3 (25kV) in Figure 3.5 at  $t = 5s$ . The RSC is blocked by setting the control mode of the DFIG- based wind farm to a var regulation mode with reference reactive power command equal to zero. Consequently, the DFIG will not be able to exchange reactive power with the power system. The DFIG-based wind turbine model in SimPowerSystem library is provided by a protective system which designed to trip the wind turbine when the voltage at the PCC drops to 75%. The circuit of the protective system is shown in Appendix B. Fig 3.7a shows that the voltage at the PCC (bus B575) during the fault is dropped to 0.65 pu, which

makes the protective system trips the wind farm where the total active power generated by the wind farm is zero as, shown in Fig 3.7b.

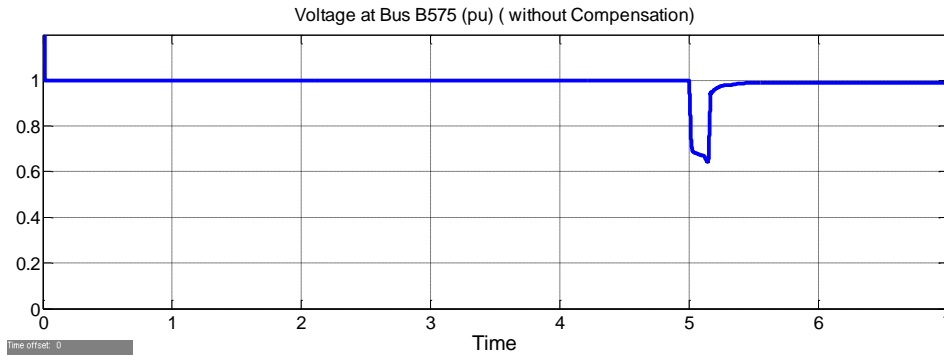


Figure 3.7a PCC (Bus B575) voltage during SLGF

Figure 3.7b also shows that, there is no reactive power is being exchanged between the DFIG-based wind farm and the grid ( $Q=0$ ), due to the blocking of the RSC.

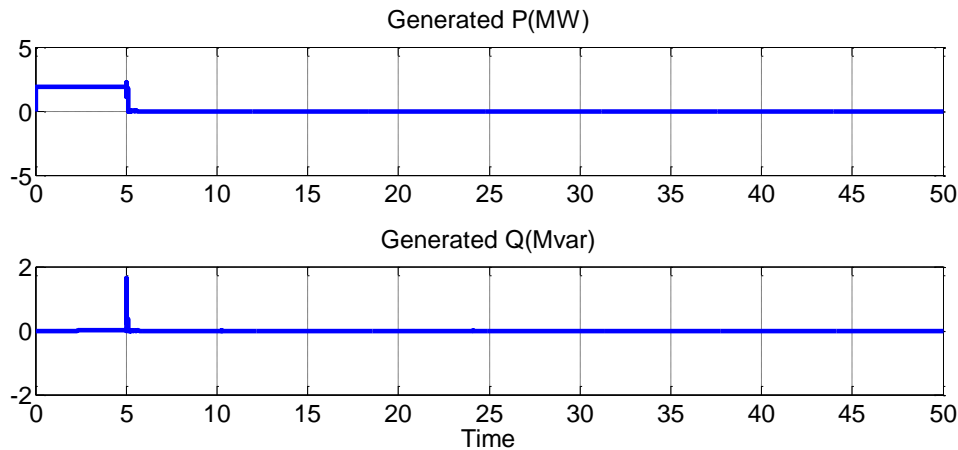


Figure 3.7b Interrupted operation of the wind turbine during a SLGF

After the installation of 10MVA STATCOM at bus B3 in Figure 3.5, it provided the required reactive power to maintain the voltage at the PCC above 0.75 pu and maintain the wind farm in service during and after the SLGF. Figure 3.7c shows how the voltage at the PCC (bus B575) is improved to 0.79 pu when a STATCOM is connected.

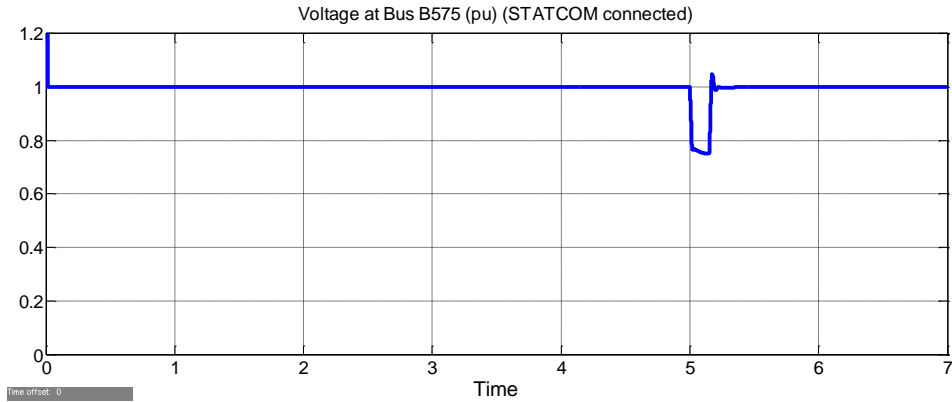


Figure 3.7c PCC (Bus B575) voltage during SLGF with a STATCOM

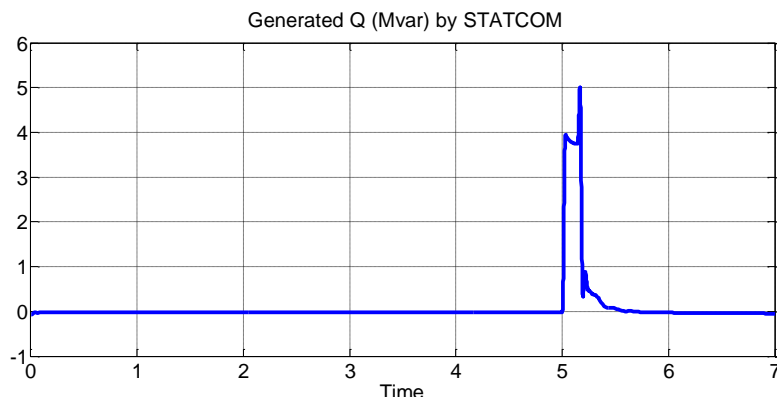


Figure 3.7d Reactive power injected by the STATCOM during SLGF

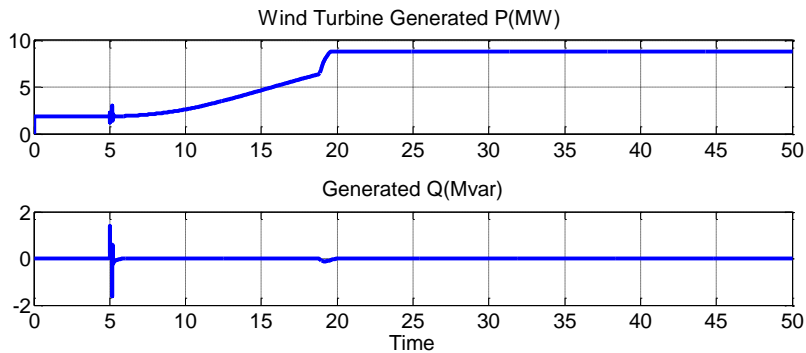


Figure 3.7e Uninterrupted operation of the wind turbine with a STATCOM during SLGF

Figure 3.7d shows the reactive power supplied by the STATCOM to maintain the wind farm in service. The RSC is blocked, and the STATCOM is providing 4MVar reactive power. This could not have been provided by the GSC, which has a rating of 3 MVA, and underlines the need for a STATCOM or some other form of reactive compensation. Figure 3.7e shows how the

wind farm remains in service during the fault and generates a full 9 MW active power when the STATCOM is connected while the RSC is blocked and the reactive power command of the GSC is set to zero.

### 3.4.3 Line to Line Fault (L-L) With STATCOM and RSC Blocking.

A temporary Line-to-Line fault is applied for 9 cycles to the bus B3 (25kV) in Fig 3.5 at  $t = 5$ s. The RSC is blocked and reactive power command of the GSC is set to zero. Figure 3.8a shows that the voltage at the PCC (bus B575) during the fault is dropped to 0.45 pu. It is clear that the line-to-line fault causes a deeper voltage sag compare with the single line-to-ground fault. The wind farm is tripped by the protective system due to this significant voltage sag that exceeded the undervoltage protection limit of 0.75 pu.

After the installation of 17MVA STATCOM at bus B3 in Figure 3.5, it provided the required reactive power to maintain the voltage at the PCC above 75 pu and maintain the wind farm in service during and after the line-to-line fault. Figure 3.8b shows how the voltage at the PCC (bus B575) is improved to 0.76 pu when a STATCOM is connected and the PCC voltage is quickly reestablished shortly after the fault has cleared.

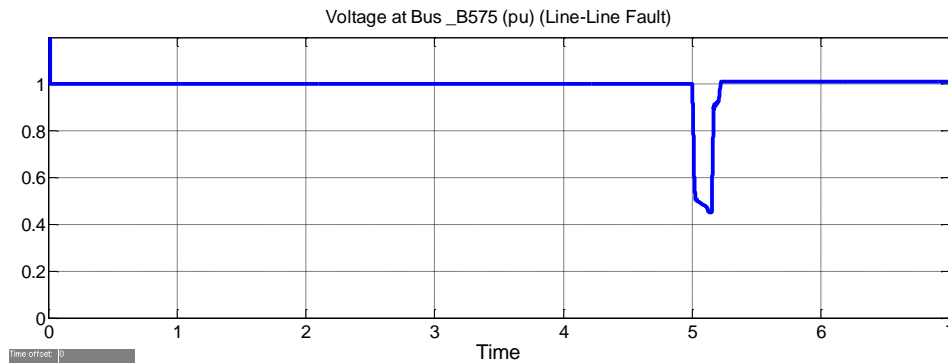


Figure 3.8a PCC (Bus B575) voltage during line to line fault

Figure 3.8c shows the reactive power supplied by the STATCOM to maintain the wind farm in service. The RSC is blocked, and the STATCOM is providing 15MVar reactive power. The amount of the reactive power injected is much higher than the injected reactive power during the single line-to-ground fault which is a realistic increase due to the difference in the voltage sag level in both cases.

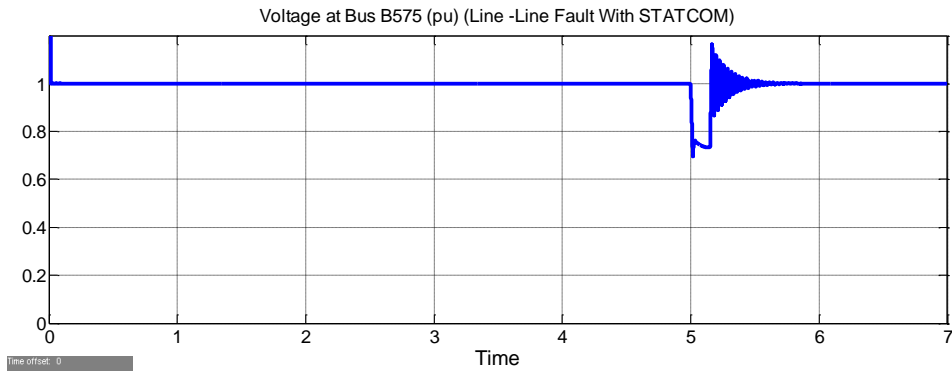


Figure 3.8b PCC (Bus B575) voltage during line to line fault with a STATCOM

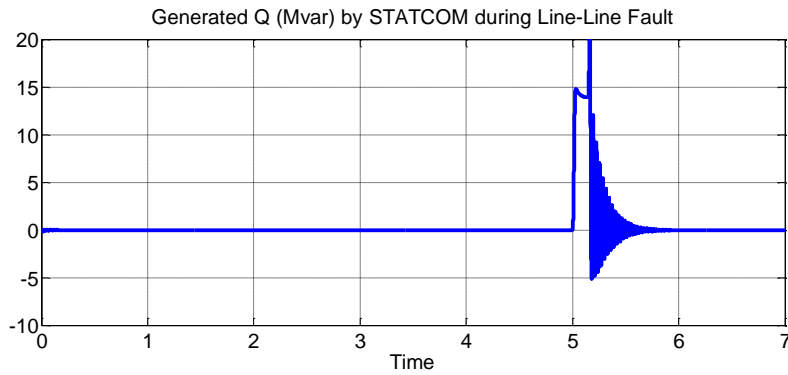


Figure 3.8c Reactive power injected by the STATCOM during line-to-line fault

Another requirement for the successful uninterrupted operation of the wind turbine is the DC-link voltage stability of variable frequency AC/DC/AC converter (VFC) in the rotor circuit. Figure 3.8d and Figure 3.8e show that the overshoot of the DC link voltage has been decreased during the fault from 1315V to 1280V when the STATCOM is installed.

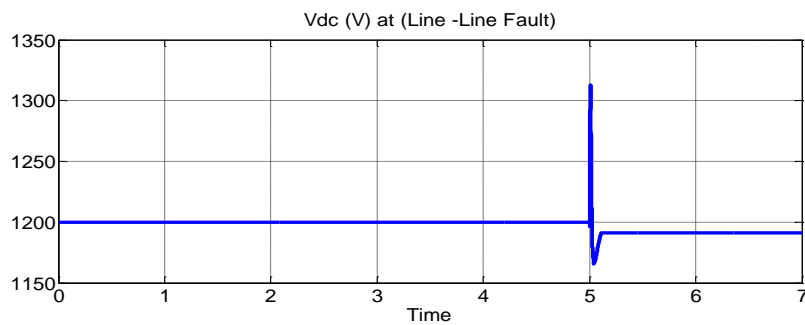


Figure 3.8d The overshoot of the DC link voltage during Line-to-Line fault without STATCOM

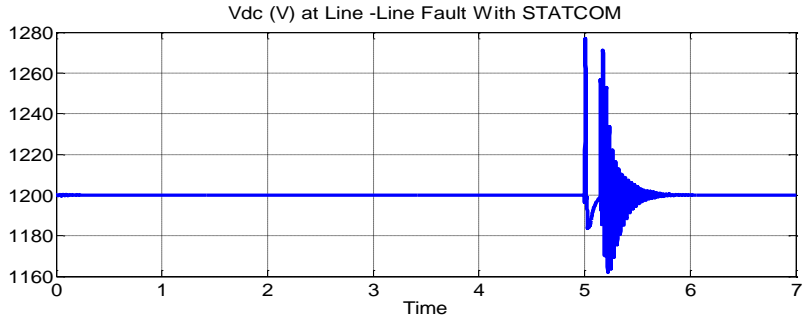


Figure 3.8e The overshoot of the DC link voltage during line-to-line fault with STATCOM

Decreasing the overshoot of the DC link voltage minimizes the danger of damaging the GSC and helps the RSC to restart when the fault has cleared. In addition, the GSC controller successfully controls the DC-link voltage back to the nominal value of 1200V when the STATCOM is installed.

**3.4.4 Voltage Sag of 30% at Bus 120kV With STATCOM Device and RSC Blocking.**

The main purpose of this section is to study how a remote fault from the point of common coupling might affect the operation of a wind farm. Therefore, a temporary voltage sag of 30% for 0.5 s at  $t = 5s$  is applied to the grid Bus (120kV) in Figure 3.5, which is far from the PCC where the DFIG-based wind farm is connected. Figure 3.9a shows that the voltage at the PCC (bus B575) during the sag is fallen to 0.7 pu. As a result, the protective system has tripped the wind farm.

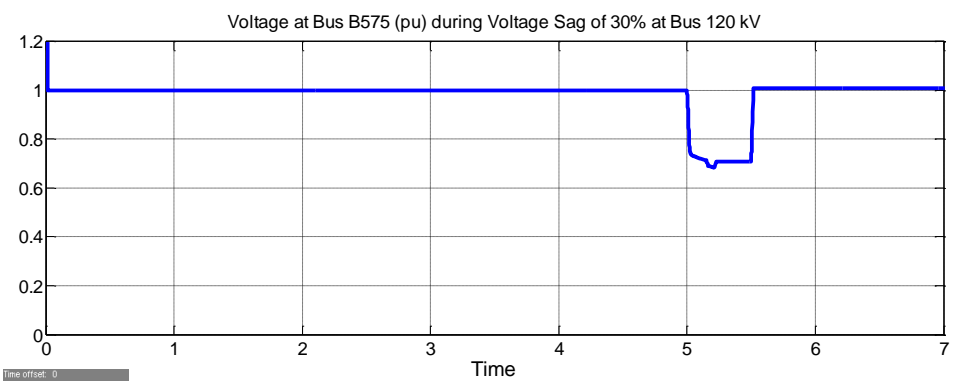


Figure 3.9a PCC (Bus B575) voltage during a voltage sag of 30% at Bus 120kV

After the installation of a 4 MVA STATCOM at bus B3 in Figure 3.5, it provided the required reactive power to maintain the voltage at the PCC above 75 pu and maintain the wind farm in service during and after the sag and achieved uninterrupted operation of the DFIG-based wind farm. Figure 3.9b shows how the voltage at the PCC (bus B575) is improved to 0.79 pu when a STATCOM is connected.

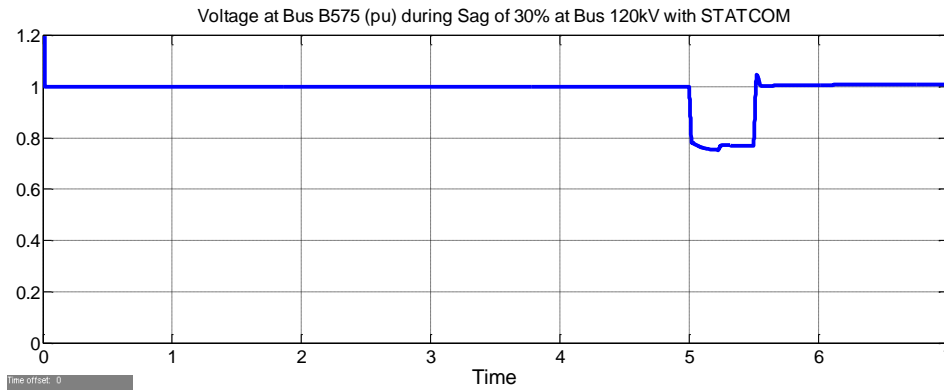


Figure 3.9b PCC (Bus B575) voltage during sag of 30% at Bus 120kV with a STATCOM

Figure 3.9c shows the reactive power amount supplied by the STATCOM to maintain the wind farm in service. The RSC is blocked, and STATCOM is providing 1.5MVar. It is obvious that the injected amount of reactive power is much less compared with the cases of SLGF and L-L fault.

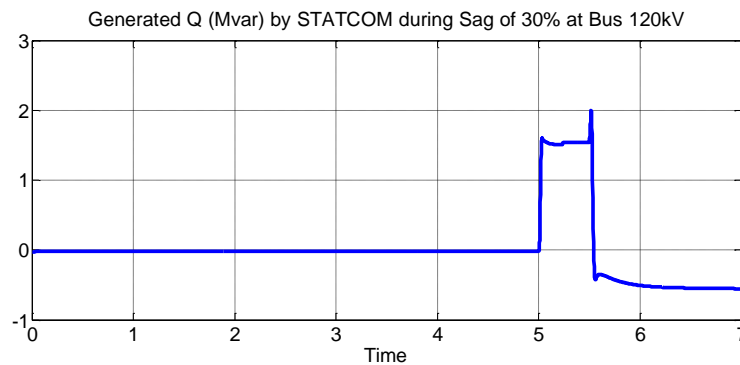


Figure 3.9c Reactive power injected by the STATCOM during sag of 30% at bus 120Kv

### 3.5 Disturbance Mitigation in the DFIG-based Wind Farm System Using the SVC

The same study has been done by integrating static var compensator (SVC) instead of STATCOM. SVC is integrated at the PCC to provide the required reactive power and support the DFIG-based wind turbine during different fault conditions. The system performance was studied

and analyzed under the same fault conditions assumed in the case of STATCOM, which include SLGF at bus B3, L-L fault at bus B3, and voltage sag of 30% at the bus 120kV.

### 3.5.1 Single Line to Ground Fault (SLGF) With SVC and RSC Blocking

Under the same SLGF conditions that applied in the case of STATCOM, the voltage at the PCC dropped to 0.65 pu as already shown in Figure 3.7a. After the installation of 15MVA SVC at bus B3 in Figure 3.5, it provided the required reactive power when the RSC was blocked and maintained the voltage at the PCC above 0.75 pu during the SLGF. Figure 3.10a shows how the voltage at the PCC (bus B575) is improved to 0.77 pu when a SVC is connected.

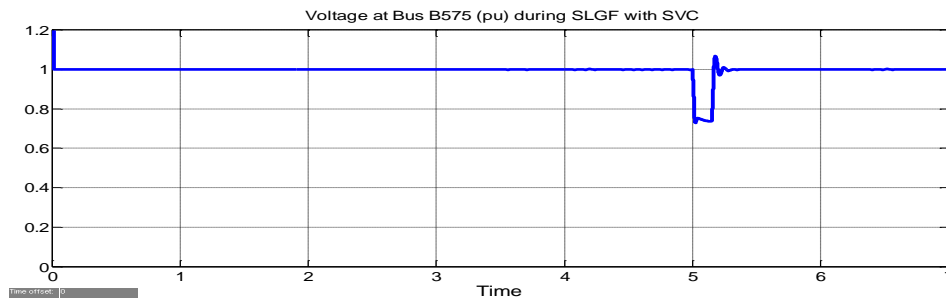


Figure 3.10a PCC (Bus B575) voltage during SLGF with a SVC

Figure 3.10b shows the reactive power supplied by the SVC to maintain the wind farm in service. The SVC provides 3 MVar reactive power to improve the voltage to 0.77 pu.

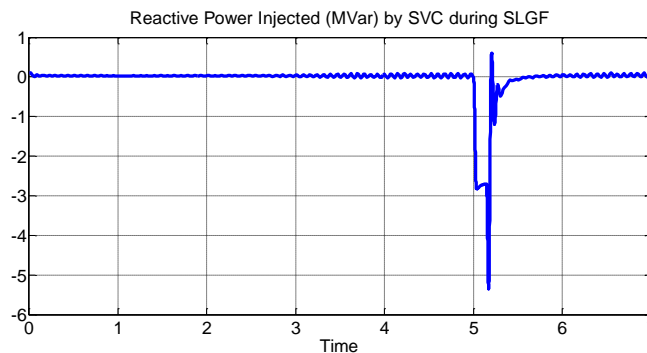


Figure 3.10b Reactive Power Injected by the SVC during SLGF

### 3.5.2 Line-to-Line Fault (L-L) With SVC and RSC Blocking.

Figure 3.10c and 3.10d show the performance of the SVC under L-L fault conditions. The voltage at the PCC was kept above the 0.75pu; consequently, uninterrupted operation of the DFIG-based wind farm was achieved. SVC is supplying 10MVar.

Figure 3.10e shows that the overshoot of the DC-link voltage decreased during the fault from 1315V to 1300V when the SVC is installed. The overshoot in the DC-link voltage does not improve much in the case of using SVC due to the small amount of reactive power injected compared with the case of STATCOM.

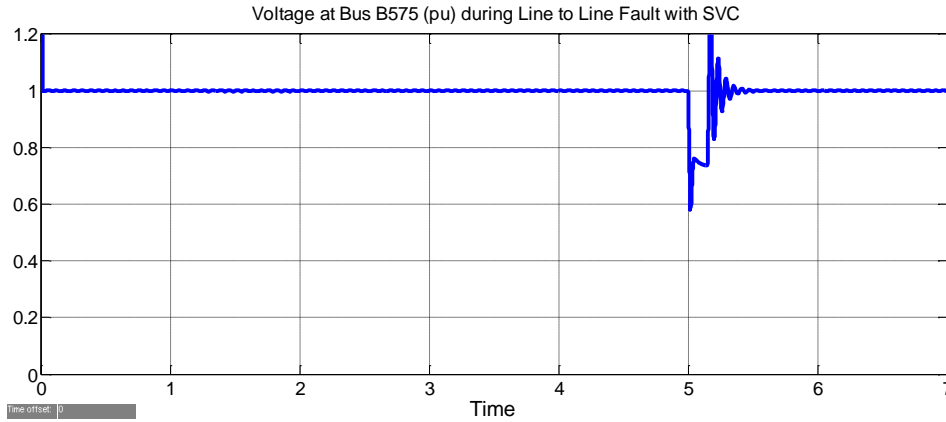


Figure 3.10c PCC (Bus B575) voltage during line-to-line Fault with SVC

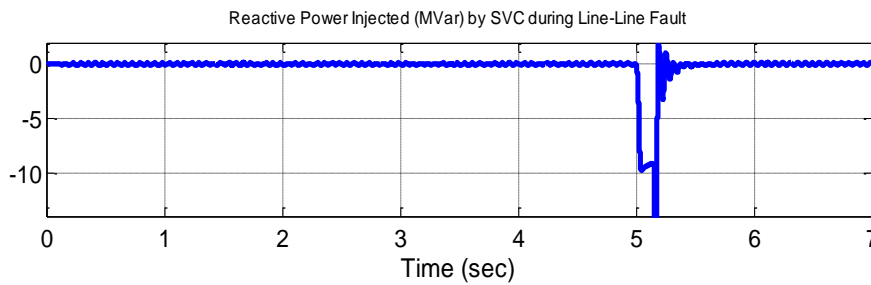


Figure 3.10d Reactive power injected by the SVC during line-to-line Fault

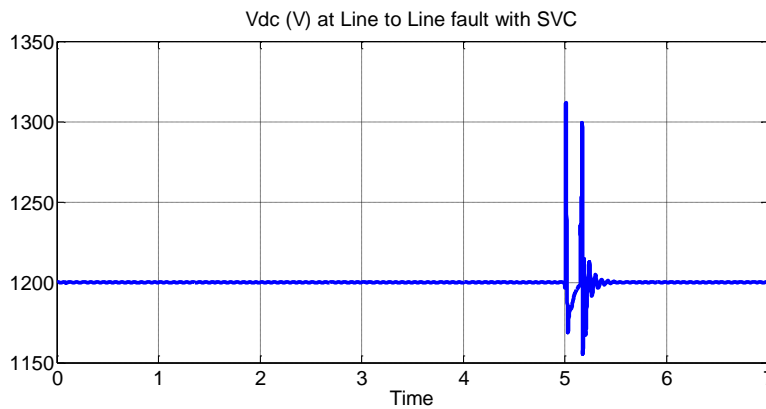


Figure 3.10e The overshooting of the DC link voltage during line-to-line fault with SVC

### 3.5.3 Voltage Sag of 30% at Bus 120kV With SVC and RSC Blocking.

The same temporary voltage sag of 30% for 0.5 s to the grid Bus (120kV) in Fig. 3.5 at  $t = 5$ s resulting from a remote fault has been applied. By installing the SVC, the voltage at the PCC was maintained above the 0.75pu; consequently, uninterrupted operation of the DFIG-based wind farm was achieved. Figure 3.10f, shows how the voltage at the PCC (bus B575) is improved to 0.78 pu when a SVC is connected.

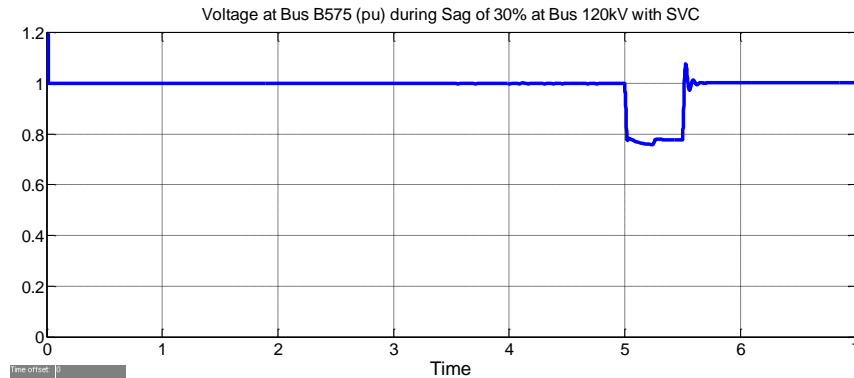


Figure 3.10f PCC (Bus B575) voltage during sag of 30% at bus 120kV with SVC

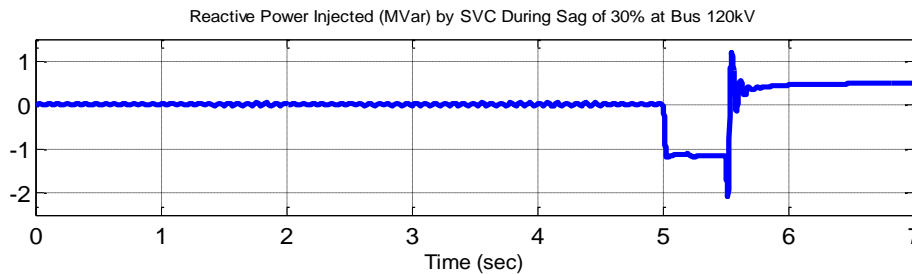


Figure 3.10g Reactive power injected by the SVC during the sag of 30% at bus 120kV

Figure 3.10g shows the reactive power supplied by the SVC to maintain the wind farm in service. The RSC is blocked, and the SVC is providing 1.2MVar.

### 3.6 Economic Comparison of STATOM and SVC

The cost of a FACTS device has two components: installation costs and operating expenses. The total installation cost includes the equipment price plus delivery and installation charges. While, operating cost includes maintenance and service charges. Typically, the operating cost for such devices is small and about 5%-10% of the total installation cost [101].

Table 3.1 Installation Cost Comparison of Shunt Controllers

<b>Shunt Device</b>	<b>Cost (US \$/kVAR)</b>
Shunt Capacitor	8 /kVAR (uncontrolled)
SVC	40/ kVAR (controlled)
STATCOM	50 /kVAR (controlled)

The cost of FACTS devices (SVC and STATCOM) is much more expensive compared with the shunt capacitor due to the cost of the controllers and the complexity of design and applications and it has added as a point of reference. The STATCOM is more expensive dynamic reactive compensation source due the type of switches used. Table 3.1 shows a summary of the installation cost of various shunt controllers [62, 63].

Table 3.2 The installation cost calculation of the SVC application

<b>Fault Type</b>	<b>kVar Injected</b>	<b>SVC Installation Cost (US \$)</b>
SLGF at Bus B3	3,000	120,000
(L-L) Fault at Bus B3	10,000	400,000
Voltage Sag of 30%	1,200	48,000

The installation cost of the SVC and STATCOM required in this study is calculated as shown in Table 3.2 and Table 3.3, respectively. The installation cost was calculated by multiplying the injected amount of kVAR in the cost of dollar per kVAR.

Table 3.3 The installation cost calculation of the STATCOM application

<b>Fault Type</b>	<b>kvar Injected</b>	<b>STATCOM Installation Cost (US \$)</b>
SLGF at Bus B3	4,000	200,000
(L-L) Fault at Bus B3	15000	750,000
Voltage Sag of 30%	1500	750,00

### 3.7 STATCOM and SVC Performance Comparison

Table 3.4 below summarizes the performances of both STATCOM and SVC for this study and also compares the amount of reactive power injected (MVar), installation cost, and the DC-link voltage overshooting. STATCOM provides more reactive power compensation compared to the SVC during all the three fault conditions. In the case of L-L fault (worst fault case applied in this study), the installation cost is an important factor to be taken into consideration. SVC can be an attractive option when a large amount of reactive power needs to be injected. This comparison

provides some basis for the integration of FACTS into DFIG by helping to achieve a better balance between both performance and cost for specific fault conditions.

Table 3.4 STATCOM compared to SVC performance

	STATCOM			SVC		
	SLGF	L-L Fault	30% Sag	SLGF	L-L Fault	30% Sag
Injected-Var (MVar)	4 MVar	15 MVar	1.5 MVar	3MVar	10 MVar	1.2 MVar
Var Cost (\$)	200,000	750,000	75,000	120,000	400,000	48,000
DC-Link Voltage (volt)	Not specified	1,280	Not specified	Not specified	1,300	Not specified

### 3.8 Summary

Dynamic reactive power compensation is the most successful technique applied to integrate the DFIG-based wind farm to the power grid during grid disturbances. This chapter has presented a comparative study of the application of both a STATCOM and a SVC to accomplish uninterrupted operation of a DFIG-based wind farm during fault conditions. They are connected at the point of common coupling (PCC) to provide voltage support and prevent the undervoltage protection from tripping the wind farm. Without STATCOM or SVC, the voltage at the PCC will fall below 0.75 (undervoltage protection limit), so that the wind turbine must be tripped from the power network.

This study has concluded that both devices produce the required reactive power to maintain a wind farm in service during the fault period. However, the ability to provide more capacitive power during a fault is one important advantage of a STATCOM over a SVC under the same fault conditions. This is due to the fact that the maximum capacitive power generated by a SVC is proportional to the square of the system voltage, while the maximum capacitive power generated by a STATCOM decreases linearly with voltage (constant current).

It was also found that integrating FACTS devices during the fault period would improve the overshooting in the DC-link voltage of the RSC, which minimizes the danger of damaging

the GSC and also helps the RSC to restart when the fault has cleared. In addition, it helps the GSC to control the DC link voltage back to the nominal value.

STATCOM has a faster and smoother response than the SVC because with the voltage source converter (VSC), the STATCOM has no delay associated with the thyristor firing (Typically, 43ms delay is associated with thyristor firing) [Reference]. The SVC is a less expensive application than a STATCOM and becomes a more attractive application when a large amount of injected reactive power is required, such as a line-to-line or three-phase fault.

Finally, the results of the comparative study presented in this chapter will help select the optimum FACTS device application that meets both cost and performance requirements for specific fault conditions.

## CHAPTER 4

### SMOOTHING OUTPUT POWER OF A GRID CONNECTED DFIG-BASED WIND TURBINE USING BATTERY ENERGY STORAGE SYSTEM (BESS)

#### 4.1 Introduction

There is a wide range of applications for battery energy storage system (BESS) at all levels of Generation, transmission, and distribution. BESS can be used to increase the reliability and security, and improve their efficiency when applied properly. Cheaper unused electricity produced at off-peak hours can be stored and used later to meet demand fluctuation. BESS can also be used for load leveling [105], voltage regulation [104], transmission and distribution facilities deferral [106]. These applications provide more uniform load factor for the generation, transmission, and distribution systems.

For wind power, the most well-known problem is the intermittency. Depending on the size of the wind farm and the strength of the grid to which it is connected, the active power variation may cause a frequency deviation, which might mistakenly trigger the protective relays which have a tripping threshold of about 1% [69]. DFIG has proven to be suitable for wind power applications due to its ability to operate stably with a rotational speed in the range of  $\pm 25\text{-}30\%$  around the synchronous speed. The variation of the wind speed is still a major issue when a severe drop or increase in the wind speed occurs [50, 67]. Controlling the output active and reactive power of the DFIG has been addressed and discussed by many researchers [67, 69]. However, the type of energy storage devices, cost, and the corresponding control topology makes a difference in specific applications.

This Chapter presents some ideas and detailed analysis of how to smooth out the output power for a grid connected DFIG. A new control strategy based on a stator flux oriented vector control is applied for both GSC and RSC in order to optimize the charge and discharge process of the battery energy storage system (BESS) and also to balance the maximum power point tracking (MPPT) as well as output power smoothing objective. Two different wind speed profiles were applied (step wind speed and somewhat random wind speed profile) during this study which enabled us to test the system under both sub-synchronous mode (lower wind speed) and super-synchronous mode (higher wind speed) of operation. A detailed design procedure to size the BESS is also described in this study. The simulation results were carried out in

MATLAB/Simulink (SimPowerSystem toolbox) environment. The configuration of the proposed DFIG with BESS connected to the DC-link is shown in Figure 4.1.

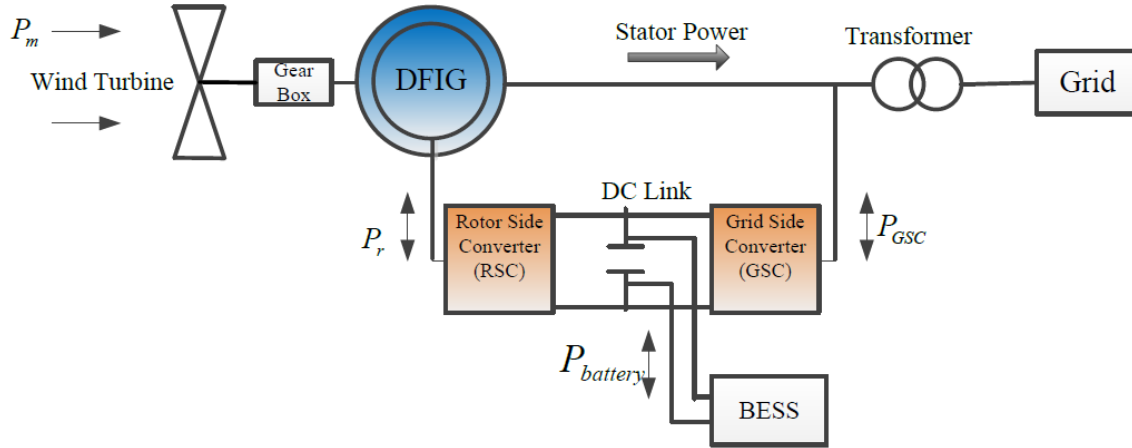


Figure 4.1 Battery Energy Storage System (BESS) connected to the DC-Link of the rotor converter of DFIG.

#### 4.2 An Overview of Energy Storage Devices

Energy storage devices provide valuable benefits to improve stability, power quality and reliability of supply. Storage technologies have been developed significantly in order to meet the challenges of practical power systems applications. Over the past decade numerous reasons have accelerated the renewable energy applications in the existing grid. However, renewable resources are intermittent and the energy output varies widely during the day. Electricity storage technologies, when properly designed and integrated, can smooth out this variability and allow unused electricity to be dispatched at a later time.

Energy storage technologies can be classified broadly into three categories depending on their applications and system requirements: short-term (a few seconds or minutes), long-term (minutes or hours) and real long-term (many hours to days) [74]. The classification is basically based on the amount of MWh that storage system can provide along with the power demand. Both discharge duration (time), and the storage system capacity (MW) can be varied in order to design a suitable energy storage system. Figure 4.2 shows the basic principle of energy storage classification. The area (stored energy in MWh) can be the same or different depending on the discharge duration. Decreasing discharge rate can be applied to make the discharge duration longer, and increasing discharge rate can be applied to make the discharge time shorter.

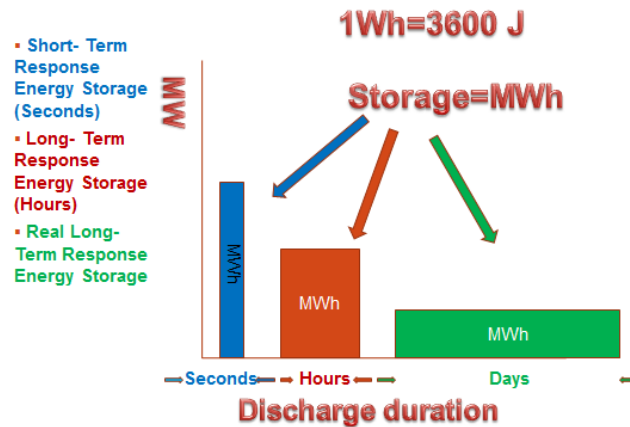


Figure 4.2 Classification of energy storage technologies

A brief description of the main energy storage devices currently being considered is presented below.

#### 4.2.1 Flywheels

Flywheel is classified as a short term response energy storage device where the energy stored in flywheel is in the form of kinetic energy in the rotating mass of a rapidly spinning flywheel [73, 74] given by:-

$$\text{Stored Energy} = \frac{1}{2} J \omega^2 \quad (4.1)$$

Where, J is the moment of inertia and  $\omega$  is the angular velocity. Such equipments have typically been used for applications requiring short discharge time such as stabilizing voltage and frequency,. The flywheels have variable storage capacity in the range of 150 kW to typically less than 100kW [107]. High efficient energy storage and relatively long life are the major advantages of flywheels. On the other hand, the high speed rotor and the possibility of it breaking loose and releasing all of its energy in an uncontrolled manner, and the current high cost are the disadvantages of the flywheels. The main characteristics of flywheels can be summarized as below [73, 92].

- Power (kW): < 100kW
- Energy (kWh): < 100kWh
- Charging-Discharging Efficiency  $\approx$  90%

- Life time (years)  $\approx$  20- 30 years
- Installation cost (\$/kWh)  $\approx$  170-420

#### 4.2.2 Supercapacitors

Supercapacitors (sometimes called ultra-capacitors) are electrochemical double layer capacitors that store energy in the electric field (like a parallel plate capacitor) and is given by:-

$$\text{Stored Energy} = \frac{1}{2} C V^2 \quad (4.2)$$

Where C is the capacitance and V is the voltage across the parallel plates. They are also classified as short-term response devices and are suitable for fast-response, short-duration applications. They are excellent for stabilizing voltage and frequency. In comparison with a battery or a traditional capacitor, the supercapacitor allows a much higher power and energy density. The supercapacitors have a variable storage power capacity range between 1kW-250kW, and typical energy storage less than 3MWh. The main characteristics of flywheels can be summarized as below [73, 92].

- Power (kW): 1kW-250 kW
- Energy (MWh): < 3
- Charging-Discharging Efficiency  $\approx$  95%
- Life time  $\approx$  30-40 years
- Price (\$/kWh)  $\approx$  85-480

It is necessary to convert from alternating current (AC) to direct current (DC) and vice versa for all storage devices except mechanical storage devices. Consequently, a power conversion system (PCS) is required that acts as a rectifier while the energy device is charged (AC to DC) and as an inverter when the device is discharged (DC to AC) as shown in Figure 4.3.

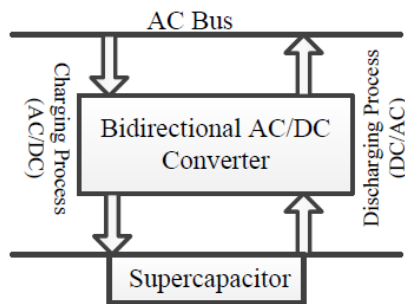


Figure 4.3 Working Scheme of Supercapacitor

The PCS also conditions the power during conversion to ensure that no damage is done to the storage device.

#### **4.2.3 Superconducting Magnetic Energy Storage System (SMES)**

Superconducting magnetic energy storage (SMES) systems convert the ac current from a power system into the dc current flowing in the superconducting coil and store the energy in the form of magnetic field. The stored energy can be released to the ac system when necessary. Power capacity of SMES is 3.0MW [73]. SMES is suitable when the application needs a fast response time, such as, power quality problems, and improve transient stability [77]. The SMES is a short-term response energy storage device. The advantages of the SMES are, efficient, reliable, and fast response time. The power quality conditioning by the SMES is considered to be very good. The disadvantages of the SMES are, cooling requirement, very expensive, sensitive to temperature, and high magnetic field. The main characteristics of the SMES can be summarized as below [73, 78].

- Power (MW): 0.3MW-3MW
- Bridging time: 10 Seconds
- Energy (MWh): 250MWh
- Charging-Discharging Efficiency  $\approx 95\%$
- Life time  $\approx 40$  years
- Price (\$/kWh)  $\approx 240-600$

The SMES has the same charging and discharging process as the supercapacitor that shown in Fig 4.3 where the SMES is charged through (AC to DC) rectifier and discharged through (DC to AC) inverter.

#### **4.2.4 Batteries**

In an electrical battery, energy is stored in the form of chemical energy. Batteries have the potential to span a broad range of energy storage applications due in part to their portability, ease of use and variable storage power capacity (100W-20MW) [107]. The current technology in batteries include: lead acid batteries, nickel-metal hydride, lithium, sodium-sulfur (NaS), alkaline and nickel cadmium. Batteries can be classified as long-term energy storage devices. Batteries can be connected in series-parallel combination to increase their power capacity for different applications. The advantages of the batteries are, there is no need to be connected to an electrical system, can be used in areas where electricity is not provided, and easily expandable. The typical

disadvantages are: expensive, life-cycle cost, and maintenance. The battery has the following characteristics [73, 107].

- Power (MW): 100W -20MW
- Energy (MWh): < 200
- Charging-Discharging Efficiency  $\approx$  70- 90%
- Life time  $\approx$  2-10 years
- Price (\$/kWh)  $\approx$  85-4800

The working scheme shown in Figure 4.3 is also valid for the battery where battery is charged through (AC to DC) rectifier and discharged to the AC system through (DC to AC) inverter.

#### **4.2.5 Fuel Cells**

A fuel cell converts stored chemical energy, in (fossil fuel, hydro carbon) gas, directly into electrical energy [73], hydrogen as energy carrier. Fuel cells can operate continuously. There are several types of fuel cells, each with its own advantages, limitations, and potential applications such as, Polymer electrolyte Fuel cells (PEM), Direct Methanol Fuel cells, and Alkaline Fuel cells, etc. The energy produced by the various types of cells depends on the operation temperature, the type of fuel cell, and the catalyst used. Hydrogen fuel cell is classified as a long-term response energy storage device and has a typical power capacity less than 20MW [73]. The advantages of the hydrogen fuel cell are less maintenance, low emissions, and low noise. However, it is very expensive. The main characteristics of the hydrogen fuel cell can be summarized as following [73, 74].

- Power (MW): <20
- Energy (MWh): <200
- Charging-Discharging Efficiency  $\approx$  70- 80%
- Life time  $\approx$  2-10 years

#### **4.2.6 Compressed Air Energy Storage (CAES)**

Compressed air energy systems (CAES) use cheaper electric power, when can not be consumed to run compressors that push air into underground reservoirs, such as mined caverns at very high pressure, and then use this air under pressure in a turbine to generate power on demand. A typical such system is shown in Figure 4.4 [103]. Currently, there are 2 large-scale demonstration plants in operation, one in Germany (290MW), and one in Alabama (110MW)

[107]. Power capacity of CAES system ranges between 100-300MW. This is classified as real long-term energy storage device that can supply power for days. The most common application is providing backup power during long blackouts. The main characteristics of the CAES can be summarized as following [73], [107].

- Power (MW): 100 -300MW
- Energy (MWh): <400-7200MWh
- Charging-Discharging Efficiency  $\approx 80\%$
- Life time  $\approx 30$  years
- Price (\$/kWh)  $\approx 12-85$

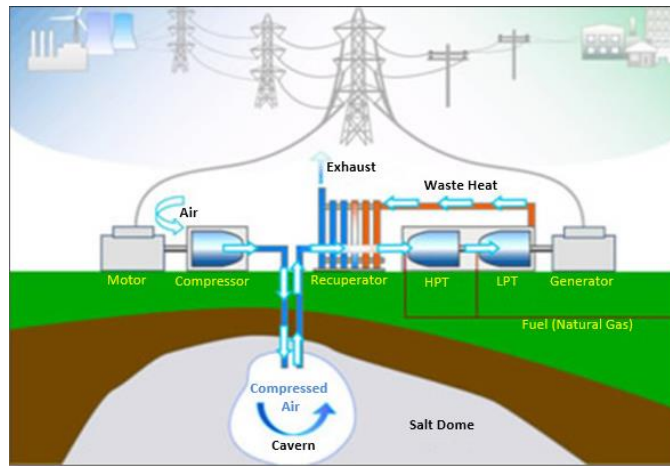


Figure 4.4 Layout of a compressed air energy storage facility [103]

#### 4.2.7 Pumped Hydro Energy Storage (PHES)

Pumped storage has been commercially implemented for load balancing for over 80 years. The method stores (potential) energy in the form of water, pumped from a lower elevation reservoir to a higher elevation when cheap electrical energy is available. Low-cost (off-peak) electric power is used to run the pumps. During periods of high electrical demand, the stored water is released through turbines Figure 4.5. Pumped Hydro typically has power capacity less than 2000MW.

The pumped storage is classified as real long-term response energy storage and typically used for application that needs power to be supplied for period between hours and days (power outages). There is over 90GW of pumped storage is in operation worldwide. In the United States, 38 plants currently provide total power capacity of 19GW [92]. The characteristics of the pumped hydro energy storage system can be summarized as following [92], [103].

- Power (MW): < 2,000MW
- Energy (MWh): <24000MWh
- Charging-Discharging Efficiency  $\approx 87\%$
- Life time  $\approx 40$  (or more) years
- Price (\$/kWh)  $\approx 45-85$

To calculate the mass power output of a PHES facility, the following relationship can be used:

$$P_c = \rho g Q H \eta_p \quad (4.3)$$

Where  $P_c$  is power capacity in Watt,  $\rho$  is mas density of water in  $\text{kg/m}^3$ ,  $g$  is acceleration due to gravity in  $\text{m/s}^2$ ,  $Q$  is the discharge through the turbines in  $\text{m}^3/\text{s}$ ,  $H$  is the effective head in m, and  $\eta_p$  is the efficiency of the pump. To evaluate the storage capacity of the PHES the following formula can be used:

$$S_c = \frac{\rho g H u \eta_T}{3.6 \times 10^9} \quad (4.4)$$

$S_c$  is the storage capacity in megawatt-hours (MWh),  $u$  is the volume of water that is drained and filled each day in  $\text{m}^3$ , and  $\eta_T$  is the turbine efficiency.

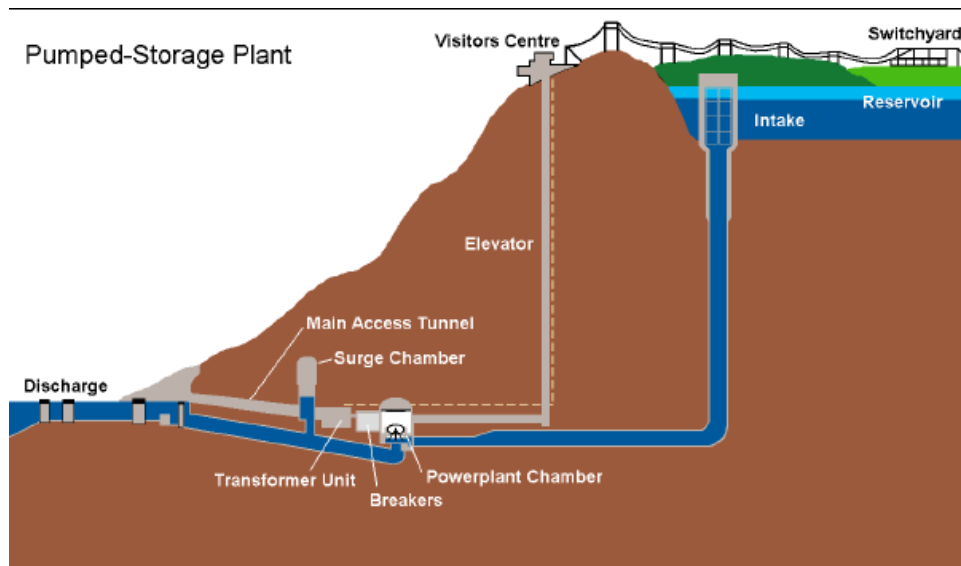


Figure 4.5 Layout of a pumped hydroelectric energy storage facility [110].

Table 4.1 summarizes the characteristics of all energy storage devices in terms, power capacity, stored energy, efficiency, cost, life time, and the device category (class).

Table 4.1 Energy Storage Devices Characteristics

Device	Power	Energy	Discharge Duration	Efficiency	Cost (\$/kWh)	Life Time (year)	Class
Flywheel	<100 kW	< 100 kWh	Sec./ Min.	90 %	170-420	20-30	Short-term
Super-capacitors	<250 kW	< 3 MWh	Sec./ Min.	95 %	85-480	30-40	Short-term
SMES	0.3– 3 MW	< 250 kWh	Sec./ Min.	90 %	240-600	40	Short-term
Batteries	< 20 MW	< 200 MWh	Min./ Hours	70 – 90 %	85-4800	2-10	Long-term
Hyd Fuel Cells	< 20 MW	< 200 MWh	Min./ Hours	70– 90%	-----	2-10	Long-term
Thermal Storage	<60 MW	< 500 MWh	Hours	<93%	50	30	Long-term
Compressed Air	100 – 300 MW	0.4-7 GWh	Days	80%	12-85	30	Real Long
Pumped Hydro	< 2 GW	< 24 GWh	Days	87%	45-85	40	Real Long

### 4.3 Why Battery Energy Storage Systems (BESS) for DFIG

Battery energy storage system (BESS) is a technology with high power density ( $\text{MW}/\text{m}^3$ ), power capacity in the range of hundreds of kW, and with the ability to respond in time frame of minutes. BESS technologies are usually appropriate to improve power quality, particularly to maintain the voltage stability during transients [92].

It's common for DFIG applications that energy storage system (ESS) is connected to the DC link of the rotor converter Figure 4.1. The rotor circuit handles only 25-30% of the DFIG rated power which means that the energy storage system needs to be designed to handle that power. ESS can effectively participate in frequency and active power regulation, unit commitment, economic dispatch, and electricity market operation. Most of the commercial-scale turbines installed today are about 2 MW [90]. Therefore, 25% of 2MW (hundreds of kW) would likely to be the power in the rotor circuits and exchanged with the ESS connected to the DC link of the rotor converter. In this case, BESS seems to be a practical choice since it accommodates this amount of power (hundreds of kW).

#### 4.4 System Configuration and Principle of Operation

Fig. 4.1 above is self-explanatory. The BESS in the DC-link could be described by its Thevenin equivalent circuit [50]. At the higher wind speeds (the machine operating at super-synchronous speed), power output of the DFIG-based wind turbine is higher as compared to the average power and, therefore, the extra power is stored in the battery. On the other hand, at the lower wind speeds (the machine operating at subsynchronous speed) the power is supplied from the battery to maintain the average power (constant power) fed to the grid. This topology, when applied properly, ensures that the power fed to the grid is always “leveled or constant” resulting in an efficient and reliable source of electrical power. The sizing and design of the BESS integrated to DFIG model is discussed next in detail.

##### 4.4.1 Design and Sizing of BESS

The proper design and sizing of the BESS is the key step to achieve a successful operation. The capacity is determined by the amount of energy to be exchanged between the BESS and the DC link. Basically, the average value of the power to be fed to the grid is calculated based on the site wind conditions. The required rating of the battery can be calculated using the following formula:

$$\text{Battery Rating} = \sum_{i=1}^n (P_{gen} - P_{avg}) * t_i \quad (4.5)$$

Where,  $P_{gen}$  is the output power of the DFIG-based wind turbine,  $P_{avg}$  is the targeted continuous average power to be fed to the grid and  $t$  is the time period for which the power difference between the instantaneous generated power and the average power fed to grid is calculated. Figure 4.6 shows a random general power curve of a wind turbine and the periods in which the battery will store the additional power ( $P_{gen} > P_{avg}$ ) and the periods in which the battery will supply the power to the machine ( $P_{gen} < P_{avg}$ ) to maintain the average power supplied to the grid. The average power can be calculated for a specific period of time (day, month, or a year). For the simplicity, in this study 1MW was selected to be the daily average power of a 1.5 MW DFIG-based wind turbine. The minimum required DC voltage level of the BESS can be determined using equation (4.6) below as a function of the grid line voltage.

$$V_{dc} = \frac{N_2}{N_1} \sqrt{\frac{2}{3}} V_{Line} \quad (4.6)$$

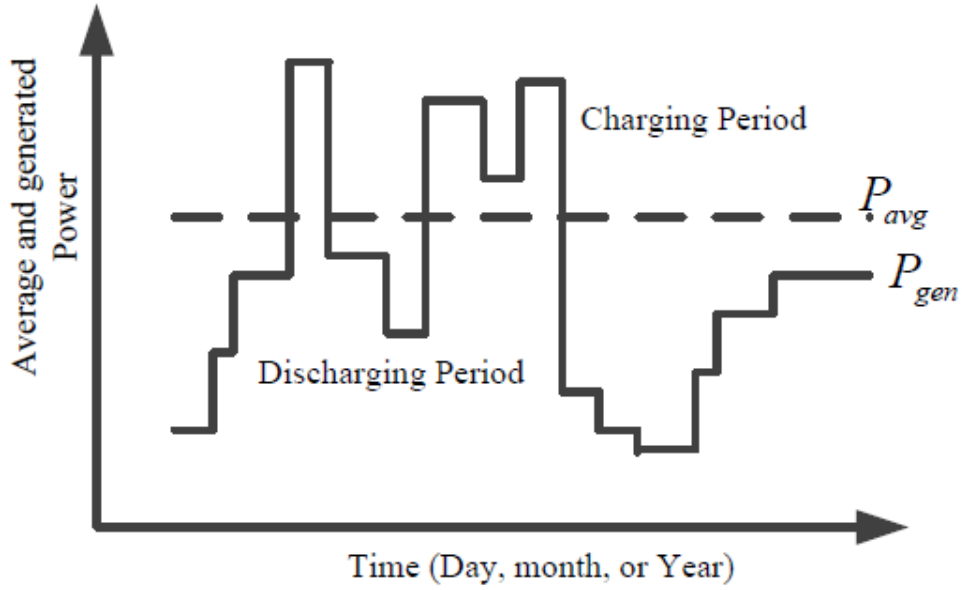


Figure 4.6 General power curve of a wind-turbine showing the characteristics of the generated power ( $P_{gen}$ ) and the average power ( $P_{avg}$ )

Connecting the battery bank to the DC link voltage ( $V_{dc}$ ) requires a number of batteries to be connected in series, parallel or series parallel combination in order to match with the DC link Voltage. Equation (4.7) is used to calculate the total numbers of batteries in series.

$$N_{Series} = \frac{V_{dc}}{V_b} \quad (4.7)$$

The total numbers of batteries in parallel are calculated as.

$$N_{Parallel} = \frac{E_b \times 1000}{V_{dc} \times P_b \times MDOD} \quad (4.8)$$

Where,  $V_{dc}$  is the minimum required dc voltage of the battery bank, ( $N_2 / N_1$ ) is the transformer turns ratio,  $V_{Line}$  is the grid line voltage,  $V_b$  is the voltage of a single battery,  $P_b$  is the capacity of a single battery in Ah,  $E_b$  is the total rating of the battery bank in kWh, and MDOD is the maximum depth of discharge of the battery.

#### 4.5 Proposed Control Strategy

Vector control is one of the most commonly used methods applied to control the flow of active and reactive power between the stator and the grid [43]. The vector control technique can

be applied on both RSC and GSC. Typically, the RSC controller aims to control the stator active and reactive power by controlling the rotor current components on d-q axis ( $i_{qr}$ ,  $i_{dr}$ ); while the objective of the GSC controller is to maintain the DC-link voltage constant regardless the magnitude and direction of the rotor power. As mentioned earlier, the GSC control scheme can also be designed to regulate the reactive power. Figure 4.7 shows the complete control scheme for both RSC and GSC of a DFIG with BESS applied in this study.

#### 4.5.1 Grid Side Converter (GSC) Controller

The main idea of this scheme is to modify the active power outer control loop of the GSC. The generated active power value of the DFIG is regulated to be constant and equal to the reference power (average power). This reference active power value is compared with the instantaneous output active power and the error is fed to a proportional–integral (PI) controller to generate the q-axis current reference component that will be compared with the q-axis actual value component of the generator current. As for reactive power control loop of the GSC, the idea is to regulate or control the stator reactive power. This control loop allows us to control the reactive power sharing between the GSC and the DFIG and then provide the total reactive power that matches the requirement of the grid ( $Q_{Grid} = Q_{Stator} + Q_{GSC}$ ). The resulted d-q reference currents that produced from comparing the reference d-q current components with actual d-q current components of the DFIG will be fed to the PWM controller of the GSC to control both active and reactive power.

In this study both active and reactive power control loops of the GSC are considered. The reference reactive power ( $Q_{ref}$ ) was set to be zero for unity power factor operation. The implementation of the reference d-q current is given in (4.9).

$$i_{qsref} = (k_{pp} - \frac{k_i}{s})(P_{avg} - P_{gen}) \quad (4.9)$$

$$Q_{ref} = 0 \Rightarrow i_{dsref} = 0 \quad (\text{unity power factor operation})$$

Where,  $k_{pp}$  and  $k_i$  are the proportional and the integral constants of the PI controller respectively. The reference d-axis current depends on the reactive power sharing between the stator and the GSC, and it is set up to be zero for unity power factor operation. Since the main focus of this work is to control only the active power output, this assumption was made in order to minimize the complexity of the control system.

These reference currents are then compared with the sensed actual stator currents ( $i_{qs}, i_{ds}$ ) and the obtained error signal is processed with a PI controller to generate the control voltages for the PWM generator to be fed to the GSC. The expressions for the control voltages to be fed to the GSC are given in equations (4.10) and (4.11) below.

$$v_{qgsc} = (k_p - \frac{k_i}{s})(i_{qsref} - i_{qs}) \quad (4.10)$$

$$v_{dgsc} = (k_p - \frac{k_i}{s})(i_{dsref} - i_{ds}) \quad (4.11)$$

Where,  $i_{qs}$  and  $i_{ds}$  are the sensed actual components of the stator currents. These control voltages ( $v_{qgsc}, v_{dgsc}$ ) are fed for PWM generation of the GSC.

#### 4.5.2 Rotor Side Converter (RSC) Controller

The objective of the RSC is to govern both the stator-side active power (generating torque) and reactive power independently by controlling the d-q components of the rotor current. The reference values of rotor currents are compared with the sensed actual values of rotor currents and the obtained error signal is processed with a PI controller to generate the control voltages for the PWM generator on the rotor side converter. The expressions for the control voltages in d-q frame are given in equations (4.12) and (4.13) below.

$$v_{qrsc} = (k_p + \frac{k_i}{s})(i_{qrref} - i_{qr}) \quad (4.12)$$

$$v_{drsc} = (k_p + \frac{k_i}{s})(i_{drref} - i_{dr}) \quad (4.13)$$

Where,  $i_{qr}$  and  $i_{dr}$  are the actual q-d axis components of the rotor currents.  $i_{qrref}$  and  $i_{drref}$  are the reference values of d-q components of the rotor currents which are generated from the reference active and reactive powers. This control voltages are fed to the PWM generator to be fed to the RSC to control the stator active and reactive power as shown in Figure 4.7.

#### 4.6 A Grid Connected DFIG Model with BESS

To evaluate the effectiveness of the proposed strategy, simulation studies are carried out using MATLAB/Simulink as shown in Appendix B.

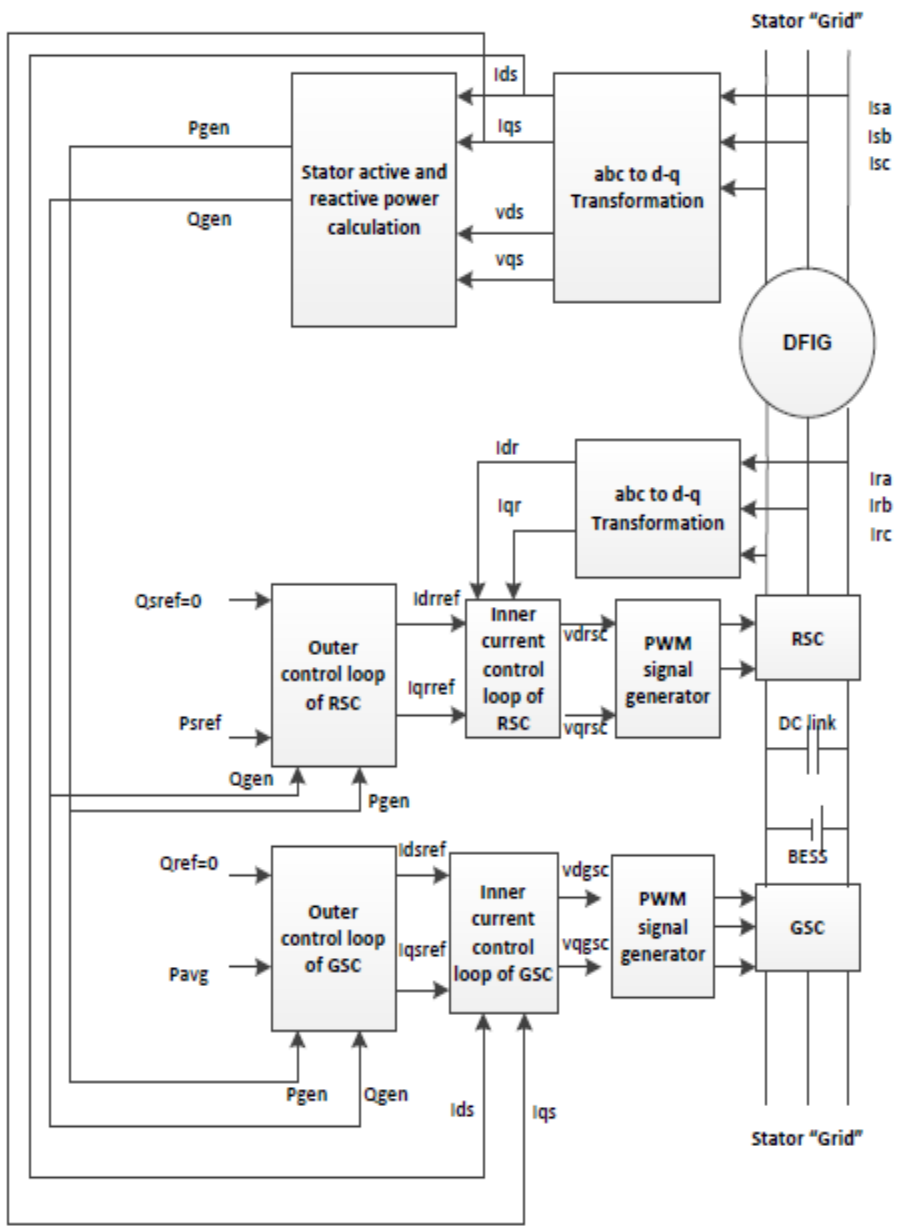


Figure 4.7 Schematic Diagram of Proposed Control Strategy for RSC and GSC of a DFIG with BESS

#### 4.6.1 Grid Connected DFIG Model

Figure 3.5 shows the single line diagram of the test system. The grid model consists of a 120kV, 60Hz, grid supply point, feeding a 25kV distribution system through 120-25kV, 47MVA step down transformer, which feeding a 575V system through 25kV-575V, 12MVA step down transformer. There are two loads in the system; one load of 2MVA, 0.9 pf (lag) at 30km from transmission line, and a static load of 500kW at 575V bus. The 25kV, 30km long line is represented as nominal- $\Pi$  line. The DFIG-based wind turbine with a rating of 1.5MW is connected at 575V bus. The GSC in DFIG maintains the DC link voltage almost constant at 1200V during normal operating condition.

#### 4.6.2 BESS Sizing

In this study, the sizing of the BESS bank is done by taking the following requirements into consideration:

- It's recommended that Battery is never discharged to below 50% of its capacity; however, many battery manufacturers recommend even shallower DOD. For off-grid applications, a 60%-80% DOD will extend battery life significantly [107]. The depth of discharge (DOD) is the limit of energy withdrawal to which you will subject the battery (or battery bank). DOD is expressed as a percent of total capacity; Figure 4.8 shows the impact of depth of discharge on the number of cycles for a typical deep-cycle lead acid battery [100].

The BESS bank in this study is being sized for reducing the output power fluctuations of DFIG due to the varying nature and unpredictability of wind. Therefore, the BESS will have a high number of charge and discharge cycles during the day. Based on this fact, 50 % DOD is selected in order to extend BESS bank life significantly.

- In the DFIG-based wind turbine application, the BESS is connected to the DC-link of rotor converter which handles 25-30% of the total rating of the DFIG [47]. Therefore, the storage capacity design of the BESS bank is selected to be 375 kW which is 25% of 1.5MW DFIG-based wind turbine used in this study.

In the battery sizing process, it is important step to determine what hour rating we would like to use. A longer hour range rating s translates to lower number per day [107], which consequently, extends the battery life. Therefore the BESS bank in this study is designed to supply power for 10hr, which translates to about 2 cycles a day. As a result of

this design, the BESS will be able to supply power of 375kW for 10h. the total kWh of the BESS is:

$$\text{Total kWh of BESS bank} = 375kW \times 10hr = 3750kWh$$

By taking into account the depth of discharge rate (DOD) of 50%, the total kWh of the BESS bank can be calculated as following:

- Total kWh of BESS bank =  $\frac{3750kWh}{0.5} = 7500kWh$

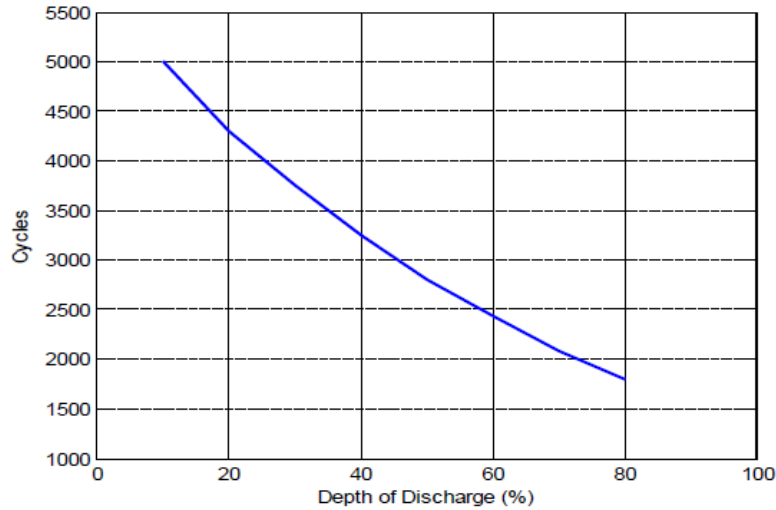


Figure.4.8 Depth of discharge % vs. Number of cycles for typical deep-cycle Lead-Acid battery [100].

- Since the BESS bank is directly connected to the DC-link of the rotor converter of the DFIG, BESS bank voltage is designed to be 1200 V which is the same as the DC-link voltage of rotor converter of the DFIG.

The commercially available battery bank consists of cells of 12 V, 24 V, and 48 V. By using 12 V cells, the number of cells required to fulfill voltage of 1200 V is  $(1200V/12V) = 100$  number of cells in series. The total ampere hour required is:

$$(7500 \times 10^3 \text{ Wh} / 1200 \text{ V}) = 6250 \text{ Ah.}$$

The 12 V cells are available with a nominal capacity between 100Ah- 800Ah [100]. In this design, the nominal capacity of each cell is taken to be 150 Ah. As a result, the number of sets of 100 series-connected cells required to be connected in parallel is  $6250 \text{ Ah} / 150\text{Ah} \approx 42$ .

The BESS bank sizing is summarized in Table 4.2 below

Table.4.2 Sizing of BESS bank

Power (kW)	Capacity	Discharge Time (hour)	DOD	Designed kWh	Nominal Voltage (Volt)	# Arrays
375Kw		10 hours	50%	7500kWh	1200 V	42

#### 4.6.3 BESS Model

A detailed procedure to select the rating of the BESS was already mentioned in earlier sections. The MATLAB-based modeling of the battery is done using the Thevenin's equivalent of it as shown in Figure 4.9 [50]. Since the battery is an energy storage unit, its energy is represented in kWh, when a capacitor is used to model the battery unit, the capacitance  $C_b$  can be determined from equation (4.14).

$$C_b = \frac{(kWh) \times 3600 \times 10^3}{1/2(V_{OCMax}^2 - V_{OCMin}^2)} \quad (4.14)$$

Where  $V_{OCMin}$  and  $V_{OCMax}$  are the minimum and maximum open circuit voltage of the battery under fully discharged and charged conditions.

The voltage of the battery in fully charged and discharged is taken as 12.8V and 11.2V, respectively. The maximum open circuit voltage ( $V_{OCMax}$ ) for the battery bank is  $12.8 \times 100 = 1280V$ , and the minimum open circuit voltage ( $V_{OCMin}$ ) is  $11.2V \times 100 = 1120V$ . By substituting the values of kWh,  $V_{OCMax}$ , and  $V_{OCMin}$  in equation (65), the value of capacitor bank capacitance obtained is 140625 F. a resistance of 10 kΩ in parallel with the  $C_b$  represents self-discharging of the battery bank.

In the Thevenin's equivalent model of the battery,  $R_s$  is the equivalent resistance (external + internal) of parallel / series combination of a battery, which is usually a small value. The parallel circuit of  $R_b$  and  $C_b$  is used to describe the stored energy and voltage during charging or discharging.  $R_b$  in parallel with  $C_b$  represents self-discharging of the battery. Since the self-

discharging current of a battery is small, the resistance  $R_b$  is large. The design details of the BESS used in this study are given in Appendix A.

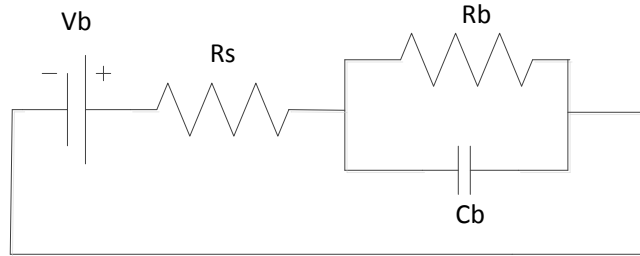


Figure 4.9 Thevenin Equivalent circuits of the BESS

#### 4.7 Simulation Results and Discussion

The proposed configuration of a grid connected DFIG based wind turbine with BESS is carried out in MATLAB/Simulink environment. The proposed control strategy is applied on both RSC and GSC in order to achieve output power smoothing of DFIG under different wind speed conditions. A stepwise wind speed profile has been applied with a different wind speed values in order to test the system under different wind speed conditions (sub-synchronous and super-synchronous mode of operation). Random wind speed profile was applied to examine the system performance under more realistic wind speed profile.

##### 4.7.1 The System Output at Steady State Conditions without BESS

A step wind speed profile has been applied with initial wind speed of 8m/s and then at  $t=5s$  wind speed increases to 14m/s. The generated active power starts increasing smoothly (together with the turbine speed) to reach its rated value of 1.5MW in approximately 18s. Over that time frame the turbine speed will have increased from 0.8pu to reach the rated value of 1.21pu of generator synchronous speed. The DC link nominal voltage of the DFIG-based wind turbine is 1200V. The overall performance of the system is shown in Figure 4.10. The main purpose of running the system in this case was to verify the system output (active power, DC link nominal voltage, and the rotor speed) at the rated wind speed (14m/s in this case).

##### 4.7.2 The System Performance with the BESS and the Proposed Control Strategy

In order to test the system under both sub-synchronous and super-synchronous modes of operation, a step wind speed profile has been applied with an initial value of 8m/s and then at

t=5s wind speed increases to 14m/s (rated wind speed), at t=40s the wind speed decreases to 10m/s (sub-synchronous mode of operation), and t=70s the wind speed goes up to reach 16m/s (super-synchronous mode of operation).

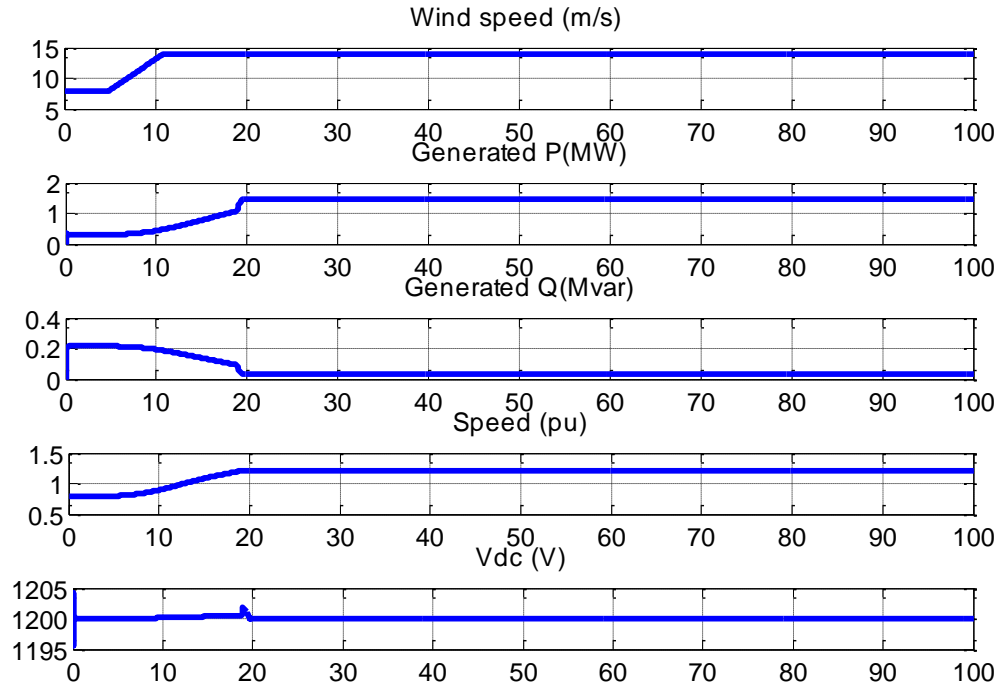


Figure 4.10 Performance of DFIG-based wind turbine without the BESS and the proposed control at rated wind speed of 14m/s

Figure 4.11a-4.11f show the performance of the proposed configuration of a DFIG-based Wind turbine at sub-synchronous speed, and super-synchronous speed. The waveforms of wind speed, reactive power, generated active power, battery power, ac rotor speed, and DC link voltage, are presented. The convention for the battery power is chosen as to be negative if the battery discharges any power and positive if power is stored in the battery.

Despite the variation in the wind speed, the value of the generated output power fed to the grid is maintained to be constant at 1MW by the modified average power control strategy. However, this is maintained by either charging or discharging the battery in the corresponding region of operation. The reactive power is maintained at a stable value of zero, demonstrating a unity power factor operation. The analysis has been performed at variable wind speeds and the generated power is maintained to be constant at the desired reference value (1 MW).

The proposed strategy also reduced the variation in the rotor speed and the DC link voltage due to the wind speed variation. The rotor speed and the DC link voltage maintained at the rated values of 1.2pu and 1200V respectively. The targeted periods are those at  $t=40s$  when the wind speed decays from 14m/s to reach the sub-synchronous speed of 10m/s and at  $t=70$  when the wind speed starts increasing from 10m/s to reach the super-synchronous speed of 16m/s. During the first period at  $t=40$  sec the output power of BESS tends to be negative (discharging power to the machine) and at  $t=70$  sec the output power of the BESS tends to be positive (charging process) as shown in Figure 4.11b.

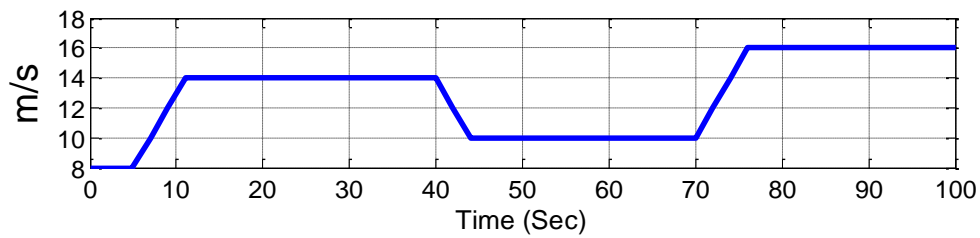


Figure 4.11 (a) Applied stepwise wind speed profile

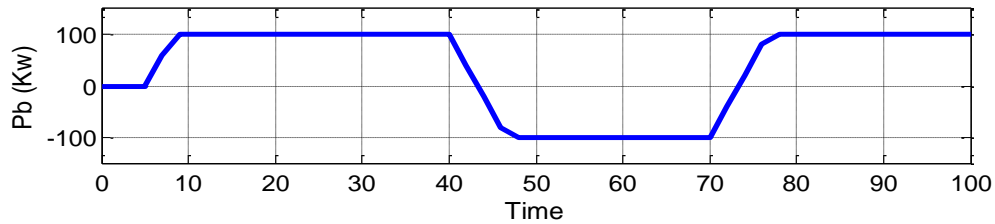


Figure 4.11 (b) Battery output power

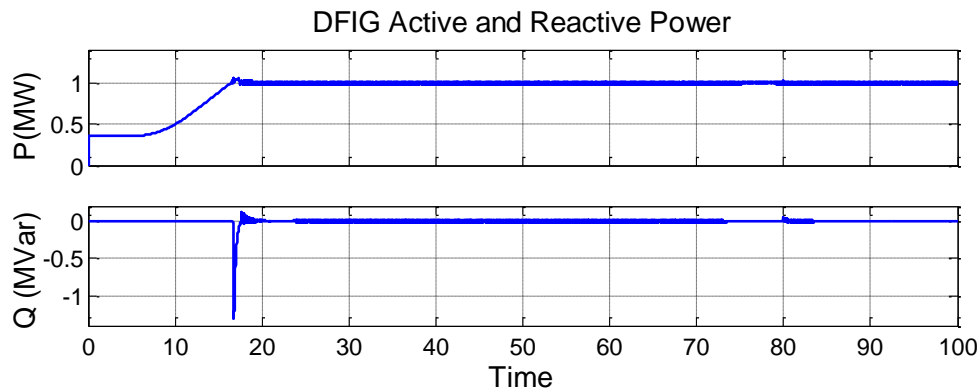


Figure 4.11 (c&d) Generated active and reactive power

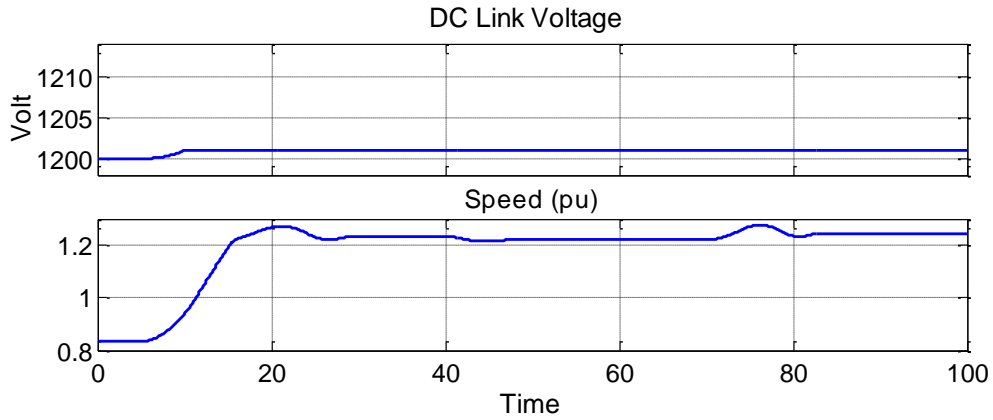


Figure 4.11 (e &f) DC Link voltage and rotor speed

Random wind speed profile was applied in order to examine the system under more realistic wind speed conditions; the system performance is shown in Figure 4.12a -4.12f.

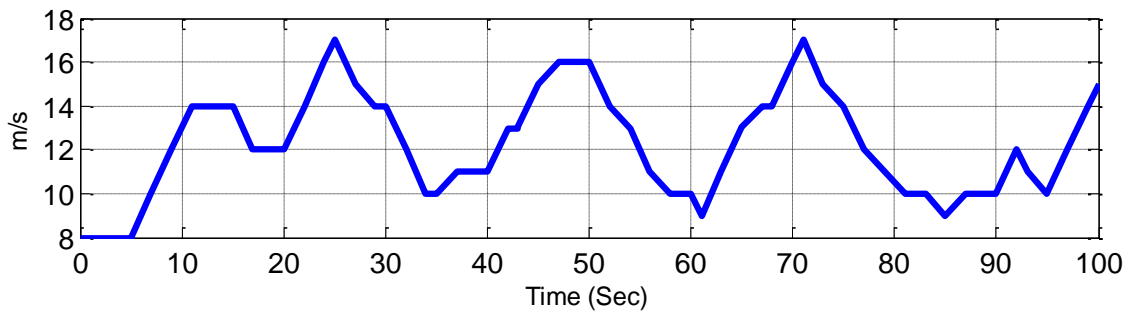


Figure 4.12 (a) Random wind speed profile

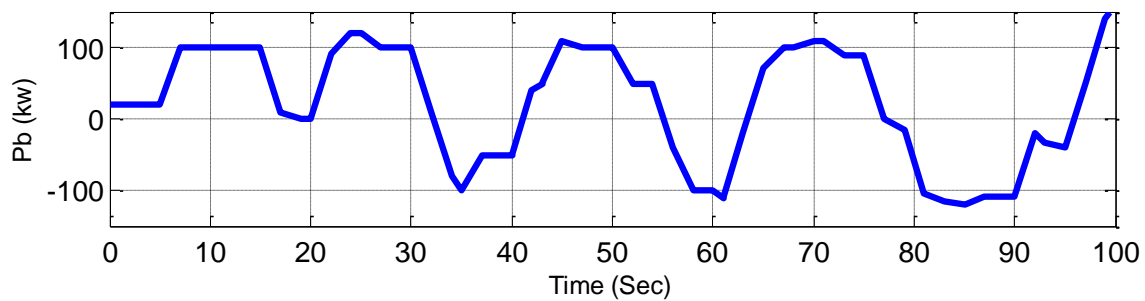


Figure 4.12 (b) Battery output power

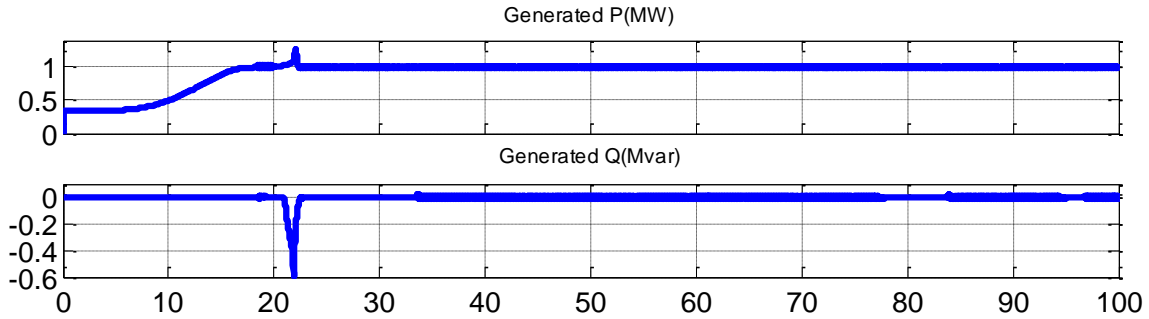


Figure 4.12 (c&d) Generated active and reactive power

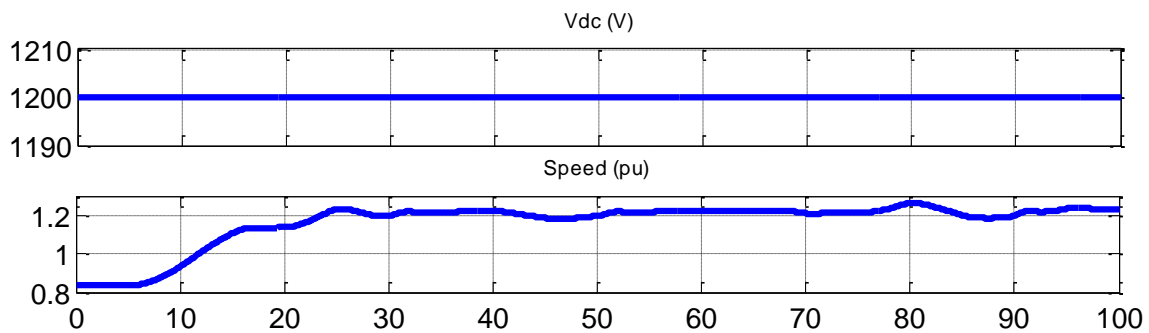


Figure 4.12 (e & f) DC Link voltage and rotor speed

Simulation results for power of the BESS unit correspond to a positive power when charging the storage unit and a negative power when discharging the power. Despite the variation in the wind speed, the value of the generated output power fed to the grid is maintained to be constant at the desired reference value 1MW.

It can also be noticed that the control strategy is sensitive to wind speed variations. More fluctuated wind speed (randomly distributed wind speed) means more difficult to demonstrate a good performance due to the high number of charge and discharge cycles.

#### 4.8 Summary

In this Chapter, a configuration of a DFIG-based wind turbine with a BESS in the DC-link has been proposed with a control strategy to maintain the generated active power output to the grid constant. A methodology to select and size of BESS has been well addressed. The effectiveness of the proposed control strategy is seen under different wind speeds. The use of BESS was one of the possible options to ensure the stable and reliable operation of a grid

connected DFIG. BESS system would help store/release the additional energy to maintain a constant power injected to the grid. During higher wind speeds, the excess energy was stored in BESS while keeping the generated active power at a constant level. During lower wind speeds, the stored energy in the batteries was supplied to the machine. This ensured the stable/constant power supply from DFIG based wind turbine under stepwise constant & random wind speed profiles.

The proposed configuration in this Chapter also provides an effective solution to the intermittency characteristic of the generated output power of DFIG due to wind speed variation. If the utility fails to maintain the grid power constant, then during periods of “over-generation,” the consumers are to be paid in return to implement “load-leveling,” and absorb the excess power. This is not a beneficial practice as the supplier loses both energy and money.

## CHAPTER 5

### CONCLUSION

#### 5.1 Summary

Wind energy in various forms has been playing a very significant role since the beginning and in the very existence of human race. It has been used for irrigation and transportation for centuries. However, the impact of generating electricity in large scale in the 21<sup>st</sup> century has taken the application of wind energy to a different level. With the steady global population growth and finite fossil fuel resources, along with political unrest in the oil producing countries, global warming and greenhouse gas emissions, sustainability of the human rest and the earth has becoming a very challenging issue for the 21<sup>st</sup> century and beyond. In the past two decades electricity production from wind globally has been growing at a fast rate. Even though the actual production of electricity is a very small fraction (somewhere in the vicinity of 1-5% overall, but for some countries in excess of 50%) of the total electricity produced, it is expected to grow steadily for the next 20-30yrs. In USA, the largest user of electricity in the world, it has been mandated by laws to produce about 10-35% of total electricity from wind and other non-hydro renewable sources by 2030 in most of the states. As a point of reference, it must be remembered that the total installed generation capacity in USA is in excess of 1.0Terawatt (Tera =  $10^{12}$ ) or 1 million MW. The annual electricity production is about 4,200TWh with a capacity factor of about 0.47. In paper 10-20% may not sound that difficult, but in reality there are many challenges and obstacles. With the advent of the many power electronics devices that provides faster response and smoother control, system integration of wind farm into the existing grid is becoming more manageable. However, when the wind and solar penetration increases in 20-30% level, there are many issues that need to be dealt with. This is primarily because these energy sources are intermittent in nature and the energy is available when the demand is typically low. In order for the grid to be dominated by non-hydro renewable energy sources, storage must be added. Unfortunately except for the pumped storage power plants (which in USA is mostly built), other forms of energy storage for large scale applications is not available and are still in research and development stage.

Recent advancement of power electronics devices and available digital control strategy, however, made the application of doubly fed induction generator (DFIG) more useful for large scale wind farm. One must, however, remember that the size of an individual DFIG unit is still

very small (2.00-5.00MW range) compared to central power plants unit size (500-1,200MW). Controlling one large unit is, in general, lot simpler than controlling a large number of smaller units. This dissertation has been predominantly focused on the various application aspects of the DFIG based wind farm design and control and proposed a number of new control strategy.

After a brief overview of wind energy growth and the basic principle of a typical wind energy conversion system, a detailed DFIG model in MATLAB/Simulink is built from fundamental principles. The simulation results confirmed the validity of the model. Vector control strategy based on stator flux oriented reference frames to control the output active power of the DFIG is presented and the simulation results are discussed at length. A new vector control strategy based on the rotor flux oriented reference frame is presented as well, and compared with the commonly used stator flux oriented vector control available in literature. The results have confirmed the validity of the new vector control strategy. This new proposed rotor flux oriented vector control strategy provides better active power tracking compare with the stator flux oriented vector control and eliminates the DC offset associated with the integration of the stator flux components to calculate the orientation angle. This feature would provide a better power tracking and easier implementation of the control method.

Reactive power requirements, control and voltage stability during fault conditions has been recognized as a potential problem in large wind farm applications. A comparative study of the application of both STATCOM and SVC to accomplish uninterrupted operation of DFIG-based wind farm during fault conditions is presented. Specific attention was given to the amount of reactive power injected, improving the DC-link overshooting, and the application cost for different fault conditions. The comparative study presented in this work will help select the optimum FACT device that meets both cost and performance requirements for specific fault conditions. It was concluded that both devices produce the required reactive power to maintain the wind farm in service. However, the ability to provide more capacitive power during a fault is one important advantage of the STATCOM over the SVC. This is because of the amount of reactive power produced by the SVC is proportional to the square of the voltage which means this reactive power output is reduced at low voltages when it is likely to be needed most. It was also found that integrating FACTS devices during the fault period would improve the overshooting in the DC link voltage of RSC which minimizes the dangerous of damaging the GSC and also helps the RSC to restart when the fault has cleared. In addition, it helps the GSC to

control the DC link voltage back to the nominal value. STATCOM has a faster and smoother response due to type of switches used compare with the using of two anti-parallel Thyristors with natural commutation in case of SVC. The SVC is less expensive than a STATCOM and becomes very attractive application when a large amount of injected reactive power is required such as line to line or 3-phase fault.

As mentioned earlier, storage is an integral part of the total solution for an intermittent (variable wind speed) wind power source. A battery energy storage System (BESS) has been integrated into a grid-connected DFIG-based wind turbine. The BESS would help in storing/releasing additional power in case of higher/lower wind speed to maintain constant grid power. This ensured the stable/constant power supply from DFIG based wind turbine. If the utility fails to maintain the grid power constant, then during periods of “over-generation,” the consumers are to be paid in return to implement “load-leveling,” and absorb the excess power. This is not a beneficial practice as the supplier loses both energy and money. In addition, placing the BESS in the DC link of the DFIG and adopting the proposed control strategy has avoided the need for a high rating of BESS.

There are many other design and control aspects of wind power generation, both small and large application that must also be studied. Researches in those areas are on-going. It is a very difficult proposition at this time for wind power alone without substantial amount of energy storage to provide continuous supply of electricity and follow the demand. Unfortunately, any form of large scale energy storage is extremely expensive. Controlling a large number of smaller machines in a wind farm to balance the power demand and controlling the voltage is not a simple task either. However, integrating wind power (10% range) to an existing grid is a different problem and more manageable. The new concept of micro-grid or distributed generation with hybrid design between wind, solar, fossil fuel, and storage is being studied by many researchers and may find applications in some specific case. It is, however, unthinkable at this time to run the entire US power grid with renewable energy sources, hydro and non-hydro combined.

## **5.2 Contributions**

Besides studying the wind power applications, the DFIG and system integration models, in general, the main contributions of this dissertation include:

1. A detailed model of all components of the DFIG-based wind turbine including the AC-DC-AC rotor converter using MATLAB/Simulink and its operation in both sub-synchronous and

super-synchronous modes is explained clearly. The simulation results confirmed the validity of the model.

2. A new vector control strategy based on the rotor flux oriented reference frame to control the output active power of DFIG is presented and compared with the commonly used strategy based on the stator flux oriented vector control. The proposed control eliminates the DC offset associated with the integration of the stator flux components to calculate the orientation angle and provides a better accurate power tracking and easier implementation of the control method. The results have confirmed the satisfaction of the both vector control strategies.
3. A comparative study utilizing both STATCOM and SVC to accomplish uninterrupted operation of DFIG-based wind farm during the different fault condition is performed. The comparison has been done in terms of the amount of reactive power injection (MVar), installation cost, and the improvement in the overshooting of the DC link voltage of the DFIG. The results will help the system planner to select the optimum FACTS device that meets both cost and performance requirements for specific fault conditions.
4. A DFIG-based wind turbine with a battery energy storage system (BESS) in the dc link of the rotor converter has been proposed with a control strategy to maintain constant active power output to the grid. A new control strategy based on a stator flux oriented vector control is applied to both GSC and RSC in order to optimize the charge and discharge process of the BESS and also to balance the maximum power point tracking (MPPT) for output power smoothing. The effectiveness of the proposed control strategy is studied under different wind speeds.
5. All the codes and model details utilized in the MATLAB/Simulink programming are included in the Appendices (including the instructions) for any future use by other researchers

### **5.3 Future Work**

This dissertation has opened many opportunities for future research on applications of the DFIG-based wind turbine system. The following items provide a short list of potential for future work:

1. Development of a detailed wind turbine model and adding it to the mathematical model of the DFIG proposed in this work where more realistic wind speed profiles can be studied.

2. Rotor flux and rotor flux oriented vector control schemes presented in this study can be adopted to decouple the control of the reactive power produced by the DFIG since only active power control is covered in this work.
3. Interaction of the DFIG- based wind farm with more realistic power grid models, where other type of generators like synchronous generators are also present. Similar study can be done in those power grids to evaluate the support provided by the use of both STATCOM and SVC.
4. Integrating battery energy storage system (BESS) using the proposed control strategy into DFIG- based wind farm consists of a group of wind turbines. Each DFIG-based wind turbine is equipped with BESS.
5. Enhancing the low-voltage ride through (LVRT) capability caused by faults and improving the stability and reliability of the DFIG wind turbine using energy storage system can be another challenging future task to be studied.
6. Study the hybrid design of a micro-grid that includes other power sources.
7. Study in-depth the design of a large wind farm and its impact on voltage stability.
8. Perform analytical study of the effects on loss of inertia when used power electronics based control system.
9. Verify the analytical results obtained from such modeling and simulation with the real world on-line testing.

#### **5.4 List of Publications**

Some of the results presented in this dissertation have already been published in the following peer-reviewed publications. Much of the written materials in this dissertation have been borrowed from these publications [identified in the parentheses]. This has been added for clarity and future references.

1. Tarek Masaud, Keun Lee, and P.K Sen, “An overview of Energy Storage Technologies in Electric Power Systems: What is the Future?,” IEEE North American Power Symposium (NAPS), Arlington, TX, USA. pp. 1-6, September 26-28, 2010. [Chapter 4].
2. Tarek Masaud, Keun Lee, P.K Sen, and Keith Malmedal, “Design and Energy Estimates for Wind Farms”, IEEE Conference, PEDES 2010, New Delhi, India, Dec 20-23. 2010, pp. 1-6. [Chapter 1].

3. Tarek Masaud, and P.K Sen, “Modeling and Control of Doubly Fed Induction Generator for Wind Power”, IEEE North American Power Symposium (NAPS), Boston, Massachusetts, Aug 4-6. 2011, pp. 1-8. [Chapter 2].
4. Tarek M. Masaud, and P.K. Sen, “Study of the Implementation of STATCOM on DFIG-Based Wind Farm Connected to a Power System,” IEEE *PES Conference on Innovative Smart Grid Technologies (ISGT)*, Washington, DC, USA. January16-20. 2012, pp. 1-7. [Chapter 3].
5. Tarek M. Masaud and P.K. Sen, “A Comparative Study of the Implementation of STATCOM and SVC on DFIG-Based Wind Farm Connected to a Power System,” IEEE Power and Energy Society (PES) General Meeting, San Diego, California, USA. July.2012. [Chapter 3].

## REFERENCES

- [1] Hyong Sik Kim and Dylan Dah-Chuan Lu, "Wind Energy Conversion System from Electrical Perspective - A Survey," *Smart Grid and Renewable Energy*, vol. 1, no. 3, pp. 119-131, Nov. 2010.
- [2] G. L. Johnsson, *Wind Energy Systems*. Englewood Cliffs, N.J., USA. Prentice-Hall, 1985.
- [3] Pao, Lucy Y, and Johnson, Kathryn E, "Control of Wind Turbines," *IEEE Control System Magazine*, vol. 31, Issue 2, pp. 44-62, April. 2011.
- [4] Pao Lucy Y, and Johnson Kathryn E, "A Tutorial on the Dynamics and Control of Wind Turbines and Wind Farms," American Control Conference, St. Louis, MO, USA, June 10 – 12. 2009. pp. 2076 – 2089.
- [5] Johnson, Kathryn E, Pao Lucy Y, Balas Mark J, Kulkarni V, and Fingersh Lee J. "Stability Analysis of an Adaptive Torque Controller for Variable Speed Wind Turbines," 43rd IEEE Conference on Decision and Control, Atlantis, Paradise Island, Bahamas, vol. 4, pp. 4087 - 4094, December 14-17. 2004. [NREL report, NREL/CP-500-36756, December 2004].
- [6] Schreck Scott J, and Robinson Michael C, "Horizontal Axis Wind Turbine Blade Aerodynamics in Experiments and Modeling," *IEEE Transactions on Energy Conversion*, vol. 22, no. 1, pp. 61-70, March. 2007.
- [7] Magdi Ragheb, and Adam M. Ragheb. Fundamental and Advanced Topics in Wind Power. Published Online by InTech. July 2011. [http://cdn.intechopen.com/pdfs/16242/InTech-Wind\\_turbines\\_theory\\_the\\_betz\\_equation\\_and\\_optimal\\_rotor\\_tip\\_speed\\_ratio.pdf](http://cdn.intechopen.com/pdfs/16242/InTech-Wind_turbines_theory_the_betz_equation_and_optimal_rotor_tip_speed_ratio.pdf). [Accessed 7-17-2013].
- [8] Françoise Mei, "Small Signal Modeling and Analysis of Doubly Fed Induction Generator in Wind Power Applications," *Ph.D. dissertation*, Control and Power Group Department of Electrical and Electronic Engineering, Imperial College London University of London. 2008.
- [9] Johnson, Kathryn E, L. Fingersh, M. Balas, and L. Pao, "Methods for Increasing Region 2 Power Capture on a Variable Speed Wind Turbine," *Journal of Solar Energy Engineering*, vol. 126, no. 4, pp. 1092- 1100, 2004.
- [10] U.S. Department of Energy Office of Energy Efficiency and Renewable Energy. (2008). 20% wind energy by 2030 [Online]. Available: <http://www.nrel.gov/docs/fy09osti/42864.pdf>. [Accessed: 4-15-2013].
- [11] Muyeen S. M, Takahashi Rion, Murata Toshiaki, and Tamura Junji "A Variable Speed Wind Turbine Control Strategy to Meet Wind Farm Grid Code Requirements," *IEEE Transactions on Power Systems*, vol. 25, no. 1, pp. 331-340, February. 2010.

- [12] National Renewable Energy Laboratory (NREL). Updated Installed Wind Capacity Map [online]. Available: <http://www.nrel.gov/wind/news/2012/1829.html>. [Accessed: 4-15-2013].
- [13] American Wind Energy Association (AWEA). AWEA U.S. Wind Industry Fourth Quarter 2012 Market Report [Online]. Available: [http://www.awea.org/learnabout/publications/reports/upload/AWEA-Fourth-Quarter-Wind-Energy-Industry-Market-Report\\_Executive-Summary-4.pdf](http://www.awea.org/learnabout/publications/reports/upload/AWEA-Fourth-Quarter-Wind-Energy-Industry-Market-Report_Executive-Summary-4.pdf). [Accessed: 4-20-2013].
- [14] Global Wind Energy Council (GWEC). Global Wind Statistics (2012) [Online]. Available: [http://www.gwec.net/wp-content/uploads/2013/02/GWEC-PRstats-2012\\_english.pdf](http://www.gwec.net/wp-content/uploads/2013/02/GWEC-PRstats-2012_english.pdf).
- [15] Johnson, Kathryn E. Adaptive Torque Control of Variable Speed Wind Turbines. *NREL Technical Report*, NREL/TP-500-36265, August. 2004.
- [16] P W Carlin, A. S. Laxson, and E.B. Muljadi. The History and State of the Art of Variable-Speed Wind Turbine Technology. *NREL Technical Report*, NREL/TP-500-28607, February. 2001.
- [17] P. Mutschler and R. Hoffmann, "Comparison of wind turbines regarding their energy generation," in Proc. 2002 IEEE 33rd Annual IEEE Power Electronics Specialists Conference, vol. 1, Cairns, Queensland., Australia, June, 23–27, pp. 6–11, 2002.
- [18] Quincy Wang, and Liuchen Chang, "An Intelligent Maximum Power Extraction Algorithm for Inverter-Based Variable Speed Wind Turbine Systems," *IEEE Transaction on Power Electronics*, vol. 19, no. 5, pp. 1242-1249, September. 2004.
- [19] Linn Takeuchi. Subcontractors and Component Suppliers in the Swedish Wind Power Industry. Department of Technology and Society Environmental and Energy Systems Studies, Lund University, Sweden, Report No. 42, May. 2003.
- [20] Jangamshetti Suresh H, and Rau V. Guruprasada, "Normalized power curves as a tool for identification of optimum wind turbine generator parameters," *IEEE Transactions on Power Conversion*, vol. 16, no. 3, pp. 283-288, September. 2001.
- [21] Senjyu Torriombu, Sakamoto Ryosei, Urasaki Naonitsii, Funabashi Toshihisa, Fujita, Hideki and Sekine Hideomi, "Output power leveling of wind turbine Generator for all operating regions by pitch angle control," *IEEE Transactions on Energy conversion*, vol. 21, no. 2, pp. 467-475, June. 2006.
- [22] Jangamshetti, Suresh H, Ran, V.G, "Optimum siting of wind turbine generators," *IEEE Transactions on Energy Conversion*, vol. 16, no. 1, pp. 8-13, March. 2001.
- [23] Bimal K. Bose, "Modern Power Electronics and AC Drives", USA, Prentice Hall PTR, Inc. City and State, 2002.
- [24] Paul C. Krause, "Analysis of Electric Machinery", McGraw-Hill, Inc. City and State, 1986.

- [25] Burack Ozpineci, and Leon.M Tolbert, “Simulink Implementaion of Induction Machine Model- A modular Approach”, Electric Machines and Drives Conference, IEMDC03.IEEE International, City and State, vol. 2, pp. 728, June. 2003.
- [26] Wei Qiao, “Dynamic Modeling and Control of Doubly Fed Induction Generators Driven by Wind Turbines,” Power Systems and Exposition IEEE/PES, vol. 2, pp. 1-8, March. 2009.
- [27] Eduard Muljadi, C. P. Butterfield, Brian Parsons, and Abraham Ellis, “Effect of Variable Speed Wind Turbine Generator on Stability of a Weak Grid,” *IEEE Transactions on Energy Conversion*, vol. 22, no. 1, pp. 29-36, March. 2007.
- [28] Eduard Muljadi, M. Singh, and V. Gevorgian, “Doubly Fed Induction Generator in an Offshore Wind Power Plant Operated at Rated V/Hz”, Energy Conversion Congress and Exposition (ECCE), Raleigh, NC, USA, pp. 779-786, 15-20 September. 2012.
- [29] Stephan Engelhardt, Istvan Erlich, Christian Feltes, J'org Kretschmann, and Fekadu Shewarega, “Reactive Power Capability of Wind Turbines Based on Doubly Fed Induction Generator,” *IEEE Transactions on Energy Conversion*, vol. 26, no. 1, pp. 364-372, March 2011.
- [30] Janka B Ekanayake, Lee Holdsworth, Xue Guang Wu, and Nicholas Jankins, “Dynamic Modeling of Doubly Fed Induction Generator Wind Turbines,” *IEEE Transactions on Power Systems*, vol. 18, no. 2, pp. 803-809, May. 2003.
- [31] Srirattanawichaikul,W, Kumsuwan Y, Premrudeepchacharn S, and Wu B, “A Vector Control of A Grid Connected 3L-NPC-VSC with DFIG Drives,” (ECTI-CON) International Conference, Chiang Mai, Thailand, pp. 828-832, May. 2010.
- [32] Lie Xu, and Yi Wang, “Dynamic Modeling and Control of DFIG-Based Wind Turbines under Unbalanced Network Conditions,” *IEEE Transactions on Power Systems*. vol. 22, no. 1, pp. 314-323, February. 2007.
- [33] Lie Xu, and Cartwright P, “Direct Active and Reactive Power Control of DFIG for Wind Energy Generation,” *IEEE Transactions on Energy Conversion*, vol. 21, no. 3, pp. 750 – 758, September. 2006.
- [34] Arantxa Tapia, Gerardo Tapia, J. Xabier Ostolaza, and Jose Ramon Saenz, “Modeling and Control of Wind Turbine Driven Doubly Fed Induction Generator,” *IEEE Transactions on Energy Conversion*, vol. 18, no. 2, pp. 194 – 204, June. 2003.
- [35] Jihen Arbi, Manel Jebali, Ilhem Slama, and Lotfi Charaabi, “Direct Virtual Torque Control for Doubly Fed Induction Generator Grid Connection,” *IEEE Transactions on Industrial Electronics*, vol. 56, no. 10, pp. 4163 – 4173, October. 2009.

- [36] S. Muller, M. Deicke and RikW. De Doncker, "Doubly fed induction generator systems for wind turbines," *IEEE, Industry Applications Magazine*, vol. 8, issue. 3, pp. 26-33, May/June 2002.
- [37] Shuhui Li, Haskew T A, and Eduard Muljadi, "Integrative Characteristic Evaluation of DFIG Maximum Power Extraction using Lookup Table Approach," IEEE PES General Meeting, Minneapolis, MN, USA, pp. 1- 8, July. 2010.
- [38] B Chitti Babu, and K.B.Mohanty, "Doubly Fed Induction Generator for Variable Speed Wind Energy Conversion Systems – Modeling and Simulation," *International Journal of Computer and Electrical Engineering*, vol. 2, no. 1, Feb. 2010.
- [39] R. Pena, J.C. Clare, G.M. Asher, "Doubly fed induction generator using back-to-back PWM converters and its application to variable speed wind-energy generation", *IEEE Proceedings on Electric Power Applications*, vol. 143, no. 3, pp. 231-241, May 1996.
- [40] Jeong-Ik Jang, Young-Sin Kim, and Dong-Choon Lee, "Active and Reactive Power Control of DFIG for Wind Energy Conversion under Unbalanced Grid Voltage," CES/IEEE 5<sup>th</sup> International Power Electronics and Motion Control Conference (IPEMC), Shanghai, China, vol. 3, pp. 1-5, Aug. 2006.
- [41] Jacomini R V, Franca A P, and Bim E, "Simulation and Experimental Studies on Double-Fed Induction Generator Power Control at Subsynchronous Operating Speed," IEEE International Conference on Power Electronics and Drive Systems (PEDS), Taipei, Taiwan, pp. 1421-1424, November. 2009.
- [42] B. K. Bose and N. R. Patel, "Quasi-fuzzy estimation of stator resistance of induction motor," *IEEE Transactions on Power Electronics*, vol. 13, no. 3, pp. 401–409, May 1998.
- [43] B. K. Bose and N. R. Patel, "Stator flux oriented vector controlled induction motor drive with space vector PWM and flux vector synthesis by neutral networks," *IEEE Transactions on Industry Applications*, vol. 37, no. 5, pp. 1308–1318, October. 2001.
- [44] S. Wang and Y. Ding, "Stability analysis of field oriented doubly-fed induction machine drive based on computer simulation," *Electric Machines and Power Systems*, vol. 21, no. 1, pp. 11–24, 1993.
- [45] Shuhui Li, Chaloo R. and Nemmers M J, "Comparative study of DFIG power control using stator-voltage and stator-flux oriented frames," IEEE PES General Meeting, Alberta, Canada, pp. 1- 8, July, 26-30. 2009.
- [46] Wei Qiao, Ganesh Kumar Venayagamoorthy, and Ronald G. Harley, "Real-Time Implementation of a STATCOM on a Wind Farm Equipped with Doubly Fed Induction Generators," *IEEE Transaction on Industry Application*, vol. 45, no. 1, pp. 98–107, Feb. 2009.

- [47] Wei Qiao, Ganesh Kumar Venayagamoorthy, and Ronald G. Harley, "Coordinated Reactive Power Control of Large Wind Farm and a STATCOM Using Heuristic Dynamic Programming," *IEEE Transaction on Energy Conversion*, vol. 24, no. 2, pp. 493–503, June. 2009.
- [48] Li Wang, and Chia-Tien Hsiung, "Dynamic Stability Improvement of an Integrated Grid-Connected Off-Shore Wind Farm and Marine-Current Farm Using a STATCOM," *IEEE Transaction on Power Systems*, vol. 26, no. 2, pp. 690–698, May. 2011.
- [49] Stephan Engelhardt, Istvan Erlich, Christian Feltes, Jorg Kretschmann, and Fekadu Shewarega "Reactive Power Capability of Wind Turbines Based on Doubly Fed Induction Generators," *IEEE Transactions on Energy Conversion*, vol. 26, no. 1, pp. 364-372, March. 2011.
- [50] Eduard Muljadi, C P Butterfield, R. Yinger, and H Romanowitz, "Energy Storage and Reactive Power Compensator in a Large Wind Farm," *NREL Conference paper*. NREL/CP-500-34701, October. 2003.
- [51] Singh S N, Jacob Østergaard, and Bharat Singh "Reactive power capability of unified DFIG for wind power generation," IEEE PES General Meeting, Minneapolis, MN, USA, pp. 1-7, July, 25-29. 2010.
- [52] K E Okedu, S M Muyeen, Rion Takahashi and Junji Tamura "Participation of FACTS in stabilizing DFIG with crowbar during grid fault based on grid codes," IEEE Conference and Exhibition (GCC), Dubai, UAE, pp. 365-368, February, 19-22. 2011.
- [53] Rafael Guerrero, "Grid code interrelation, wind generation evaluation and reactive compensation. Special topics inside a grid code," Integration of Renewables into the Distribution Grid, (CIRED Workshop), Lisbon, Portugal, pp. 1-4, May, 29-30. 2012.
- [54] Ha Thu Le, and Surya Santoso, "Increasing Wind Farm Transient Stability by Dynamic Reactive Compensation: Synchronous- Machine-Based ESS versus SVC," IEEE Power and Energy Society (PES) General Meeting, Minneapolis, Minnesota USA, 25-29 July. 2010.
- [55] "Simulink7 User's Guide," The MathWorks, Inc, October. 2008.
- [56] Hydro-Quebec, "SimPowerSystems™ User's Guide, R2012b" The MathWorks, Inc. September. 2012. [Only Online: upon request from Matworks.com].
- [57] Yanqiang shi, Hong Shen, Lei Dong, Bin Huang, Jian Ding, and Dezhi Chen, "The Coordination Control of Voltage and Reactive Power Between Wind Turbines and SVC Technology,' International Conference on Power System Technology (POWERCON), Hangzhou, China, 24-28 Oct. 2010.

- [58] Mehrdad Fazli, Ali Reza Shafighi, Ali Fazli, and Heidar Ali Shayanfar, “Effects of STATCOM on Wind Turbines Equipped with DFIGs During Grid Faults,” World Non-Grid-Connected Wind Power and Energy Conference (WNWEC) , Nanjing, China, 5-7 Nov.2010.
- [59] H. Gaztanaga, I. Etxeberria-Otadui, D. Ocnasu, and S. Bacha, “Real-Time Analysis of the Transient Response Improvement of Fixed-Speed Wind Farms by Using a Reduced-Scale STATCOM Prototype,” *IEEE Transactions on Power System*, vol. 22, no. 2, pp. 658–666, May. 2007.
- [60] A. P. Jayam, and B. H. Chowdhury, “Improving the Dynamic Performance of Wind Farms with STATCOM,” IEEE Power System Conference and Exposition, Seattle, USA, March, 15-18. 2009.
- [61] Z. Saad-Saoud, M. L. Lisboa, J. B. Ekanayake, N. Jenkins, and G. Strbac, “Application of STATCOM to Wind Farms,” *Generation, Transmission and Distribution, IEE Proceedings*, vol. 145, no. 5, pp. 511–516, September. 1998.
- [62] GE, ‘Guide for Economic Evaluation of Flexible AC Transmission Systems (FACTS) in Open Access Environment,’ *Technical Report*, EPRI-TR 108500. GE, New York, 1997.
- [63] J. V. Coevering, J. P. Stovall, R. L. Hauth, P. J. Tatto, B. D. Railing and B. K. Johnson, “The Next Generation of HVDC- Needed R&D, Equipment Costs, and Cost Comparisons,” Proc. EPRI Conference of Future of Power Delivery, Washington DC, 1996.
- [64] Faruk A. Bhuiyan, and Amirnaser Yazdani, ”Multimode Control of a DFIG-Based Wind Power Unit for Remote Applications,” *IEEE Transaction on Power Delivery*, vol. 24, no. 4, pp. 2079 – 2089, October. 2009.
- [65] Y. Mishra, S. Mishra, and Fangxing Li “Coordinated Tuning of DFIG-Based Wind Turbines and Batteries Using Bacteria Foraging Technique for Maintaining Constant Grid Power Output,” *IEEE Systems Journal*, vol. 6, Issue. 1, pp. 16-24, March. 2012.
- [66] Chad Abbey and Géza Joos, “Supercapacitor Energy Storage for Wind Energy Applications,” *IEEE Transaction on Industry Applications*, vol. 43, Issue 3, pp. 769-776, May. 2007
- [67] Liyan Qu, and Wei Qiao, “Constant Power Control of DFIG Wind Turbines With Supercapacitor Energy Storage,” *IEEE Transaction on Industry Applications*, vol. 47, no. 1, January. 2011.
- [68] Banakar H, Baike Shen and Boon-Teck Ooi, “Strategies to Smooth Wind Power Fluctuation of Wind Turbine Generator,” *IEEE Transactions on Energy Conversion*, vol. 22, Issue 2, pp. 341-349, June. 2007.
- [69] Rasool Aghatehrani, Rajesh Kavasseri, and Ravi Chandra Thapa, “Power Smoothing of the DFIG Wind Turbine Using a Small Energy Storage Device,” IEEE PES General Meeting, Minneapolis, MN, USA, pp. 1-6, July. 2010.

- [70] Simoes, M G, “EGGN 581: Modern Adjustable Speed Electric Drive,” Colorado School of Mines Course, Spring 2009.
- [71] M. Aktarujjaman, M.E. Haque, and K. M. Muttaqi, “Control Dynamics of a Doubly Fed Induction Generator Under Sub- and Super-Synchronous Modes of Operation,” IEEE PES General Meeting, Pittsburgh, PA, USA, pp. 1- 9, July 20-24. 2008.
- [72] Shien, He , Weizhou Wang, Huaisen Jia, Gang Cui, Fujun Wang, and Jun Liu, “Integration of wind farm into Gansu power grid and its operation,” International Conference on Sustainable power generation and supply (SUPERGEN), Nanjing, China, pp. 1-5, April 6-7. 2009.
- [73] “Energy Storage: The missing Link in The Electricity Value Chainl,” An ESC white paper, Energy Storage Council (ESC), St. Louis, MO, May 2002.
- [74] Sérgio Faias, Patrícia Santos, Jorge Sousa, and Rui Castro, “An Overview on Short and Long-Term Response Energy Storage Devices for Power Systems Applications,” Technical University of Lisbon, IST/TUL, Lisboa, Portugal, 2007.
- [75] Zhang Chi, Tseng King-Jet Jet, “A Novel Flywheel Energy Storage System With Partially-Self-Bearing Flywheel-Rotor,” *IEEE Transactions on Energy Conversion*, vol. 22, no. 2, pp. 477-487. June. 2007.
- [76] Paulo F. Ribeiro, Brian K. Johnson, Mariesa L. Crow, Aysen Arsony, and Yilu Liu, “Energy Storage Systems for Advanced Power Applications,” *Proceedings of the IEEE*, vol. 89, no. 12, pp. 1744 – 1756, December. 2001.
- [77] Ali Hasan Hasan, Wu Bin, and Dougal, Roger A, “An Overview of SMES Applications in Power and Energy Systems,” *IEEE Transactions on Sustainable Energy*, vol. 1, no. 1, pp. 38-47, April. 2010.
- [78] Yunus, A. M Shiddiq, Masoum, Mohammad A S and Abu-Siada, Ahmed, “Application of SMES to Enhance the Dynamic Performance of DFIG During Voltage Sag and Swell,” *IEEE Transactions on Applied Superconductivity*, vol. 22, no. 4, pp. 570-579, Aug. 2012.
- [79] Jin Chi, and Wang Peng, “Enhancement of low voltage ride-through capability for wind turbine driven DFIG with active crowbar and battery energy storage system,” IEEE Power and Energy Society (PES) General Meeting, Minneapolis, Minnesota USA, pp. 1-8, July 25-29. 2010.
- [80] Williams, Mark C, “Fuel Cells and The world Energy Future ,” IEEE Power and Energy Society (PES) Summer Meeting, Vancouver, BC, Canada, July 15-19. 2001.
- [81] Ellis, Michael W, Von Spakovsky Michael R, and Nelson, Douglas J, “Fuel Cell Systems: Efficient, Flexible Energy Conversion for the 21st Century,” *Proceedings of the IEEE*, vol. 89, no. 12, pp. 1808-1818, December. 2001.

- [82] Schainker R B, Nakhamkin M, “Compressed -Air Energy Storage (CAES): Overview, Performance and Cost Data for 25MW to 220MW Plants,” *IEEE Transactions on Power Apparatus and Systems*, vol. 104, no. 4, pp. 790-795, July. 1985.
- [83] Schoenung S, Burns C “Utility energy storage applications studies ,” *IEEE Transactions on Energy Conversion*, vol. 11, no. 3, pp. 658-665, September. 1996.
- [84] Pickard W F, “The history, Present State, and Future Prospects of Underground Pumped Hydro for Massive Energy Storage,” *Proceedings of IEEE*, vol. 100, no. 2, pp. 473-483, February. 2012.
- [85] Jalal Kazempour S, Hosseinpour M, Moghaddam M P, “Self-Scheduling of a Joint Hydro and Pumped-Storage Plants in Energy, Spinning Reserve and Regulation Markets,” *IEEE Power and Energy Society (PES) General Meeting, Calgary, Alberta, Canada*, pp. 1-8, July 26-30. 2009.
- [86] Figueiredo F. Cristina, and Flynn Peter C, “Using diurnal power price to configure pumped storage,” *IEEE Transaction on Energy Conversion*, vol. 21, no. 3, pp. 804-809, September. 2006.
- [87] I.H. Wong, “An underground Pumped Storage Scheme in the Bukit Timah Granite of Singapore,” *Tunnelling and Underground Space Technology*, vol. 11, no. 4, pp. 485-489, October. 2006.
- [88] Palle B, Simoes M G, "Dynamic Integration of a Grid Connected DFIG Wind Turbine with a Fuel Cell," *Industry Applications Conference, 2007. 42nd IAS Annual Meeting. Conference Record of the 2007 IEEE*, 23-27 Sept. 2007. pp. 650-655.
- [89] J Charles Smith, “Winds of Change: Issues in Utility wind integration,” *Utility Wind Integration Group (UWIG)*. [Online]. Available: <http://www.uwig.org/smitheditorial.pdf>. [Accessed: 4-20-2013].
- [90] Muljadi E, and Gevorgian V “Short-Circuit Modeling of a Wind Power Plant,” *IEEE PES General Meeting, Detroit, Michigan, USA*, pp. 1- 9, July, 24-29. 2011.
- [91] Xu Xiaokang, Edmonds Michael J S, Bishop Martin, and Sember, Jim “Application of Distributed Static Compensators in Wind Farms to Meet Grid Codes,” *Power and Energy Engineering Conference (APPEEC), Shanghai, China*, pp. 1-5, March, 27-29. 2012.
- [92] “Challenges of Energy Storage Technologies!”, A report from the APS Panel on Public Affairs Committee on Energy and Environment. May, 2007. [Online]. Available: <http://www.aps.org/policy/reports/popa-reports/upload/Energy-2007-Report-ElectricityStorageReport.pdf>. [Accessed: 4-15-2013 ].

- [93] Kunte R. S, Pallem Chandralekha, and Mueller, D. "Wind Plant Reactive Power and Voltage Compliance with Grid Codes," Power Electronics and Machines in Wind Applications (PEMWA), IEEE conference, Denver, Colorado, USA, pp. 1-4, July 17-19. 2012.
- [94] A A Edris, R Adapa, M H Baker, L Bohmann K Clark, K Habashi, L Gyugyi, J Lemay, A S Mehraban, A K Myers, J Reeve, F Sener, D R Torgerson, and R R Wood "Proposed Terms and Definitions for Flexible AC Transmission System(FACTS)," IEEE Transactions on Power Delivery, vol. 12, Issue 4, pp. 1848–1853, October 1997.
- [95] Li H, and Chen Z, "Overview of Different Wind Generator Systems and Their Comparisons," Renewable Power Generation, IET, vol. 2, no. 2, pp. 123-138, June. 2008.
- [96] Brahma S M, Chaudhary M, and Ranade S J, "Some findings about equivalencing wind farms with Type 1 and Type 2 induction generators," North American Power Symposium (NAPS), Boston, MA, USA, pp. 1-6, 4-6 Aug. 2011.
- [97] Walling R A, Gursoy E, and English B, "Current Contributions from Type 3 and Type 4 Wind Turbine Generators During Faults," Transmission and Distribution Conference and Exposition (T&D), IEEE PES, pp.1-6, 7-10 May. 2012.
- [98] Hiskens I A, "Dynamics of Type-3 Wind Turbine Generator Models," IEEE Transactions on Power Systems, vol. 27, no. 1, pp. 465-474, Feb. 2012.
- [99] Reigh A Walling, and Reichard M L, "Short Circuit Behavior of Wind Turbine Generators," Protective Relay Engineers, 2009 62nd Annual Conference for , College station, Texas, USA, pp. 492-502, March 30 - April 2. 2009.
- [100] Lee Keun H, Malmedal K, and Sen P K, "Conceptual Design and Cost Estimate for a Stand-Alone Residential Photovoltaic System," IEEE Green Technologies Conference, IEEE. pp. 1-6, 19 -20 April. 2012.
- [101] Yan Zhang, and Milanovic J V, "Voltage Sag Cost Reduction with Optimally Placed FACTS devices," 9th International Conference on Electrical Power Quality and Utilisation (EPQU), Barcelona, Spain, pp. 1-6, 9-11 October. 2007.
- [102] Singh B, Saha R, Chandra A, and Al-Haddad K, "Static Synchronous Compensators (STATCOM): A review," *Power Electronics*, IET, vol. 2, no. 4, pp. 297-324, July. 2009.
- [103] David Connolly, "A review of Energy Storage Technologies for The integration of Fluctuating Renewable Energy" Review for Ph.D Project, University of Limerick, Ireland, October. 2010. [Online]. Available:  
<http://dconnolly.net/files/A%20Review%20of%20Energy%20Storage%20Technologies.pdf>.  
[Accessed 04-29-2013].

- [104] Kawabe K, and Yokoyama A, "Improvement of Angle and Voltage Stability by Control of Batteries Using Wide-Area Measurement System in Power Systems," 3rd IEEE PES Innovative Smart Grid Technologies Europe (ISGT Europe), Berlin, Germany, pp. 1-7, 14-17 Oct. 2012.
- [105] Papić I, "Simulation Model for Discharging A lead-Acid Battery Energy Storage System for Load Leveling," *IEEE Transactions on Energy Conversion*, vol. 21, no. 2, pp. 608-615, June. 2006.
- [106] Dusonchet, L Ippolito M G, Telaretti E, and Graditi G, "Economic Impact of Medium-Scale Battery Storage Systems in Presence of Flexible Electricity Tariffs for End-User Applications," 9<sup>th</sup> International Conference (European Energy Market), Florence, Italy, pp. 1-5, 10-12 May. 2012.
- [107] Smith S C, Sen P K, and Kroposki B, "Advancement of Energy Storage Devices and Applications in Electrical Power System," IEEE Power and Energy Society General Meeting (PES), Pittsburgh, PA, USA, pp. 1-8, 20-24 July. 2008.
- [108] U.S. Energy Information Administration (EIA). Annual Energy Review 2011. September, 2012. [Online]. Available: <http://www.eia.gov/totalenergy/data/annual/pdf/aer.pdf>. [Accessed: 04-25-2013].
- [109] Johnson, Kathryn E., "EGGN 589: Design and Control of Wind Energy Systems," Colorado School of Mines Course, Spring 2010.
- [110] Tennessee Valley Authority (TVA), [Online]. Available: <http://www.tva.gov/power/pumpstorart.htm>. [Accessed: 07-28-2013].
- [111] P.K. Sen, "EGGN 389: Fundamentals of Electric Machinery," Colorado School of Mines Course, Fall 2010.

**APPENDIX A**  
**SYSTEM PARAMETERS**

Table. A1  
DFIG Model Parameters [25]

Parameter (Notation)	Value (Unit)
Rated Power (P)	30 kW
Number of Poles (p)	2
Frequency (f)	50 Hz
Voltage (V)	220/380 Volt
Stator Resistance ( $R_s$ )	0.19Ω/phase
Rotor Resistance ( $R_r$ )	0.39Ω/phase
Stator Leakage Inductance ( $L_{ls}$ )	0.00021H/phase
Rotor Leakage Inductance ( $L_{lr}$ )	0.0006 H/phase
Magnetizing Inductance ( $L_m$ )	0.004 H/phase

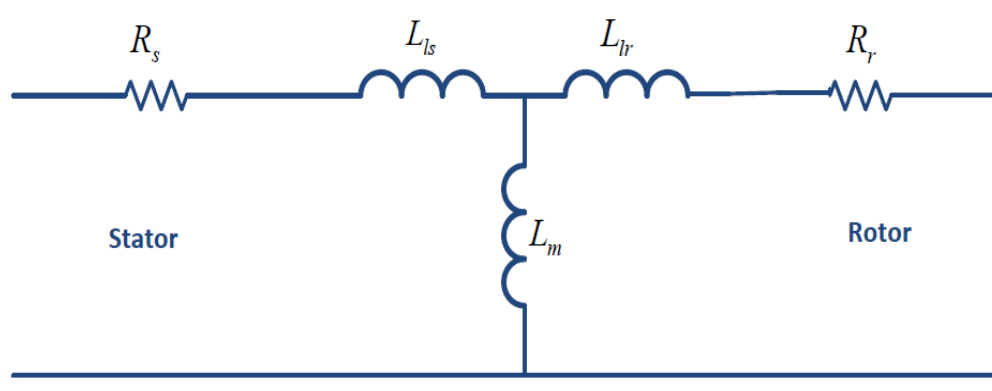


Figure A1 Parameters of induction machine equivalent Circuit

Table. A2  
Grid Connected DFIG-based Wind Farm Parameters [56]

Wind Turbine		Generator Parameters	
Rated Capacity	(6 Turbines × 1.5MW each), Total: 9 MW	$P_{rated}$	6 × 1.5 MW
Cut –in Wind speed	3.5 m/s	$V_{rated}$	575 V
Cut-out Wind speed	25 m/s	$r_s$	0.00706pu
Rated Wind speed	14 m/s	$r_r$	0.005pu
No. of Blades	3	$l_{ls}$	0.171pu
Rotor Diameter	82.5 m	$l_{lr}$	0.156pu
Swept area	5,346 m <sup>2</sup>	$L_m$	2.9pu
Rotor speed	10.1-18.7 rpm	$pf$	0.9 (lag)

Table A3  
Parameters of DFIG-based Wind Turbine with Battery Energy Storage System (BESS)

Wind Turbine		Generator Parameters		BESS Parameters (Thevenin Equivalent)	
Rated Capacity	1.5MW	$P_{rated}$	1.5 MW	Battery Nominal Voltage ( $V_b$ )	1200 V
Cut –in Wind speed	3.5 m/s	$V_{rated}$	575 V	Internal Resistance ( $R_b$ )	10,000 $\Omega$
Cut-out Wind speed	25 m/s	$r_s$	0.00706 pu	Internal Capacitance ( $C_b$ )	140,625 F
Rated Wind speed	14 m/s	$r_r$	0.005 pu	Battery series resistance ( $R_s$ )	0.00085 $\Omega$
No. of Blades	3	$l_{ls}$	0.171pu		
Rotor Diameter	82.5 m	$l_{lr}$	0.156 pu		
Swept area	5346 m <sup>2</sup>	$L_m$	2.9 pu		
Rotor speed	10.1-18.7 rpm	$pf$	0.9		

## APPENDIX B

### MATLAB/Simulink

Figure B1. Implementation of DFIG in MATLAB/Simulink (Mathematical Model)  
 (The implementation of the set of equations from (2-4) to (2-17) in Chapter 2, Section 2.5.1).  
 The Model along with it's instructions are included for future references.

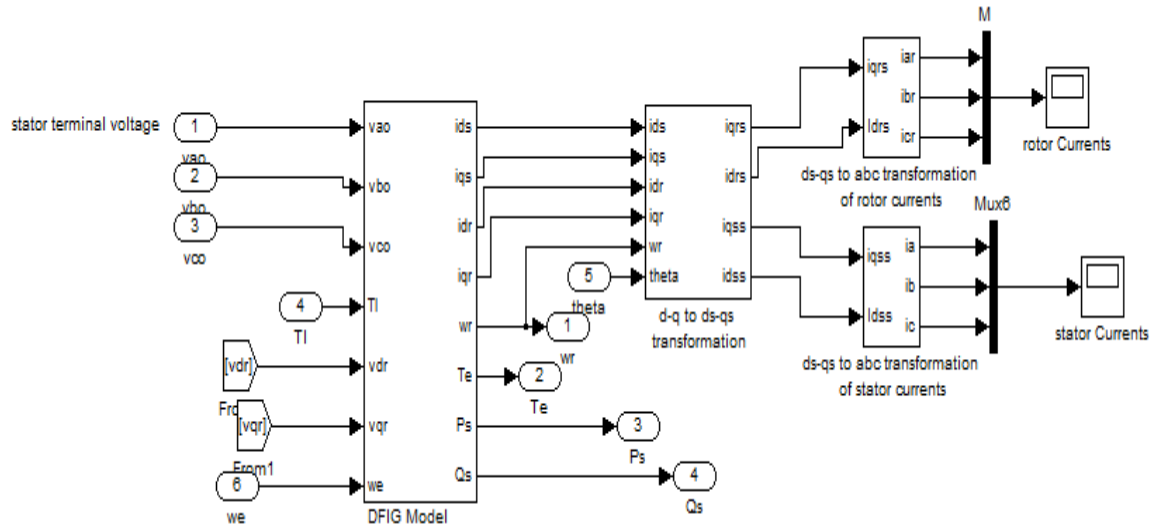


Figure B2. Implementation of AC-DC-AC converter in MATLAB/Simulink

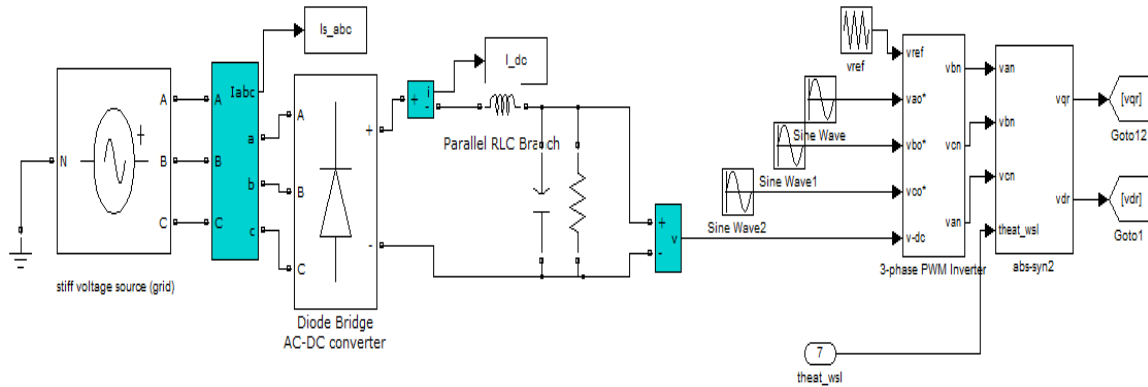


Figure B3. Implentation of Statot flux-oriented vector control in MATLAB/Simulink (All controller equations are explained in Chapter 2, Section 2.8.1 ). The coltroller implementation along with instructons are included for future references.

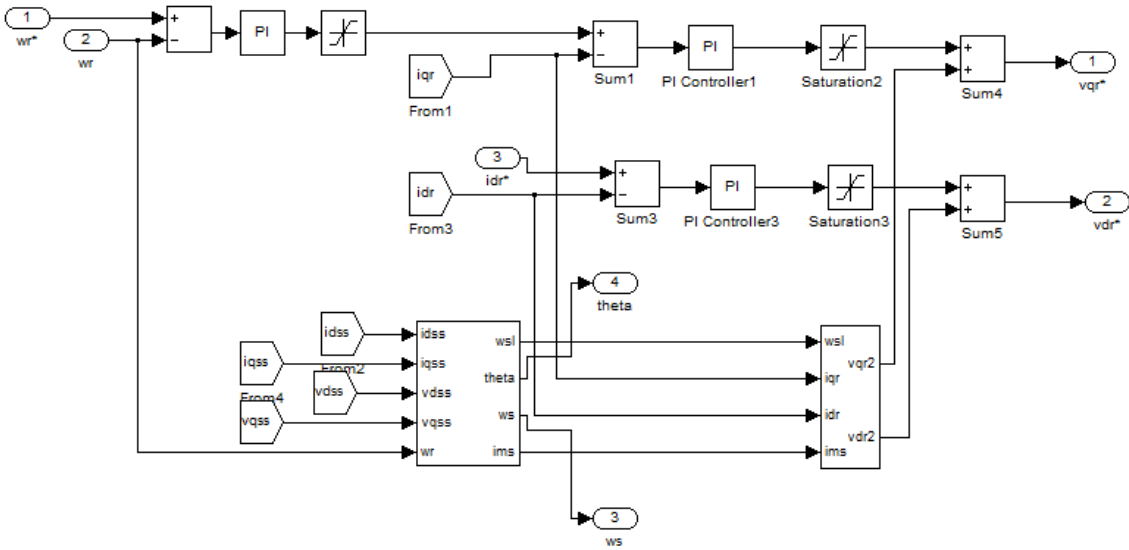


Figure B4. Implentation of Rotor flux-oriented vector control in MATLAB/Simulink (All controller equations are explained in Chapter 2, Section 2.8.2). The controller is included for future references.

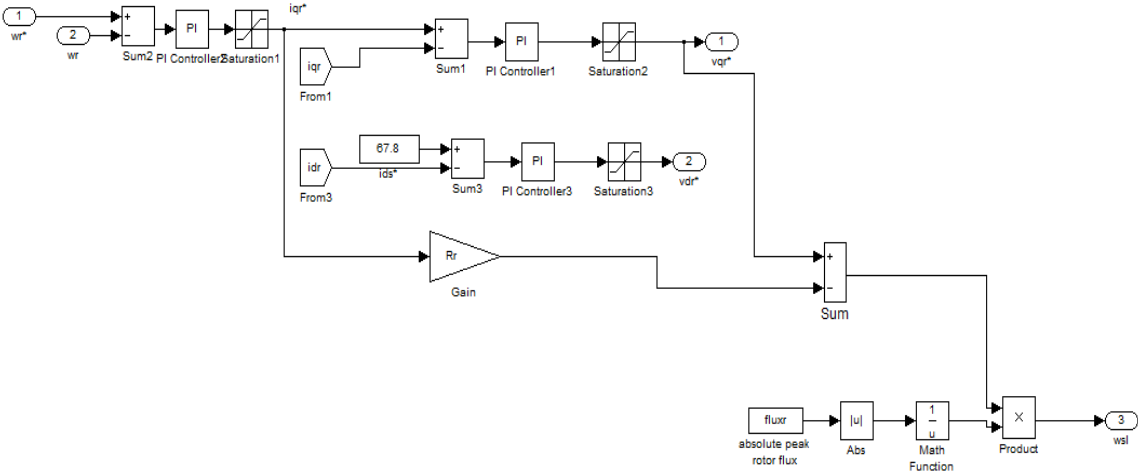


Figure B5. MATLAB/Simulink diagram of the test System (DFIG-based wind Farm connected to power Grid) is shown in Chapter3, Figure 3.5. The entire test System is available in SimPowerSystem Library in any MATLAB /Simulink Version and more details can be found in [56]. This system is used for both FACTS devices and BESS studies. The SimPowerSystem of the test system along with the description file are included for future references.

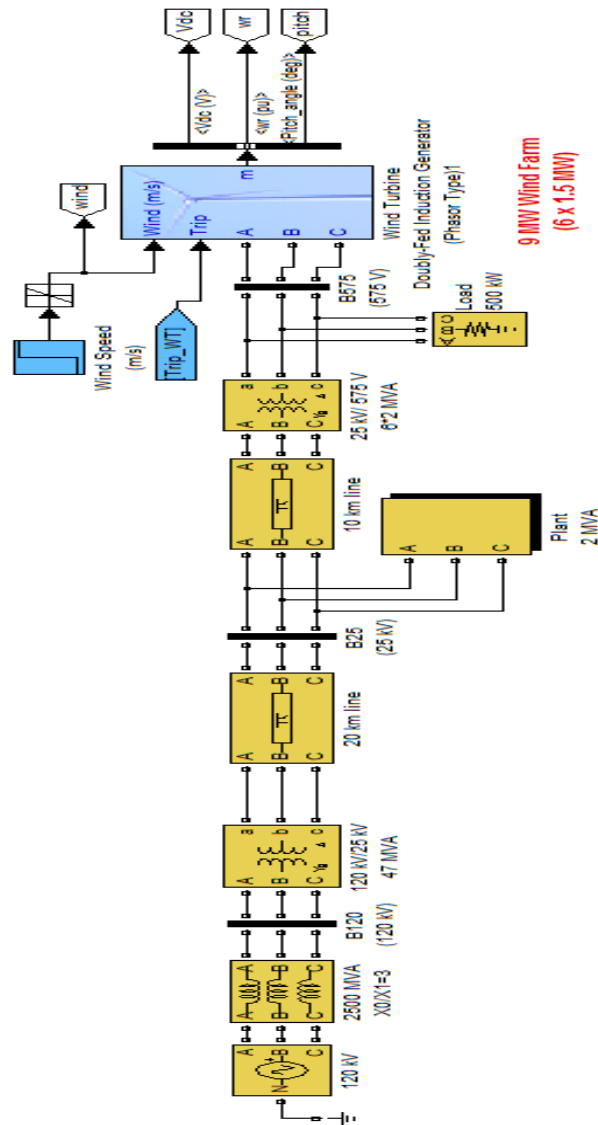






Figure B8. MATLAB/Simlink (SimPowerSystem) diagram of Phasor Model of Static Var Compensator (SVC) (This Phasor Model is available in SimPowerSystem Library and can be operated in two different modes: the voltage regulation mode and the Var control mode)

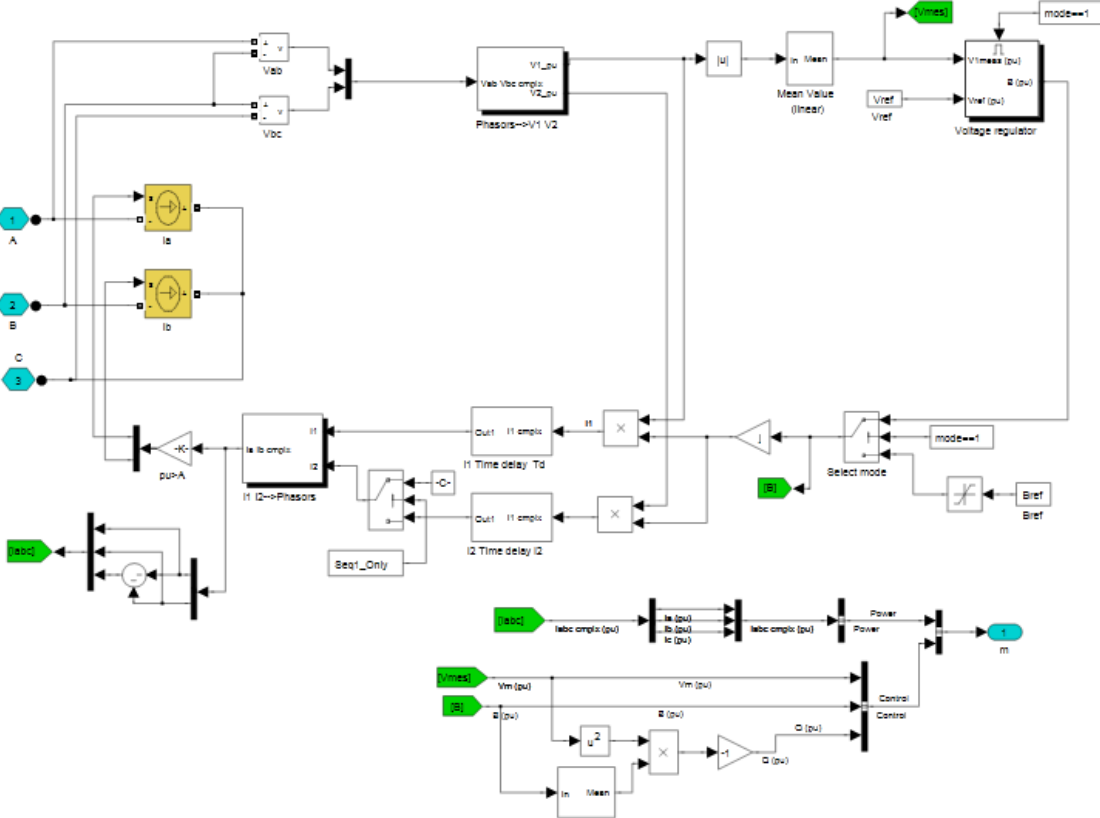




Figure B10. DFIG-based wind turbine protection system in MATLAB/Simulink (SimPowerSystem). (Overvoltage, undervoltage, overcurrent, Dc overvoltage, Overspeed, underspeed)

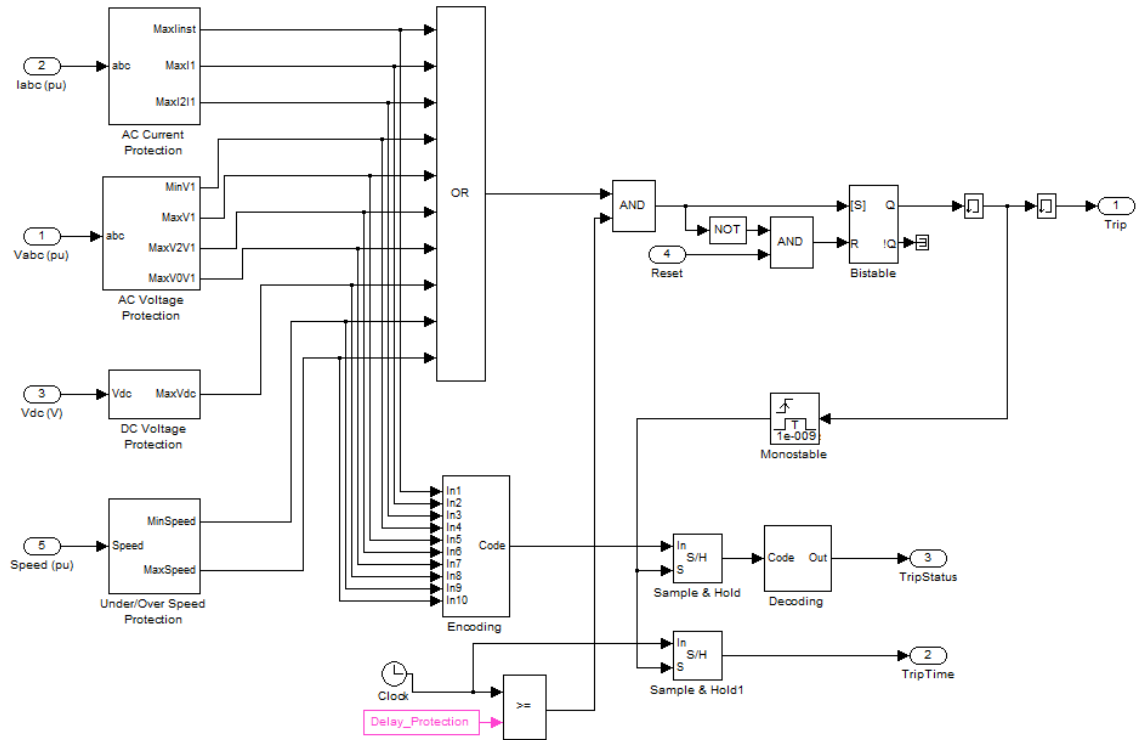


Figure B11. MATLAB/Simulink (SimPowerSystem) diagram of a grid connected DFIG-Based wind turbine with BESS

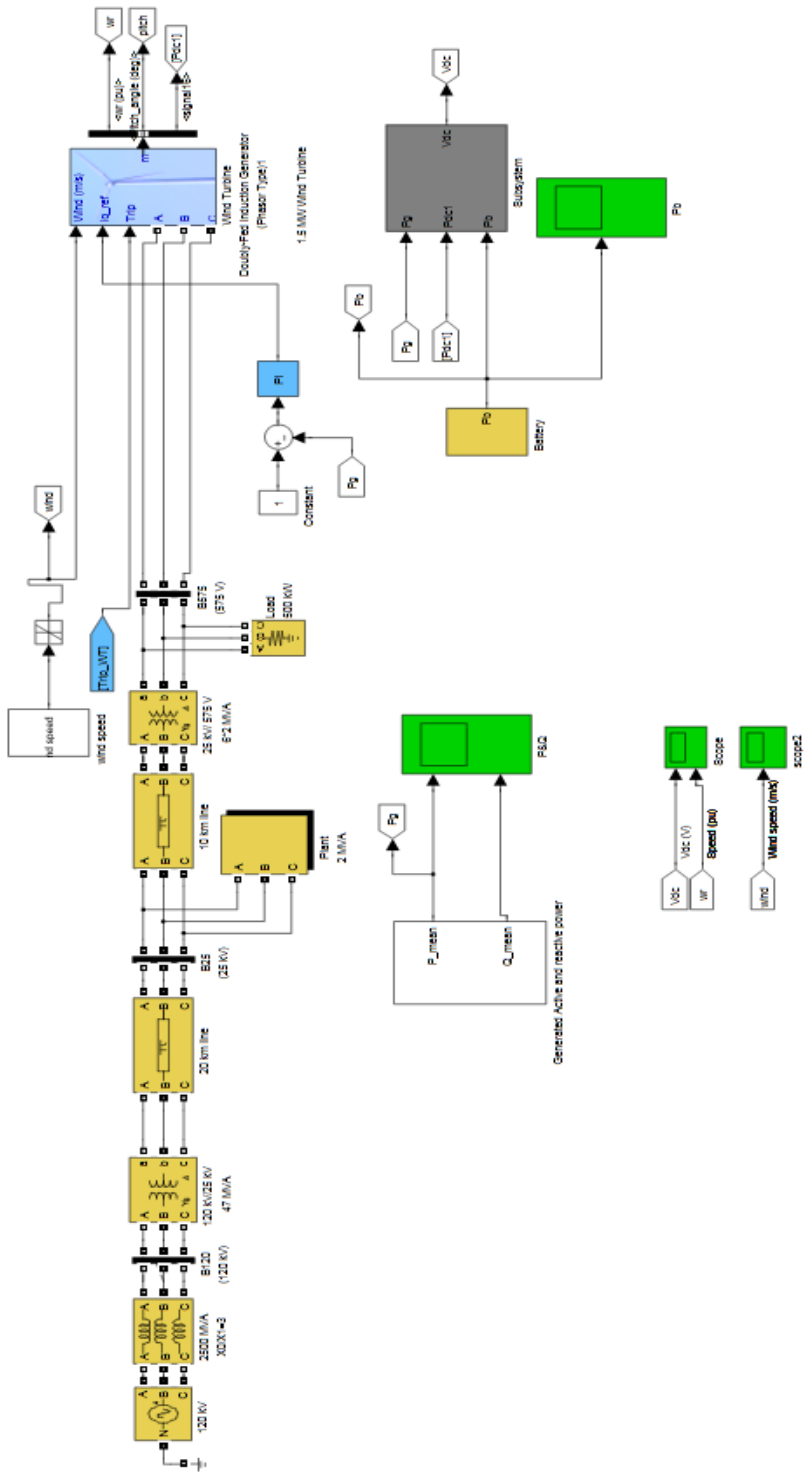


Figure B12. Battery Model Implementation in MATLAB/Simulink (SimPowerSystem), The equivalent circuit diagram is shown in Chapter.4, Figure 4.8.

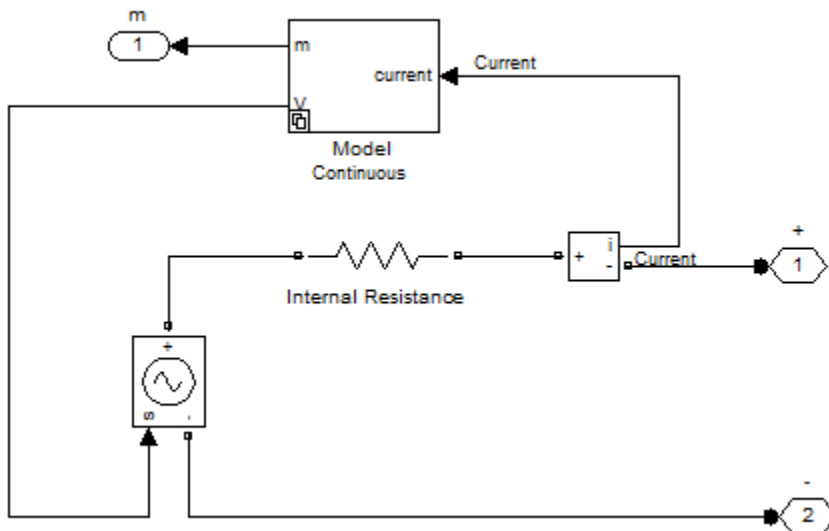


Figure B13. Implementation of the proposed control strategy of GSC in MATLAB/ Simulink of a DFIG with BESS. The control strategy is explained in Chapter 4, section 4.5.1.

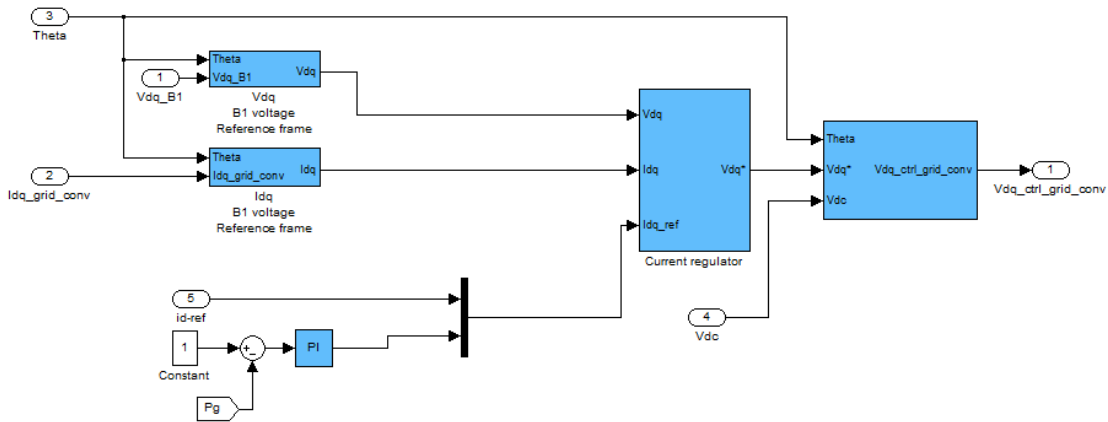
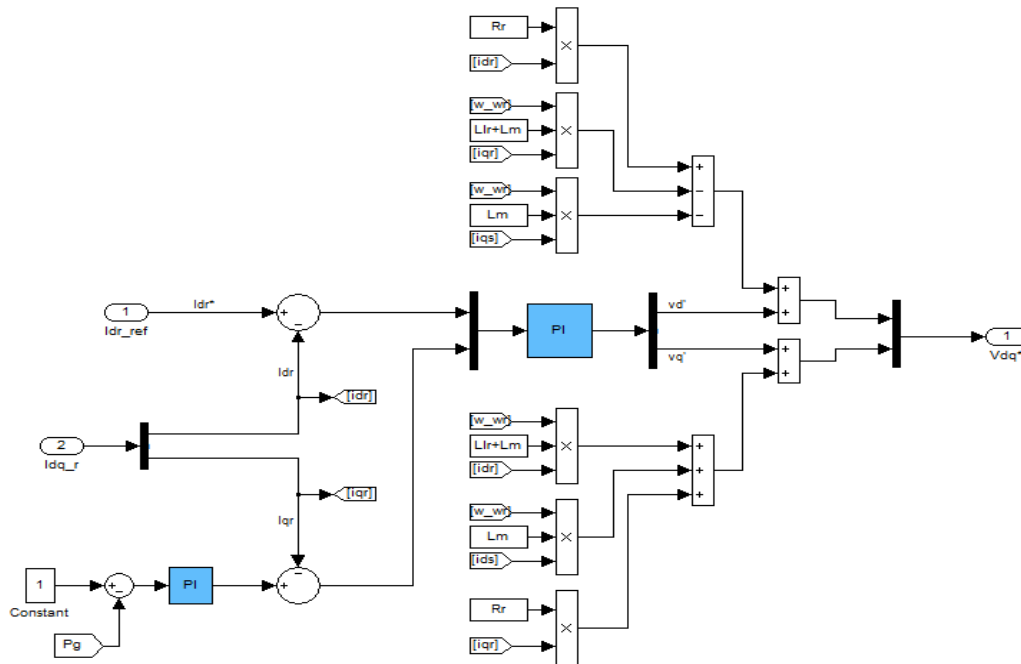


Figure B14. Implementation of the proposed control strategy of RSC in MATLAB/ Simulink of a DFIG with BESS. The control strategy is explained in Chapter 4, section 4.5.2.



## APPENDIX C

### PRINCIPLE OF d-q TRANSFORMATION [23, 24]

Note: This principle has been well-developed and understood by the engineers and scientists for long time. This short section is added here for the completeness of this dissertation.

The per-phase (or single-phase) equivalent circuit (lumped) model of the induction machine is valid only for steady-state calculations. In any variable speed application (like adjustable speed drives or DFIG), the machine normally has an element with a feedback loop, and therefore its transient behavior must be taken into consideration. In order to understand the principle of the vector control, and the transient behavior of the machines, a good understanding of the d-q model is necessary.

In the d-q dynamic model, the machine is represented by an equivalent two-phase machine, as shown in Figure C.1, in which  $d^s - q^s$  represents the stator direct and quadrature axes, and  $d^r - q^r$  represents the rotor direct and quadrature axes, and  $\theta_r$  is the arbitrary angle between the corresponding d or q axes of the stator or the rotor.  $\omega_e$  is counterclockwise angular frequency (or speed).

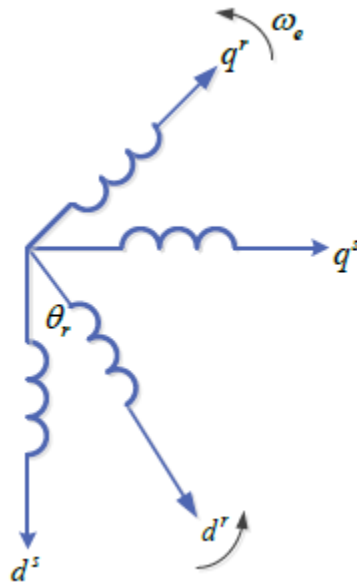


Figure C.1 Equivalent two-phase machine

In the 1920's, R. H. Park proposed the d-q transformation in order to overcome the problem associated with the time-varying inductances in the transient analysis of synchronous

machine. He replaced the variables (voltage, current and flux linkage) associated with the stator windings with variables associated with fictitious winding rotating with the rotor at synchronous speed. In other words, he referred the stator variables to a reference frame fixed on the rotor and rotating at the synchronous speed. This was quite helpful in solving synchronous machine problems, since the rotor at steady-state always runs at synchronous speed. This method of d-q transformation is called Park Transformation. Later, in the 1930s, another scholar named H. C. Stanley proposed a new method of d-q transformation by transforming the rotor variables to variables associated with fictitious stationary windings. In this method, all the rotor variables are referred to a stationary reference frame fixed on the stator. The last method of d-q transformation was proposed by G. Kron, who transformed both rotor and stator variables to a synchronously rotating reference frame that moves with the rotating magnetic field. This is extremely helpful in dealing with induction machine problems, since the rotor speed is actually variable. The time varying inductances can be eliminated by referring both stator and rotor variables to a common reference frame which can be rotating at any speed. For this application, it is the most common practice to use the synchronous speed.

Figure C.2 depicts the forward and the backward (reverse process) d-q transformation utilized to develop the d-q model of the induction machine. The transformation procedures include transforming the stator 3-phase stationary reference frame (a, b, c) variables into 2-phase stationary reference frame ( $d^s - q^s$ ) variables and then transforming those to synchronously rotating reference frame ( $d^e - q^e$ ), and vice versa.

The formula to transform the stator 3-phase stationary reference frame (a, b, c) variables (Voltage in this case) into a 2-phase stationary reference frame ( $d^s - q^s$ ) can be represented in the matrix form as shown in equations (C.1) and (C.2).  $d^s - q^s$  is assumed to be oriented by an arbitrary angle  $\theta$  as shown in Figure C.3 below.  $v_{os}^s$  is the zero sequence component which is normally not taken into account (neglected) since the machine is ungrounded and assumed to operate under balanced condition. This is also shown in Figure C.3.

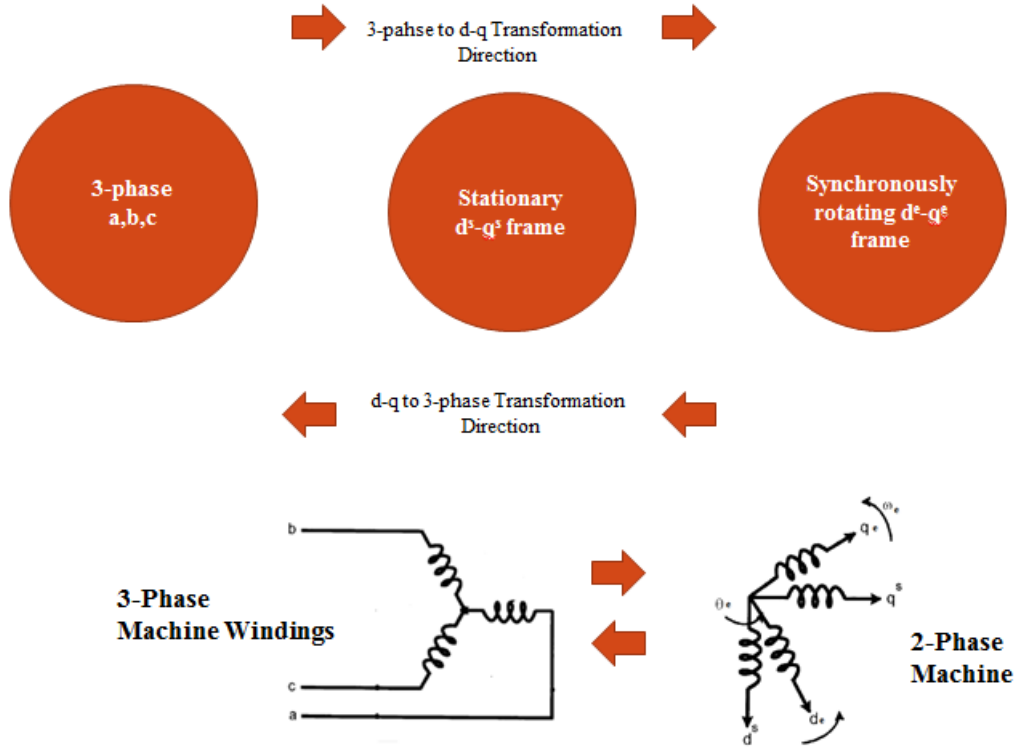


Figure C.2 The d-q transformation approach for stator windings

$$\begin{bmatrix} V_a \\ V_b \\ V_c \end{bmatrix} = \begin{bmatrix} \cos \theta & \sin \theta & 1 \\ \cos(\theta - 120) & \sin(\theta - 120) & 1 \\ \cos(\theta + 120) & \sin(\theta + 120) & 1 \end{bmatrix} \begin{bmatrix} v_{qs}^s \\ v_{ds}^s \\ v_{os}^s \end{bmatrix} \quad (C.1)$$

The corresponding inverse relation is

$$\begin{bmatrix} v_{qs}^s \\ v_{ds}^s \\ v_{os}^s \end{bmatrix} = \frac{2}{3} \begin{bmatrix} \cos \theta & \cos(\theta - 120) & \cos(\theta + 120) \\ \sin \theta & \sin(\theta - 120) & \sin(\theta + 120) \\ 0.5 & 0.5 & 0.5 \end{bmatrix} \begin{bmatrix} V_a \\ V_b \\ V_c \end{bmatrix} \quad (C.2)$$

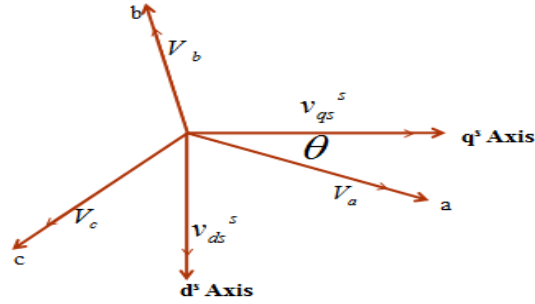


Figure C.3 Stator three- phase frame (a, b, c) to  $d^s - q^s$  stationary reference frame

By ignoring the zero-sequence component and setting  $\theta = 0$  (for simplification), the  $q^s$  axes is aligned with the phase-a axes. Equations (C1) and (C.2) and the transformation formula can then be simplified as below.

$$\begin{aligned}
 V_a &= v_{qs}^s \\
 V_b &= -\frac{1}{2}v_{qs}^s - \frac{\sqrt{3}}{2}v_{ds}^s \\
 V_c &= -\frac{1}{2}v_{qs}^s + \frac{\sqrt{3}}{2}v_{ds}^s
 \end{aligned} \tag{C.3}$$

The corresponding inverse relation becomes

$$\begin{aligned}
 v_{qs}^s &= V_a \\
 v_{ds}^s &= -\frac{1}{\sqrt{3}}V_b + \frac{1}{\sqrt{3}}V_c
 \end{aligned} \tag{C.4}$$

Equations (C.3) and (C.4) represent the forward and backward transformation formula to transform stator 3-phase stationary reference frame variables to a 2-phase  $d^s - q^s$  stationary reference frame.

The next step is to transform the stationary reference frame  $d^s - q^s$  variables to a synchronously rotating reference frame  $d^e - q^e$  variables. Figure C.4 shows the synchronously rotating axes  $d^e - q^e$ , which rotate at synchronous speed  $\omega_e$  with respect to the stationary axes  $d^s - q^s$ . The angle,  $\theta_e = \int \omega_e dt$ .

Based on Figure C.4, the relationship between the stationary frame and the synchronously rotating frame can be generated as shown in equations (C.5) and (C.6).

$$v_{qs} = v_{qs}^s \cos \theta_e - v_{ds}^s \sin \theta_e \quad (C.5)$$

$$v_{ds} = v_{qs}^s \sin \theta_e + v_{ds}^s \cos \theta_e$$

$$v_{qs}^s = v_{qs} \cos \theta_e + v_{ds} \sin \theta_e \quad (C.6)$$

$$v_{ds}^s = -v_{qs} \sin \theta_e + v_{ds} \cos \theta_e$$

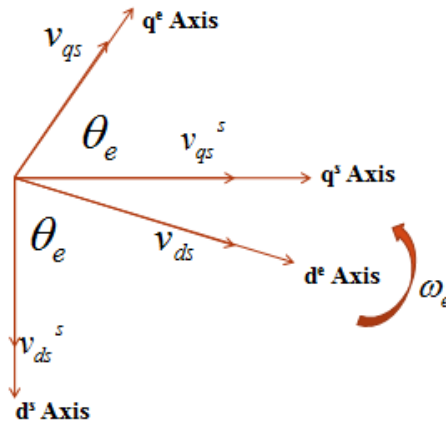


Figure C.4 Stationary frame  $d^s - q^s$  to synchronously rotating frame  $d^e - q^e$  transformation

## APPENDIX D

### SUPPLEMENTAL FILES

First supplemental file shows the implementation of DFIG in MATLAB/Simulink “Mathematical Model” (The implementation of the set of equations from (2-4) to (2-17) in Chapter 2, Section 2.5.1). The simple idea behind this model is that building a d-q induction machine model in which the rotor circuit is connected to a constant voltage source (Grid) via AC-DC-AC converter. Each equation is implemented and can be accessed by opening the subsystems blocks in the model; each block solves one of the model equations. This model is useful to understand the sub-synchronous and super-synchronous modes of operation of the DFIG. The second file shows a MATLAB/Simulink model of the test System (DFIG-based wind farm connected to a power Grid) that is shown in Chapter3, Figure 3.5. The entire test System is available in SimPowerSystem Library in any MATLAB /Simulink Version and more details can be found in [56]. The system is included here for future references. In this work, this system is used for both FACTS devices and BESS studies.

DFIG_Model.zip	Files containing an implementation of DFIG in MATLAB/Simulink “DFIG_Model1” (The implementation of the set of equations from (2-4) to (2-17) in Chapter 2, Section 2.5.1. Files include an input data MATLAB file “PARAM” of this model. Files also include a detailed description and instructions of the model in a pdf file “Description”.
DFIG Model_SimPowerSystem.zip	Files containing a SimPowerSystem model of a Grid connected DFIG “wind_power_dfig”. Files also include a detailed description and instructions of this model in a pdf file “SimPowerSystem_DFIG Model description”.